UNIVERSITÀ DEGLI STUDI DI PADOVA

Dipartimento di Fisica e Astronomia "Galileo Galilei"

Master Degree in Physics

Final Dissertation

Quantum droplets and bright solitons in mixtures of Bose-Einstein condensates

Thesis supervisor

Prof. Francesco Ancilotto

Candidate

Elena Poli

Academic Year 2019/2020

Acknowledgements

I sincerely thank Prof. Ancilotto for his guidance, his constant support and the time he spent helping me.

I would like to thank my parents and my brother for having always encouraged me to follow my own path and for always believing in me.

Thanks to Michele for always being by my side.

Contents

Introduction

In nature, liquid droplets reveal the equilibrium between mutual attractive and repulsive forces between atoms or molecules. The formation of such self-bound states is known to belong to the liquid phase of conventional condensed matter, with typical densities of the order of 10^{22} atoms/cm^3. However, recently the realization of a stable, self-bound quantum droplet has been achieved on an unexpected density regime. The prediction of this state was made by D.S. Petrov [1]: the origin of the self-bound droplet comes from the interplay of repulsive and attractive interaction between atoms in a mixture of Bose-Einstein condensates (BEC).
The basic theory of Bose-Einstein condensation was predicted by Satyendra Nath Bose and Albert Einstein in 1924 [2]. Basically, a BEC is a direct consequence of the quantum statistics of indistinguishable particles with integer spin, called bosons. Einstein proposed that cooling a gas system made of bosonic atoms at a very low temperatures would lead to a new state of matter characterized by the macroscopic occupation of the ground state [3]. In 1938, F. London had the intuition that the BEC was the mechanism at the basis of the superfluidity phenomenon in liquid helium [4] and, since then, numerous theoretical studies were developed to better understand the relationship between condensation and superfluidity. Despite its prediction in the early 1920s, it took some decades before the condensation of bosonic gases was eventually experimentally observed. Most of the theories in Bose-Einstein condensation, in fact, implies the condition of weakly interacting atoms and this can be satisfied only in ultradilute and ultracold systems. Only in 1980s new techniques like laser cooling and magneto-optical trapping were developed to cool and trap neutral atoms and, eventually, in 1995 the experimental group of Eric Cornell and Carl Wieman at the University of Colorado at Boulder and the one of Wolfgang Ketterle at MIT managed to reach the proper conditions and observe a BEC in atomic vapours of ^{87}Rb [5] and ^{23}Na [6], respectively. For the experimental achievement of Bose-Einstein condensation in dilute gases of alkali atoms and for early fundamental studies of the properties of the condensates Cornell, Ketterle and Wieman won the Nobel prize in 2001.
After this discovery, a new chapter in condensed matter physics began and the interest towards ultracold atoms increased in the theoretical and experimental research community. The purpose of this work is to study a system made of a binary mixture of Bose-Einstein condensates, where the realization of the new liquid phase predicted by D.S. Petrov takes place. A mixture can be composed of atoms of the same species in different spin states, different isotopes or different atoms. In this kind of system, the high tunability of the interparticle interaction among atoms of the same or different species and the beyond mean field physics play a crucial role for the stability of a self-bound state, opening the possibility to create liquid droplets in the contest of ultracold gases but with an extremely low density compared to any other existing liquids.
Recently, the homonuclear mixture composed by a spin mixture of ^{39}K were studied and

observed in free space [7] and in presence of an external potential [8, 9]. In the latter case, by using an optical waveguide, which leads to a dimensionality reduction of the system into a quasi-1D configuration, the crossover between a self-bound quantum droplet and the bright soliton state was studied, stressing the connection between these two localized states of different nature [10]. However, ^{39}K homonuclear mixtures lead to the formation of short-lived droplets: they evaporate after few milliseconds (~ 8 ms) because of the loss due to the three-body recombination phenomenon [7].

In this work, we will study a binary heteronuclear Bose-Bose mixture made of ^{41}K-^{87}Rb: the main motivation of this choice just comes from the longer droplet lifetime due to a lower three-body recombination rate of the system, as proved experimentally by recent works [11]. This mixture leads to the droplet formation in free space with a lifetime around ~ 28 ms, about three times longer than the measured lifetime of ^{39}K droplets. This crucial difference between dissipation processes in the two mixtures is related to the density of the two self-bound states: experimentally, ^{41}K-^{87}Rb droplets are more dilute than ^{39}K ones and, since the finite lifetime τ_{life} depends on the total density ρ according to $\tau_{\text{life}} \sim \rho^{-2}$ [1], the longer lifetime is explained. The main consequence is that this mixture could allow for a deeper experimental investigation of this new phase transition.

The chapter organization is reported below.

In chapter 1, we review the main properties of the Bose-Einstein condensates of non-interacting bosons and the description at mean-field level of a system of indistinguishable interacting bosons at zero temperature, focusing on the experimental tools that allow to tune the interaction strength. The bosonic binary mixture made of ^{41}K-^{87}Rb is presented and a simple model to predict the self-bound droplet formation is discussed, highlighting the fundamental role of quantum fluctuations embodied in the Lee-Huang-Yang energy contribution.

In chapter 2, the properties of the homogeneous mixture of ^{41}K-^{87}Rb are studied in the regime in which a self-bound state is expected: in particular, the equilibrium bulk densities and the compressibility of the system are computed by means of numerical simulations.

In chapter 3, the surface properties of a ^{41}K-^{87}Rb self-bound quantum droplet are discussed: the density profile of the droplet along the radial direction and the surface tension are studied with (*i*) a variational approach, (*ii*) a numerical method and (*iii*) by solving numerically the two coupled Gross-Pitaevskii equations associated to the components of the mixture. The critical number of particles for the droplet stability is also computed with a variational method.

In chapter 4, the total energy of a droplet is computed as a function of the total number of particles and the validity of the liquid-drop model for this kind of system is verified. From the Tolman length calculation, the curvature correction is applied to the surface tension.

In chapter 5, the bright soliton state is first studied in a single species BEC of ultracold and ultradilute atoms and then in the ^{41}K-^{87}Rb mixture in an optical waveguide.

Chapter 1

Self-bound states in binary mixtures of Bose-Einstein condensates

In this chapter we present a general introduction to Bose-Einstein condensation for non-interacting bosons and the mean-field description of a system made of identical interacting bosons. In particular, the origin of the contact pseudopotential and its strength tunability are explained. Then, a mean-field description of the ^{41}K-^{87}Rb bosonic mixture is provided within the Density Functional Theory framework. Finally, the first beyond-mean-field Lee-Huang-Yang correction due to quantum fluctuations will be introduced, showing how it leads to the formation of a self-bound state in the mixture.

1.1 Bose-Einstein condensation

A Bose-Einstein condensate is a state of matter that involves ultracold bosons close to zero temperature, as predicted by Satyendra Nath Bose and Albert Einstein in 1924. The phase transition described by a macroscopic occupation of the ground state of the system below a critical temperature T_c is linked to the quantum statistic of bosons.
The description of a non-interacting Bose gas provides the simplest example which predicts correctly some significant properties of real Bose systems. Let's consider a system with N identical non-interacting bosons: the main property of the many body wavefunction Φ is its symmetry with respect to the exchange of two coordinates $\mathbf{r}_i$ and $\mathbf{r}_j$ such that

$$\Phi(\mathbf{r}_1, \mathbf{r}_2, ..., \mathbf{r}_i, ..., \mathbf{r}_j, ..., \mathbf{r}_N) = \Phi(\mathbf{r}_1, \mathbf{r}_2, ..., \mathbf{r}_j, ..., \mathbf{r}_i, ..., \mathbf{r}_N). \tag{1.1}$$

At zero temperature, all particles occupy the ground state and the many body wavefunction reads:

$$\Phi(\mathbf{r}_1, \mathbf{r}_2, ..., \mathbf{r}_N) = \prod_i \phi_0(\mathbf{r}_i) \tag{1.2}$$

and total macroscopic density of the system can be computed as:

$$\rho(\mathbf{r}) = N|\phi_0(\mathbf{r})|^2. \tag{1.3}$$

At finite temperature, the population of excited states is allowed according to the Bose-Einstein distribution. The natural description of a Bose gas at finite temperature is

provided by the grand canonical ensemble and so, if $\langle N \rangle$ is the total average number of particles, $\langle N_\alpha \rangle$ is the average number of particle in the state α, $\beta = k_B T$ and μ is the chemical potential, one has:

$$\langle N \rangle = \sum_\alpha \langle N_\alpha \rangle = \sum_\alpha \frac{1}{e^{\beta(\mathcal{E}_\alpha - \mu)} - 1} \tag{1.4}$$

Consequently, at finite temperature the total number of particles and so the total density $\rho = N/V$ can be split in two components, the fraction of atoms in the ground state and the fraction of atoms in the excited states:

$$\begin{aligned} \rho =& \rho_0 + \rho_{\text{exc}} \\ =& \rho_0 + \frac{1}{V} \sum_{\alpha \neq 0} \frac{1}{e^{\beta(\mathcal{E}_\alpha - \mu)} - 1} \end{aligned} \tag{1.5}$$

Taking into account the behaviour of the chemical potential μ of the system visible in figure 1.1, it is clear that for a system at finite temperature $T < T_c$ we can put $\mu = 0$. Since we are working with a free non-interacting system, the label α which distinguishes different states can be identified as the momentum $\mathbf{k}$ of the particle. We can pass from the discrete summation to a integral in the continuum space of momenta and compute it:

$$\frac{1}{V} \sum_{\mathbf{k} \neq 0} \frac{1}{e^{\beta \mathcal{E}(\mathbf{k})} - 1} \to \frac{1}{(2\pi)^3} \int d\mathbf{k} \frac{1}{e^{\beta \mathcal{E}(\mathbf{k})} - 1} = \rho \left(\frac{T}{T_c} \right)^{3/2} \tag{1.6}$$

where $T_c = \frac{2\pi\hbar^2}{m} \left(\frac{\rho}{\xi(3/2)} \right)^{2/3}$ is the critical temperature under which the condensation phase takes place [12].
Inserting this result in (1.5) we can compute the condensate fraction at temperature T:

$$\frac{N_0}{N} = 1 - \left(\frac{T}{T_c} \right)^{3/2} \tag{1.7}$$

The behaviour of the condensate fraction in function of the reduced temperature is visible in figure 1.2. Notice that, for $T < T_c$, the condensate fraction is finite and it corresponds to a macroscopic occupation of the ground state.
Although it was predicted in 1920s, the condensation of bosonic gases was experimentally observed for the first time in 1995. In fact, the advent of laser cooling and new trapping techniques in the 1980s opened up a new approach to ultracold physics and the group of Eric Cornell and Carl Wieman at the University of Colorado at Boulder and the one of Wolfgang Ketterle at MIT succeeded to reach the proper conditions to observe the Bose-Einstein condensation in dilute gases of alkali atoms of ^{87}Rb [5] and ^{23}Na [6], respectively. For this experimental achievement and for early studies about condensates properties, Cornell, Ketterle and Wieman won the Nobel prize in 2001. The figure 1.3 shows the particles momentum distribution in the first observation of a Bose-Einstein condensate. From the left to the right, the three density profiles correspond to decreasing temperatures: the first one is still in the classical regime, where the density distribution is given by the classical Boltzmann law, the last one corresponds to a quasi-pure condensate. The BEC is observed with the appearance of a narrow peak in the momentum distribution, corresponding to the macroscopic accumulation of atoms in the single particle ground state of the system.

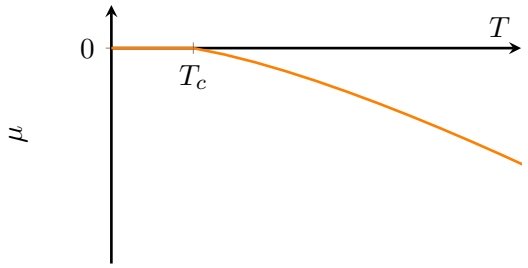

Figure 1.1: Chemical potential of an ideal Bose gas: for $T \geq T_c$ it is a negative quantity, for $T < T_c$ we have $\mu = 0$.

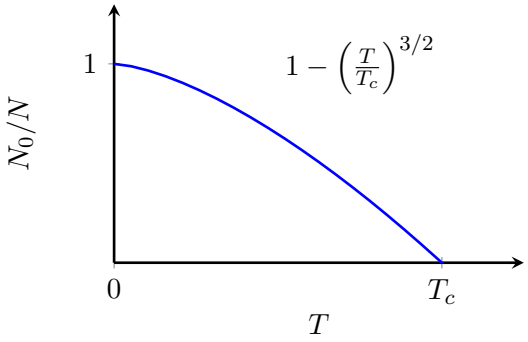

Figure 1.2: The condensate fraction N_0/N vs. the normalized temperature T/T_c in a uniform 3D system.

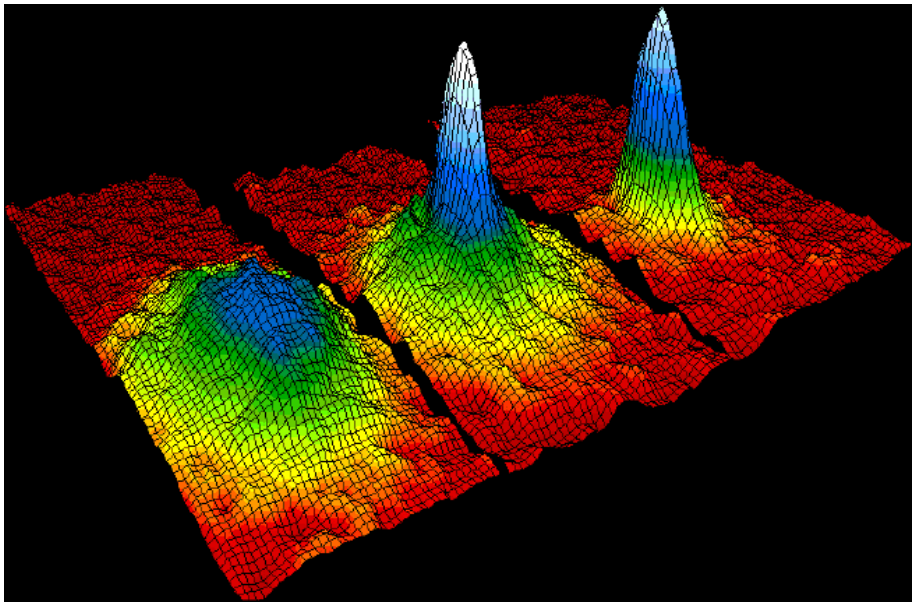

Figure 1.3: Momentum distribution data for a gas of rubidium atoms that experimentally confirms the discovery of the Bose–Einstein condensation. The left plot shows the density profile just before the appearance of a Bose–Einstein condensate, the central one is just after the appearance of the condensate and the right plot, after further evaporation, corresponds to a quasi-pure condensate.

1.2 Ultracold and ultradilute interacting bosons

So far we considered an ideal system of non-interacting bosons. However, experimentally we always deal with interactions that affect the properties of the gas. The condensates we are going to study are always very diluted, i.e. for a given number density ρ the range of interparticle interaction r_0 is much smaller than the average distance d between them:

$$r_0 \ll d \sim 1/\rho^{1/3} \tag{1.8}$$

This assumption allows to neglect interactions between three or more particles: in this way, we can consider only a two-body short range interaction potential. Then, we are dealing with an ultracold system at temperatures of the order of tens of nK for which the de Broglie thermal wavelength λ_T is larger than the range of interparticle interaction r_0:

$$\lambda_T = \frac{h}{\sqrt{2\pi m k_B T}} \gg r_0 \tag{1.9}$$

In this regime collisional events are limited to the elastic scattering, i.e. the two final states have the same relative kinetic energy E before and after the collision. In this case, the interaction depends on a single parameter, the *s-wave scattering length* a_s. In fact, the large values of λ_T make impossible the resolution of the scatterer, for this reason it is not important what precise potential V(r) is responsible for the scattering, but only how the potential behaves at large length scales. Formally, in scattering theory the outgoing wave for $r \to \infty$ is decomposed in the following way:

$$\Phi(r) \sim e^{i\mathbf{k}\cdot\mathbf{r}} + f(k,\theta)\frac{e^{i\mathbf{k}\cdot\mathbf{r}}}{r} \tag{1.10}$$

The first term is the incoming wave and the second one is the scattered wave, whose amplitude $f(k,\theta)$ depends on the interaction potential. The angle between the incoming and outgoing direction is represented by θ.
Assuming a central potential, the amplitude factor can be decomposed in angular components:

$$f(k,\theta) = \sum_l (2l+1) f_l(k) P_l(\cos\theta) \tag{1.11}$$

where $f_l(k)$ is the partial wave scattering amplitude and $P_l(\cos\theta)$ are the Legendre polynomial basis in which $f(k,\theta)$ is decomposed. The physical quantity related to the scattering amplitude is the total cross section σ defined as:

$$\sigma = \int |f(k,\theta)|^2 d\Omega \tag{1.12}$$

Recalling that we are assuming low energy interactions between ultracold bosons, the *s-wave* scattering with outgoing spherical waves dominates and the limit of the total cross section is:

$$\lim_{k\to 0} \sigma = 4\pi a_s^2 \tag{1.13}$$

In particular, the radial spherical outgoing wave at long distance goes like $\sim \sin k(r - a_s)$ were a_s is the s-wave scattering length. It is positive for repulsive interaction and negative otherwise and this parameter contains all the physical information about the ultracold atoms interaction.
Under this assumptions, the unknown short range interaction potential can be replaced by

a contact pseudopotential dependent only on the s-wave scattering length a_s parameter, which is proportional to the interaction strength. So, the ultracold atom-atom interaction can be written as:

$$V(r, r') = \frac{4\pi\hbar^2 a_s}{m}\delta(r - r') \tag{1.14}$$

This expression for the interaction potential simplifies the discussion of interacting bosons in the limit of large number N of particles: we can describe this system at a mean field level using the **Hartree equation** for bosons.
Let's consider the many body Hamiltonian

$$\begin{aligned}\hat{H} &= \sum_{i=1}^{N}\left(-\frac{\hbar^2}{2m}\nabla_i^2 + U(\mathbf{r}_i)\right) + \frac{1}{2}\sum_{\substack{i,j=1\\ i\neq j}}^{N} V(\mathbf{r}_i, \mathbf{r}_j) = \\ &= \sum_{i=1}^{N}\hat{h}(\mathbf{r}_i) + \frac{1}{2}\sum_{\substack{i,j=1\\ i\neq j}}^{N} V(\mathbf{r}_i, \mathbf{r}_j)\end{aligned} \tag{1.15}$$

where $U(\mathbf{r})$ is the external potential and $V(\mathbf{r}_i, \mathbf{r}_j)$ is the two body interaction potential. Experimentally, external trapping potentials have a fundamental role in the realization of a BEC with atomic gases. Usually, the harmonic confinement approximates very well the shape of the trapping potential. For example, a confinement along the three dimensions can be described by:

$$U(\mathbf{r}) = \frac{1}{2}m\omega_x^2 x^2 + \frac{1}{2}m\omega_y^2 y^2 + \frac{1}{2}m\omega_z^2 z^2 \tag{1.16}$$

where ω_x, ω_y and ω_z are the characteristic frequencies along the three directions. The size of the condensate is given by the harmonic oscillator length [13]:

$$a_{ho} = \sqrt{\frac{\hbar}{m\omega_m}} \tag{1.17}$$

where $\omega_m = \sqrt[3]{\omega_x\omega_y\omega_z}$ is the geometrical average of the three characteristic frequencies. The external trap allows to build also systems with quasi-1D or quasi-2D geometries: this is a very important tool to investigate BEC properties conferred by the dimensional reduction of the system.
The Hartree approximation of the many body wavefunction, under the assumption that all the interacting particles are in the same single-particle ground state, is:

$$\Phi(\mathbf{r}_1, \mathbf{r}_2, ..., \mathbf{r}_N) = \phi(\mathbf{r}_1)\phi(\mathbf{r}_2)\cdots\phi(\mathbf{r}_N) \tag{1.18}$$

This is a mean field approximation, since Bogoliubov in 1947 proved that an interacting bosonic system a fraction of system does not belong to the ground state because of interaction: this phenomenon is called quantum depletion [14]. For a system of ultracold and ultradilute bosonic gas the MF assumption is reliable, while in the case of strongly-interacting bosonic system like the superfluid ^{4}He it is not [15]. The many body wavefunction is normalized:

$$\int d\mathbf{r}_1 ... d\mathbf{r}_N \, |\Phi(\mathbf{r}_1, \mathbf{r}_2, ..., \mathbf{r}_N)|^2 = 1 \tag{1.19}$$

It is easy to demonstrate that, from this condition, also the single-particle wavefunction $\phi(\mathbf{r})$ is normalized to 1. Thus, the total energy functional is:

$$E[\Phi] = \langle \Phi | \, H \, | \Phi \rangle = \int d\mathbf{r}_1 ... d\mathbf{r}_N \, \Phi(\mathbf{r}_1, \mathbf{r}_2, ..., \mathbf{r}_N)^* \hat{H} \Phi(\mathbf{r}_1, \mathbf{r}_2, ..., \mathbf{r}_N) \tag{1.20}$$

Inserting (1.15) and (1.18) in the expression of the total energy we can get the Hartree energy functional for bosons:

$$E\left[\phi\left(\mathbf{r}\right)\right] = N \int d\mathbf{r} \phi(\mathbf{r})^* \hat{h}(\mathbf{r}) \phi(\mathbf{r}) + \frac{1}{2} N(N-1) \int d\mathbf{r} \int d\mathbf{r}' |\phi(\mathbf{r})|^2 V(\mathbf{r}, \mathbf{r}') |\phi(\mathbf{r}')|^2 \tag{1.21}$$

We can replace the general interaction potential $V(\mathbf{r}, \mathbf{r}')$ with the pseudopotential previously seen in formula (1.14).
For a conserved big number of particles N, such that $N-1 \sim N$, we can minimize this energy functional with respect to the wavefunction imposing the stationarity condition and the normalization constraint. This constraint is equivalent to using the grand canonical energy:

$$E \longrightarrow E - \mu \int d\mathbf{r} |\phi(\mathbf{r})|^2 \tag{1.22}$$

The result of this functional minimization is the so-called time independent Gross-Pitaevskii equation (1961):

$$\left(-\frac{\hbar^2}{2m} \nabla^2 + U(\mathbf{r}) + \frac{N 4\pi \hbar^2 a_s}{m} |\phi(\mathbf{r})|^2 \right) \phi(\mathbf{r}) = \mu \phi(\mathbf{r}) \tag{1.23}$$

If now we define the **condensate wave-function** $\Psi = \sqrt{N}\phi$ we obtain the final form of the Gross-Pitaevskii equation for the condensate wave function:

$$\left(-\frac{\hbar^2}{2m} \nabla^2 + U(\mathbf{r}) + \frac{4\pi \hbar^2 a_s}{m} |\Psi(\mathbf{r})|^2 \right) \Psi(\mathbf{r}) = \mu \Psi(\mathbf{r}) \tag{1.24}$$

From this equation, the condensate wavefunction $\Psi(\mathbf{r})$ can be computed iteratively starting from a trial wavefunction until the self-consistence is reached. The choice of the condensate wave function is convenient because it is normalized to the total number of particles N and we can make a link with the local numerical density of the system in the following way:

$$\rho(\mathbf{r}) = |\Psi(\mathbf{r})|^2 \tag{1.25}$$

In other words, for a weakly interacting Bose gas at very low temperature the density of condensate coincides with the numerical density of the gas.
Notice also that, unlike the ideal Bose gas, the ground state energy of the interacting system E_0, in the absence of an external potential, is

$$E_0 = \frac{1}{2} N \frac{4\pi \hbar^2 a_s}{m} \rho \tag{1.26}$$

and it is different from zero because of the interaction. In conclusion, this formalism allows for a simple treatment of the weakly interacting and diluted bosonic system.

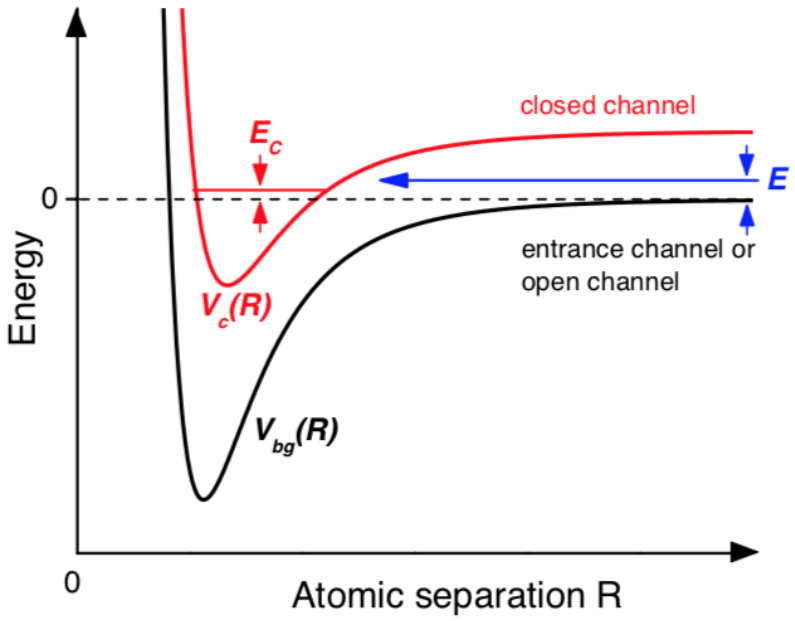

Figure 1.4: Basic scheme of Feshbach resonance channel (taken from [16]).

1.3 Feshbach resonances

Another important property of the ultracold and ultradilute Bose gases is the experimental possibility of tuning the interaction strength. In particular, the so-called Feshbach resonance is the most used tool for the tuning of scattering length by means of an external uniform magnetic fields [16].
The physical origin and the properties of a Feshbach resonance can be seen in figure 1.4. The two-body potential V_{bg} is the background potential that connects two free atoms of the ultracold gas, it is the entrance channel for elastic collision processes at a very low energies. The potential V_c is the closed channel and it can allow for bound states near the zero threshold of the open channel. A Feshbach resonance occurs when the bound state in the closed channel energetically approaches the scattering state in the open channel and the energy difference can be controlled via an external uniform magnetic field. If we define the background scattering length a_{bg} far from the resonant condition, the scattering length a_s near the resonance condition follows the following law:

$$a_s(B) = a_{bg}\left(1 - \frac{\Delta B}{B - B_0}\right) \tag{1.27}$$

where B is the external magnetic field, B_0 is the resonant magnetic field and ΔB is the resonance width. This tool can be used not only for the scattering process involved between two identical particles but also for atoms in different internal states (homonuclear mixtures) and also atoms of different species (heteronuclear mixtures): it is very powerful since it makes possible to investigate different regimes by simply changing the external field.

1.4 Bosonic binary mixture within the DFT formalism

In this thesis work, we will study a binary heteronuclear mixture of Bose-Einstein condensates made of ^{41}K and ^{87}Rb atoms. In this kind of system it is possible to change at will the intraspecies and interspecies interactions as explained in section (1.3): this opens the possibility to investigate a new unconventional liquid phase regime at very low densities as discussed in the following. We will study the system within the **Density Functional Theory** (DFT) framework, which allows for a description of the total energy expression in function of the spatially dependent density of the system, thanks to the relation seen in formula (1.25).
In addition, it will be applied the **Local Density Approximation** (LDA). According to this approximation, a component $F[\rho]_{\mathrm{LDA}}$ of the total energy functional can be written in the following way:

$$F[\rho]_{\mathrm{LDA}} = \int d\mathbf{r}\rho(\mathbf{r})f(\mathbf{r})_{\mathrm{hom}} \tag{1.28}$$

where $\rho(\mathbf{r})$ is the spatial density of the system and $f(\mathbf{r})_{\mathrm{hom}}$ is the energy density of the component F in the homogeneous system. In other words, in the context of LDA we consider the system homogeneous inside the infinitely small element of volume and we integrate all over the volume.
Recalling that the density ρ is linked to the condensate wave function Ψ by the relation

$$\rho = |\Psi|^2 \tag{1.29}$$

the total energy functional for a Bose-Bose mixture (within the mean field approximation) with two components of mass m_1 and m_2 in a volume V is:

$$E = \int d\mathbf{r} \left\{ \sum_{i=1,2} \left[\frac{\hbar^2}{2m_i} |\nabla\sqrt{\rho_i}|^2 + \frac{1}{2} g_{ii}\rho_i^2 \right] + g_{12}\rho_1\rho_2 \right\} \tag{1.30}$$

In particular:

- The index $i = 1$ is referred to the first atom species, ^{41}K, the index $i = 2$ is referred to the second atom species, ^{87}Rb.

- The kinetic term can be written in the above form thanks to the following relations:

$$\int d\mathbf{r}\nabla(\Psi^*\nabla\Psi) = 0 = \int d\mathbf{r}\nabla\Psi^*\nabla\Psi + \int d\mathbf{r}\Psi^*\nabla^2\Psi \tag{1.31}$$

$$\Downarrow$$

$$\int d\mathbf{r}\Psi^*\nabla^2\Psi = -\int d\mathbf{r}|\nabla\Psi|^2 = -\int d\mathbf{r}|\nabla\sqrt{\rho}|^2 \tag{1.32}$$

- For simplicity, interactions are written in terms of the coupling constants g defined as:

$$g_{11} = \frac{4\pi\hbar^2 a_{11}}{m_1} \tag{1.33}$$

$$g_{22} = \frac{4\pi\hbar^2 a_{22}}{m_2} \tag{1.34}$$

$$g_{12} = \frac{2\pi\hbar^2 a_{12}}{m_r} \tag{1.35}$$

The scattering length a_{11} describes the intraspecies interaction between ^{41}K atoms, a_{22} describes the intraspecies interaction between ^{87}Rb atoms and a_{12} describes the interspecies interaction between ^{41}K and ^{87}Rb atoms. Notice that, for this last case, the coupling constant contains the reduced mass $m_r = \frac{m_1 m_2}{m_1+m_2}$.

- The external potential is not present: we will see that a self-bound state remains stable without the need of any external confining potential provided by a magnetic trap (even if, as discussed in section 1.2, experimentally it is necessary for the BEC formation process).

The mean field energy density of a homogeneous mixture of bosons reads:

$$\mathcal{E}_{MF} = \frac{1}{2} g_{11}\rho_1^2 + \frac{1}{2} g_{22}\rho_2^2 + g_{12}\rho_1\rho_2 \tag{1.36}$$

We can define a useful parameter to characterize the different regimes of the system:

$$\delta g = g_{12} + \sqrt{g_{11} g_{22}} \tag{1.37}$$

For a fixed value of the intraspecies scattering length $a_{11}, a_{22} > 0$ (and thus $g_{11}, g_{22} > 0$), we can express the mean field energy density in function of this parameter:

$$\mathcal{E}_{MF} = \frac{1}{2}(\sqrt{g_{11}}\rho_1 - \sqrt{g_{22}}\rho_2)^2 + \delta g \rho_1 \rho_2 \tag{1.38}$$

According to the value of the parameter g_{12} we can identify different regimes:

- If all interactions are repulsive and if $g_{12} > \sqrt{g_{11} g_{22}}$, we have the so called **immiscible region** where the two species are not spatially overlapping.

- If $-\sqrt{g_{11} g_{22}} < g_{12} < \sqrt{g_{11} g_{22}}$ we are in the weakly interspecies interacting regime, the two densities distribution are almost the same of a single species BEC and for this reason it is called **miscible region**.

- If $g_{12} < -\sqrt{g_{11} g_{22}}$, or equivalently $\delta g < 0$, we can see in which conditions energy is minimum. First of all, the first term of equation (1.38) must be equal to zero: this is equivalent to fix the ratio between densities such that

  $$\rho_1/\rho_2 = \sqrt{g_{22}/g_{11}}. \tag{1.39}$$

  Thus, it is easy to note that the second term of equation (1.38), in the case of $\delta g < 0$, is minimum for $\rho_1, \rho_2 \to \infty$: this is the **mean field collapse region** where the system is unstable and the condensate collapses.

The fixed and positive values of the parameters a_{11} and a_{22} that we will use for this thesis work are those appropriate to a ^{41}K-^{87}Rb mixture, i.e.:

$$\begin{array}{c|c} a_{11} & 65\, a_0 \\ a_{22} & 100.4\, a_0 \end{array} \tag{1.40}$$

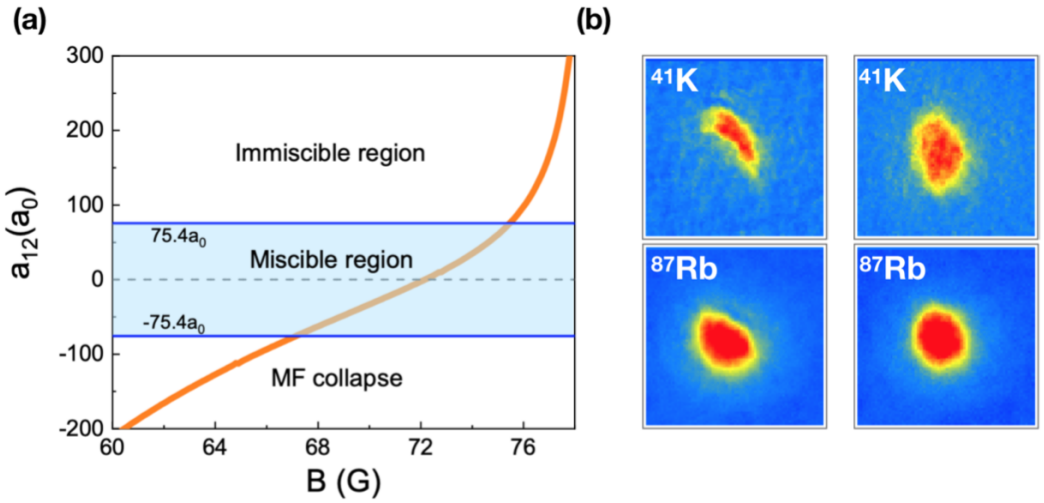

Figure 1.5: (a) Different regimes of the Bose-Bose mixtures in function of the tunable parameter a_{12} and the respective experimental external uniform magnetic field connected by means of Feshbach resonances. (b) Absorption images of the dual-species BEC. First column: immiscible regime with $a_{12} = 255a_0$. Second column: miscible regime with $a_{12} = 10a_0$. Figures taken from [11].

From this choice, the critical value of a_{12} (i.e. such that $|g_{12}| = \sqrt{g_{11}g_{22}}$) is:

$$a_{12c} = -\frac{\sqrt{g_{11}g_{22}}m_r}{2\pi\hbar^2} = -75.4\, a_0 \tag{1.41}$$

and for values $a_{12} < a_{12c}$ the system is expected to undergo a collapse at a mean-field level.
We are using, here and in the following, atomic units (a.u.), obtained by putting equal to 1 some fundamental constants: the Bohr radius a_0, the Hartree energy E_h, the electron mass m_e, the electron charge e and the reduced Planck constant $\hbar$.
The immiscible and miscible regions have been observed experimentally [11], thanks to the high tunability of interaction by means of Feshbach resonances previously discussed. In figure 1.5 some experimental results are reported [11]. In particular, in 1.5(a) the orange line shows the one-to-one correspondence between the external field and the scattering length and thus the corresponding regime of the system. In 1.5(b), the absorption images in columns show the immiscible and miscible regimes: in the first one the density distributions of the two species are not overlapped while in the second one they perfectly are and the system behaves like a single species BEC.

1.5 Beyond mean field correction: the Lee-Huang-Yang term and the self-bound droplet formation

The mean field prediction that the system will undergo a collapse when $g_{12} < -\sqrt{g_{11}g_{22}}$ fails once quantum fluctuations are taken into consideration. This correction is contained in the Lee-Huang-Yang term which represents the first beyond mean-field correcting term to the MF equation of state of a uniform and weakly-interacting system of Bose particles with hard-sphere interaction [17, 18].

We can write this term within the local density approximation [19]:

$$E_{\mathrm{LHY}} = \int d\mathbf{r}\, \mathcal{E}_{\mathrm{LHY}}(\rho_1(\mathbf{r}), \rho_2(\mathbf{r})) \tag{1.42}$$

where $\mathcal{E}_{\mathrm{LHY}}$ is the Lee-Huang-Yang energy density for the homogeneous system.
For a single-component weakly interacting Bose-Einstein condensate the expression of the Lee-Huang-Yang energy density for an homogeneous system reads [18]:

$$\mathcal{E}_{\mathrm{LHY}} = \frac{64}{15\sqrt{\pi}} g a^{3/2} \rho^{5/2} \tag{1.43}$$

where a is the scattering length, $g = \frac{4\pi\hbar^2 a}{m}$ the corresponding coupling constant and ρ the particle density. It was computed by observing that the energy per particle in the ground state can be obtained as a power series expansion in the parameter ρa^3.
However, in this work, we will use the expression of the Lee-Huang-Yang energy density extended to the case of a binary mixture [20]:

$$\mathcal{E}_{\mathrm{LHY}}(\rho_1(\mathbf{r}), \rho_2(\mathbf{r})) = \frac{8}{15\pi^2} \left(\frac{m_1}{\hbar^2}\right)^{\frac{3}{2}} (g_{11}\rho_1(\mathbf{r}))^{\frac{5}{2}} f\left(\frac{m_2}{m_1}, \frac{g_{12}^2}{g_{11}g_{22}}, \frac{g_{22}\rho_2(\mathbf{r})}{g_{11}\rho_1(\mathbf{r})}\right) \tag{1.44}$$

To simplify the notation, we can define the following variables:

$$z = \frac{m_2}{m_1} \qquad u = \frac{g_{12}^2}{g_{11}g_{22}} \qquad x = \frac{g_{22}\rho_2}{g_{11}\rho_1} \tag{1.45}$$

For an homonuclear mixture with equal mass components ($z = 1$) the dimensionless positive function f inside the Lee-Huang-Yang energy functional is analytically known [1]:

$$f(1, u, x) = \frac{\sum_{\pm} \left(1 + x \pm \sqrt{(1-x)^2 + 4ux}\right)^{5/2}}{4\sqrt{2}} \tag{1.46}$$

Instead, the analytical expression of the function f for an heteronuclear mixture is not known. In the region where $u \sim 1$, close to the mean field collapse condition with $\delta g < 0$ and small compared to the value of constant $g_{ij}\ \forall\, i, j$, the dimensionless function f is the result of a rather complicated numerical integral in the variable k [21]:

$$f(z, 1, x) = \frac{15}{32} \int_0^\infty k^2 \mathcal{F}(k, z, x)\, dk \tag{1.47}$$

with

$$\begin{aligned}
\mathcal{F}(k,z,x) = &\left\{\frac{1}{2}\left[k^2\left(1+\frac{x}{z}\right) + \frac{1}{4}k^4\left(1+\frac{1}{z^2}\right)\right] + \left[\frac{1}{4}\left[\left(k^2+\frac{1}{4}k^4\right) - \left(\frac{x}{z}k^2 + \frac{1}{4z^2}k^4\right)\right]^2 + \frac{x}{z}k^4\right]^{\frac{1}{2}}\right\}^{\frac{1}{2}} \\
&+ \left\{\frac{1}{2}\left[k^2\left(1+\frac{x}{z}\right) + \frac{1}{4}k^4\left(1+\frac{1}{z^2}\right)\right] - \left[\frac{1}{4}\left[\left(k^2+\frac{1}{4}k^4\right) - \left(\frac{x}{z}k^2 + \frac{1}{4z^2}k^4\right)\right]^2 + \frac{x}{z}k^4\right]^{\frac{1}{2}}\right\}^{\frac{1}{2}} \\
&- \frac{1+z}{2z}k^2 - 1 - x + \frac{1}{1+z}\frac{1}{k^2}\left[(1+xz)^2 + z(1+x)^2\right]
\end{aligned} \tag{1.48}$$

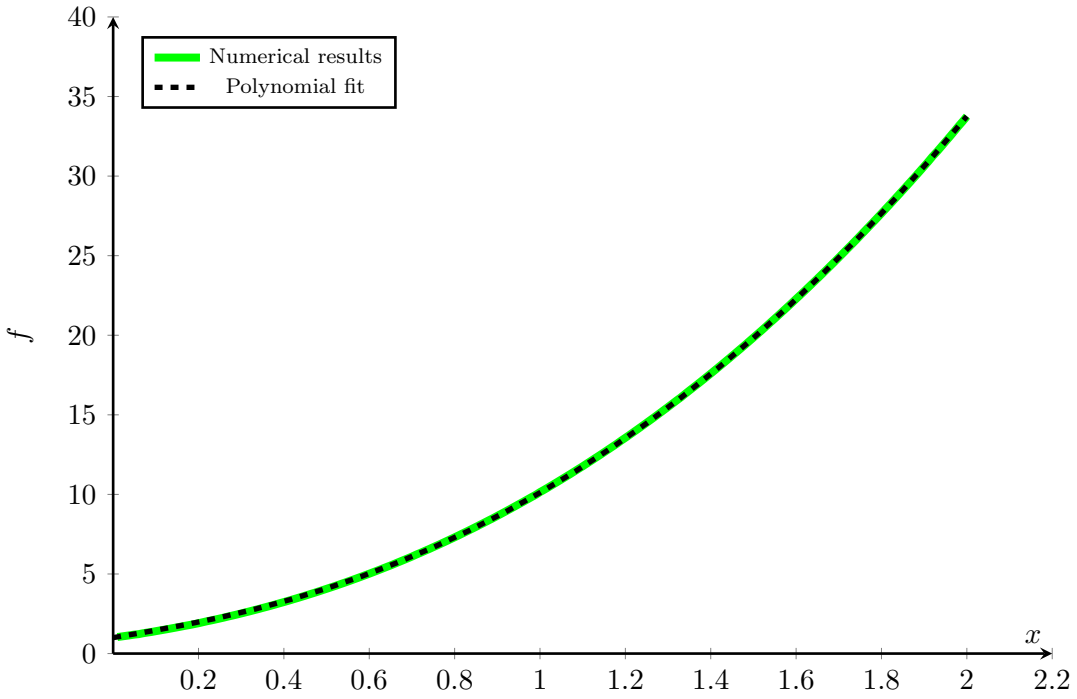

Figure 1.6: Plot of the dimensionless function f (1.47) for $z \sim 2.1$: comparison between numerical results and polynomial fit with function $f(x) = 1 + ax + bx^2 + cx^3 + dx^{3/2}$.

In particular, the result of this numerical integral can be parametrized by a more manageable analytical formula that reproduces very well the behaviour of the numerical curve in the region we are interested to work with. For the case of ^{41}K-^{87}Rb mixture, we want to approximate the function $f(z, u, x)$ with $z = \frac{87}{41} \sim 2.1$, $u \sim 1$ and with $x \sim 0.85$. This last result is found keeping into account that, working close to the critical point, the ratio between densities is similar to that one found from the mean field analysis seen in the previous section, i.e. $\frac{\rho_2}{\rho_1} = \sqrt{\frac{g_{11}}{g_{22}}}$ such that $x \sim \sqrt{\frac{g_{22}}{g_{11}}} \sim 0.85$.
We made a fit with a polynomial function $f(x) = 1 + ax + bx^2 + cx^3 + dx^{3/2}$ in order to use a simple expression that predicts very well the trend of the function f in the desired interval: results are visible in figure 1.6 and in table 1.1.

a	5.19 ± 0.03
b	7.53 ± 0.02
c	0.476 ± 0.001
d	-4.08 ± 0.05

Table 1.1: Fit parameters from polynomial function $f(x) = 1 + ax + bx^2 + cx^3 + dx^{3/2}$.

At this point, for a fixed value of the density ratio between the two equilibrium densities of the two species $\rho_1/\rho_2 = \sqrt{g_{22}/g_{11}}$, the function f becomes a constant factor denoted as $\bar{f}$. In the region where $\delta g < 0$, the mean-field interaction term and the beyond-mean-field correction have opposite sign. In fact, the effective single-component energy density func-

tional of the homogeneous mixture, obtained by adding the LHY term to equation (1.36), reads:

$$\mathcal{E}_{\text{hom}} = \beta\rho_1^2 + \gamma\rho_1^{5/2} \tag{1.49}$$

with

$$\beta = g_{11} + g_{12}\sqrt{\frac{g_{11}}{g_{22}}} = \delta g\sqrt{\frac{g_{11}}{g_{22}}} < 0 \tag{1.50}$$

and

$$\gamma = \frac{8}{15\pi^2}\left(\frac{m_1}{\hbar^2}\right)^{3/2} g_{11}^{5/2}\bar{f} > 0 \tag{1.51}$$

Notice that:

- The mean field term is negative and it describes an attractive interaction proportional to ρ^2, it dominates at small densities.
- The repulsive LHY term is positive and proportional to $\rho^{5/2}$, it dominates at large densities.

This behaviour ensures the presence of an energy minimum for a finite value of ρ_1 and ρ_2 and so the stability of the system in this regime. Other conditions are necessary to predict a stable isolated self-bound state [22]: the pressure P must be equal to zero, the chemical potential μ must be negative to avoid evaporation and also the energy must be negative. For the effective single-component mixture with total energy E and volume V, the first condition

$$P = -\frac{E}{V} = \left(-\mathcal{E}_{\text{hom}} + \rho_1\frac{\partial\mathcal{E}_{\text{hom}}}{\partial\rho_1}\right)\Big|_{\rho_1=\rho_1^*} = 0 \tag{1.52}$$

is satisfied by

$$\rho_1^* = \left(\frac{2\beta}{3\gamma}\right)^2 \tag{1.53}$$

Inserting this solution in the chemical potential expression for the effective single-component mixture with N_1 particles of the species 1

$$\mu = \frac{\partial E}{\partial N_1} = \frac{\partial\mathcal{E}_{\text{hom}}}{\partial\rho_1} = 2\beta\rho_1 + \frac{5}{2}\gamma\rho_1^{3/2} \tag{1.54}$$

one has:

$$\mu\big|_{\rho_1=\rho_1^*} = \frac{11}{3}\beta\left(\rho_1^*\right)^2 < 0 \tag{1.55}$$

Also the energy density for $\rho_1 = \rho_1^*$ is negative

$$\mathcal{E}_{\text{hom}}\big|_{\rho_1=\rho_1^*} = \frac{5}{3}\beta\left(\rho_1^*\right)^4 < 0 \tag{1.56}$$

and thus it is also the total energy, since for an homogeneous system the total energy $E = V\mathcal{E}_{\text{hom}}$ is simply the energy density multiplied by the volume V.
This simple toy model with an effective single-component homogeneous energy density functional reveals that the mixture can exist as a self-bound state in equilibrium with vacuum without any external trapping. Thus, the addition of the Lee-Huang-Yang correction has a crucial effect: the competition between the mean-field repulsion term and the beyond-mean-field attraction term leads to the formation of a self bound state, whereas absence of the LHY correction leads to the collapse of the system as predicted by the mean-field approximation seen in the previous section.

Chapter 2

Bosonic binary mixture: the homogeneous system

In this chapter we discuss the properties of the homogeneous ("bulk") mixture of ^{41}K-^{87}Rb in the regime in which a self bound state is expected as a result of competitive effects of MF and LHY contributions, as discussed in the previous chapter. A numerical computation of the equation of state is provided by imposing thermodynamic and mechanical stability. The equilibrium bulk densities of the two species and the compressibility of the system are computed for different values of the interspecies interaction parameter a_{12}.

2.1 The equation of state of a self-bound mixture

The equilibrium properties of the self-bound mixture of ^{41}K-^{87}Rb can be studied imposing the thermodynamic and mechanical stability conditions, resulting from the competition between MF attraction and LHY repulsion.
Recalling that the energy density of the homogeneous binary system is

$$\mathcal{E}(\rho_1,\rho_2)_{\text{hom}} = \frac{1}{2}g_{11}\rho_1^2 + \frac{1}{2}g_{22}\rho_2^2 + g_{12}\rho_1\rho_2 + \mathcal{E}_{\text{LHY}} \tag{2.1}$$

with $\mathcal{E}_{\text{LHY}}$ given by equation (1.44), the realizability of a self bound state is possible only if it is at equilibrium with vacuum and this condition is satisfied if the pressure P is equal to zero. Assuming a temperature $T = 0$, a fixed total number of particles N and recalling that for an homogeneous system the total energy is $E = \mathcal{E}V$ with V the volume occupied, the pressure of the binary system can be computed as:

$$\begin{aligned} P(\rho_1,\rho_2) = -\frac{\partial E}{\partial V} &= -\mathcal{E} + \sum_i \frac{\partial \mathcal{E}}{\partial \rho_i}\rho_i \\ &= -\mathcal{E} + \mu_1\rho_1 + \mu_2\rho_2 \end{aligned} \tag{2.2}$$

where $\mu_1 = \frac{\partial E}{\partial N_1} = \frac{\partial \mathcal{E}}{\partial \rho_1}$ and $\mu_2 = \frac{\partial E}{\partial N_2} = \frac{\partial \mathcal{E}}{\partial \rho_2}$ are chemical potentials of the two species by definition. Explicitly:

$$\mu_1 = \frac{\partial \mathcal{E}}{\partial \rho_1} = g_{11}\rho_1 + g_{12}\rho_2 + \frac{\partial \mathcal{E}_{\text{LHY}}}{\partial \rho_1} \tag{2.3}$$

$$\mu_2 = \frac{\partial \mathcal{E}}{\partial \rho_2} = g_{22}\rho_2 + g_{12}\rho_1 + \frac{\partial \mathcal{E}_{\text{LHY}}}{\partial \rho_2} \tag{2.4}$$

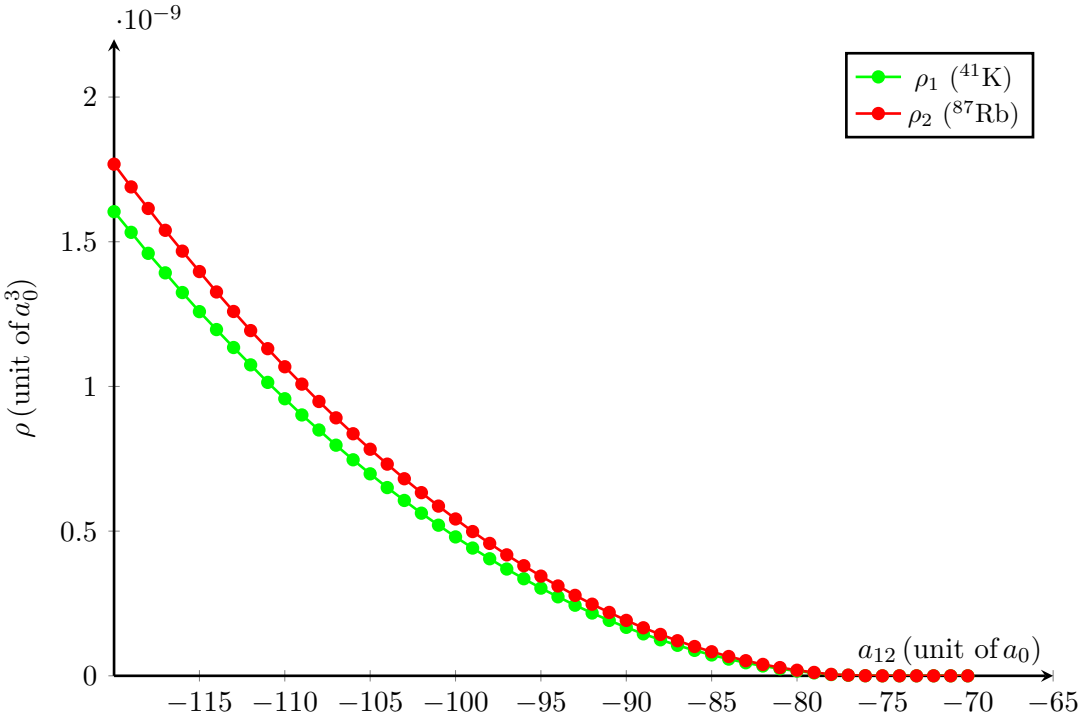

Figure 2.1: Densities ρ_1 and ρ_2 of the equilibrium configurations of the system in the self-bound regime as a function of the value of the s-wave scattering length a_{12}.

with [19]

$$\frac{\partial \mathcal{E}_{\mathrm{LHY}}}{\partial \rho_1} = \frac{8}{15\pi^2}\left(\frac{m_1}{\hbar^2}\right)^{3/2} g_{11}^{5/2}\rho_1^{1/2}\left[\frac{5}{2}\rho_1 f - \frac{g_{22}\rho_2}{g_{11}}\frac{\partial f}{\partial x}\right] \tag{2.5}$$

$$\frac{\partial \mathcal{E}_{\mathrm{LHY}}}{\partial \rho_2} = \frac{8}{15\pi^2}\left(\frac{m_1}{\hbar^2}\right)^{3/2} g_{11}^{3/2} g_{22}\rho_1^{3/2}\frac{\partial f}{\partial x} \tag{2.6}$$

The function f in the last expressions is the one defined in the previous chapter in section 5.2.
For a fixed value of the interparticle s-wave scattering length a_{12}, it is possible to locate the stable bulk configuration by using the following numerical procedure:

- Mechanical stability: find the curve $P(\rho_1, \rho_2) = 0$ in the plane (ρ_1, ρ_2) (using equation (2.2)).
- Thermodynamic stability: find the portion of plane in which both chemical potentials μ_1 and μ_2 are negative (using equations (2.3) and (2.4)).
- Minimization of energy: select the point $(\rho_{1,\mathrm{bulk}}, \rho_{2,\mathrm{bulk}})$ which satisfies the previous conditions and for which energy per particle $\frac{E}{N} = \frac{\mathcal{E}V}{N} = \frac{\mathcal{E}}{\rho}$ is minimum.

The calculated densities ρ_1 and ρ_2 of the equilibrium configuration and bulk energies for each value of the scattering length a_{12} are shown in figure 2.1 and figure 2.2, respectively.
Figures (2.3) and (2.4) illustrate the detailed procedure for the cases $a_{12} = -85\,a_0$ and $a_{12} = -96\,a_0$.
The solid blue line marks the configurations (ρ_1, ρ_2) at zero pressure while the green region contains the configurations for which both chemical potentials μ_1 and μ_2 are negative. The

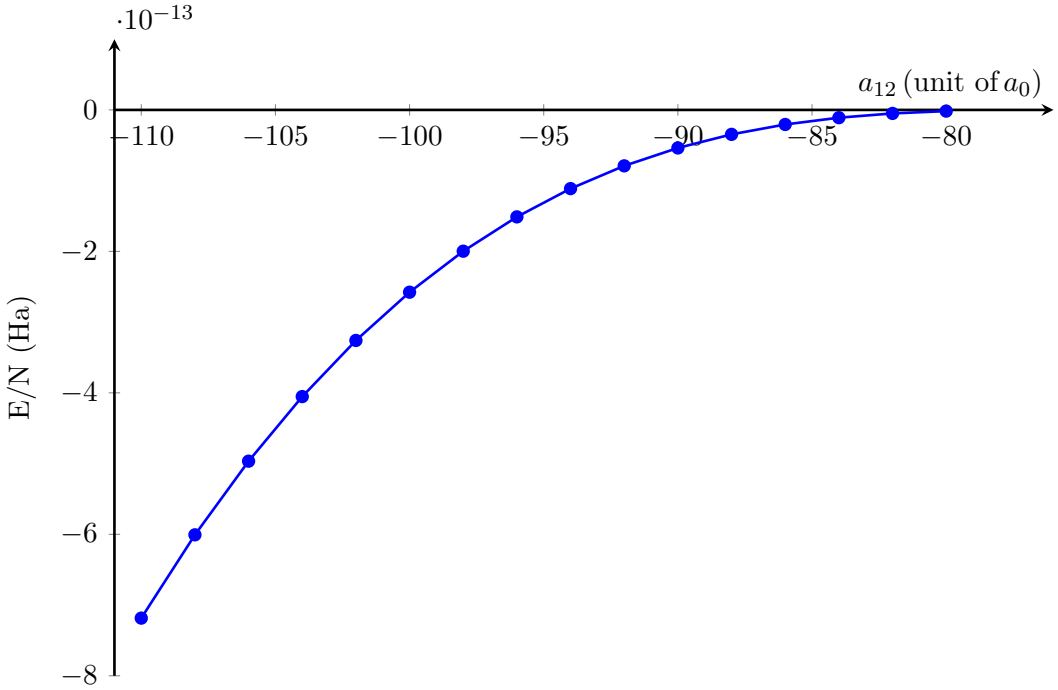

Figure 2.2: Energy per particle of the system in the self-bound regime in the equilibrium configuration as a function of the value of the s-wave scattering length a_{12}.

red point selects the minimum energy configurations among those which satisfy previous conditions.
Notice that the order of magnitude of numerical densities are around $10^{-9} - 10^{-10}$ in units of a_0^3 (a.u.) which corresponds to $10^{14} - 10^{15}$ atoms/cm^3 in real units: these states have densities of eight or nine orders of magnitude smaller than the liquid phase of common matter.
For $a_{12} > a_{12c}$ there are no stable equilibrium bulk densities for the system in consideration: the energy functional of the homogeneous binary mixture has only the MF interaction terms and the LHY term, hence, without any external trap, the system cannot remain spatially confined out of the self-bound regime, where the interspecies interaction is still attractive but not strong enough to compensate the LHY repulsion. For this reason, the gas evaporates and the corresponding equilibrium densities ρ_1 and ρ_2 are zero. As a last observation, the ratio between equilibrium densities ρ_1 and ρ_2 as a function of the interspecies scattering length a_{12}, shown in figure 2.5, converges quite linearly to the critical ratio $\frac{\rho_1}{\rho_2} \sim 0.85$, previously seen in formula (1.39).

2.2 Compressibility

Another interesting property that we can get from the bulk analysis is the compressibility, which measures the relative change of volume as a consequence of a pressure variation at constant temperature. The inverse of the compressibility is defined as:

$$\kappa = -V \left(\frac{\partial P}{\partial V} \right)_N \tag{2.7}$$

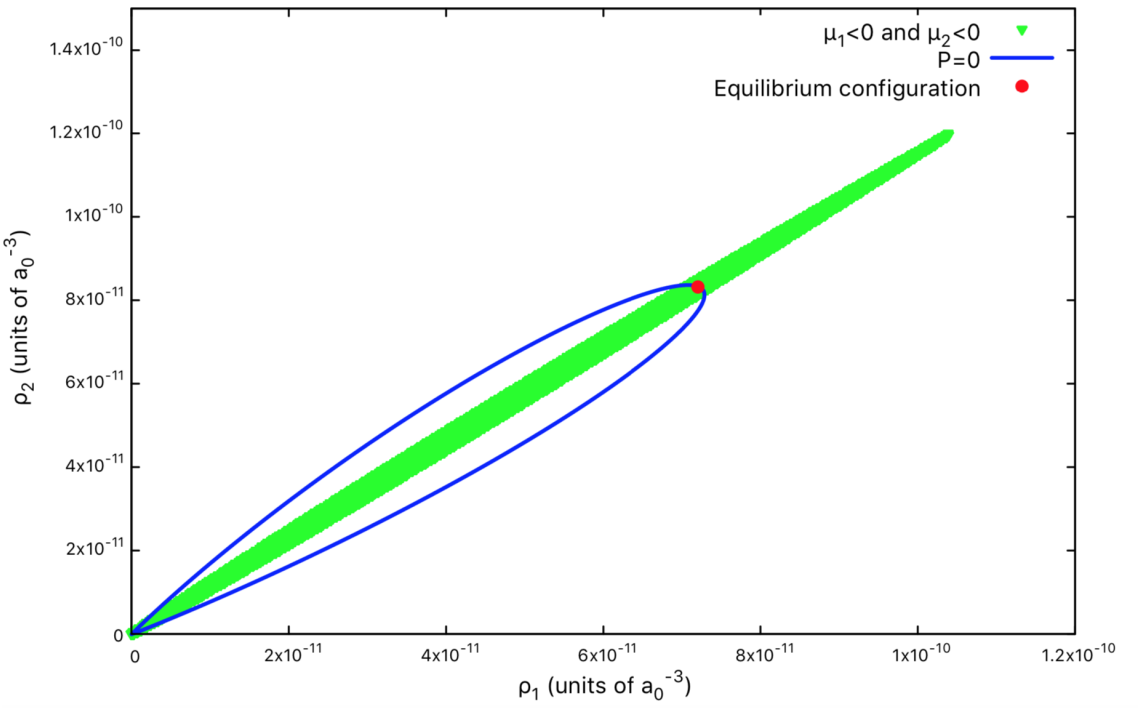

Figure 2.3: Equation of state for $a_{12} = -85\, a_0$.

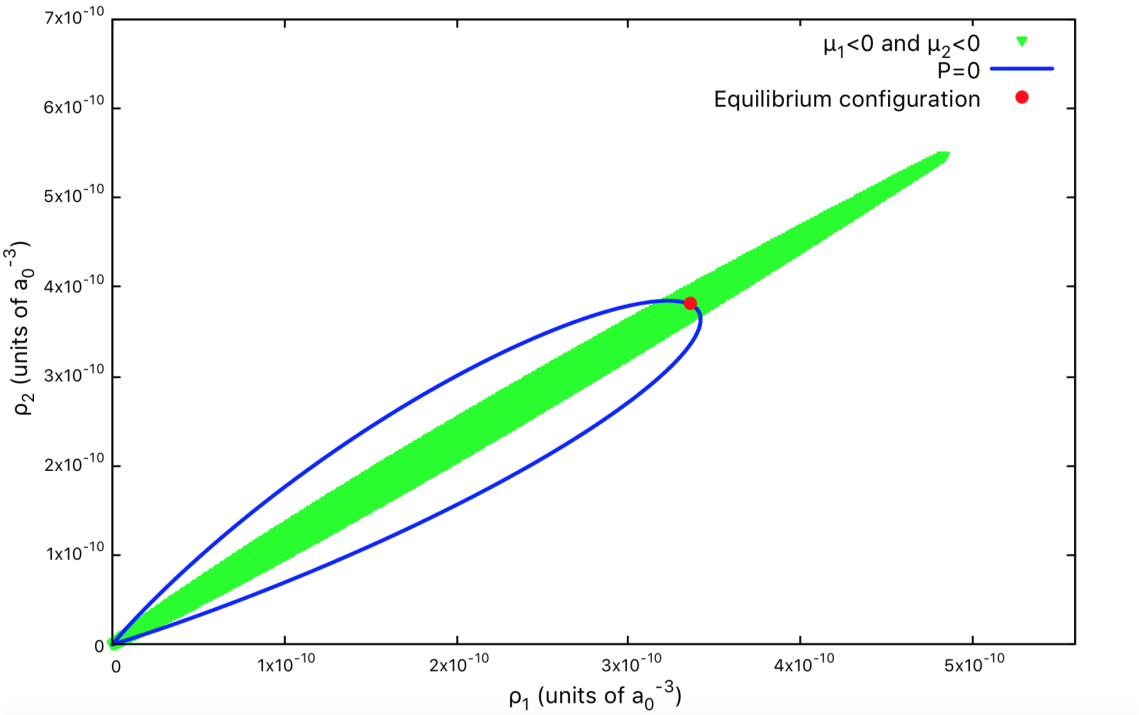

Figure 2.4: Equation of state for $a_{12} = -96\, a_0$.

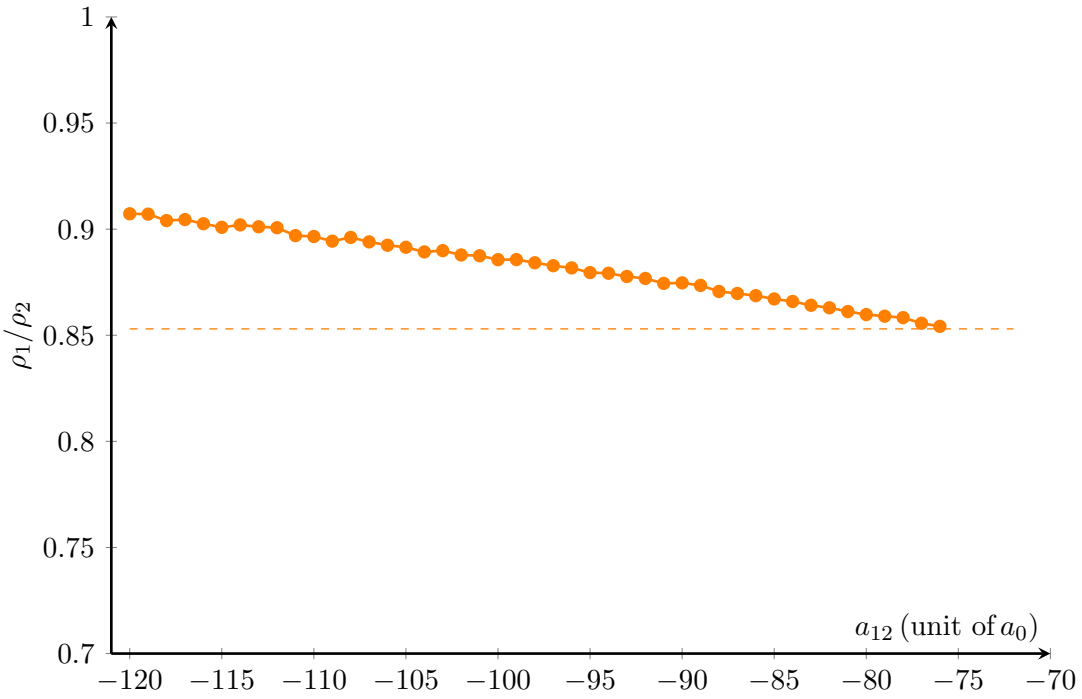

Figure 2.5: Ratio between equilibrium densities of the two species as a function of the value of the interspecies s-wave scattering length a_{12}.

and it must be greater than zero to assure the mechanical stability of the system.
The compressibility of a binary mixture in the MF approach with the addition of the beyond-MF term of LHY can be expressed as [19]:

$$\kappa^{-1} = \left(g_{11}\rho_1^2 + g_{22}\rho_2^2 + 2g_{12}\rho_1\rho_2 + \frac{15}{4}\mathcal{E}_{\mathrm{LHY}} \right)^{-1} \tag{2.8}$$

where ρ_1 and ρ_2 are the equilibrium densities of the homogeneous system computed in the previous section and $\mathcal{E}_{\mathrm{LHY}}$ is given by equation (1.44).
Results are reported in figure 2.6.
This bulk property will be a fundamental ingredient in the computation of the Tolman length, a quantity connected to the surface curvature's correction applied to the surface tension [23], as we will see in chapter 4.

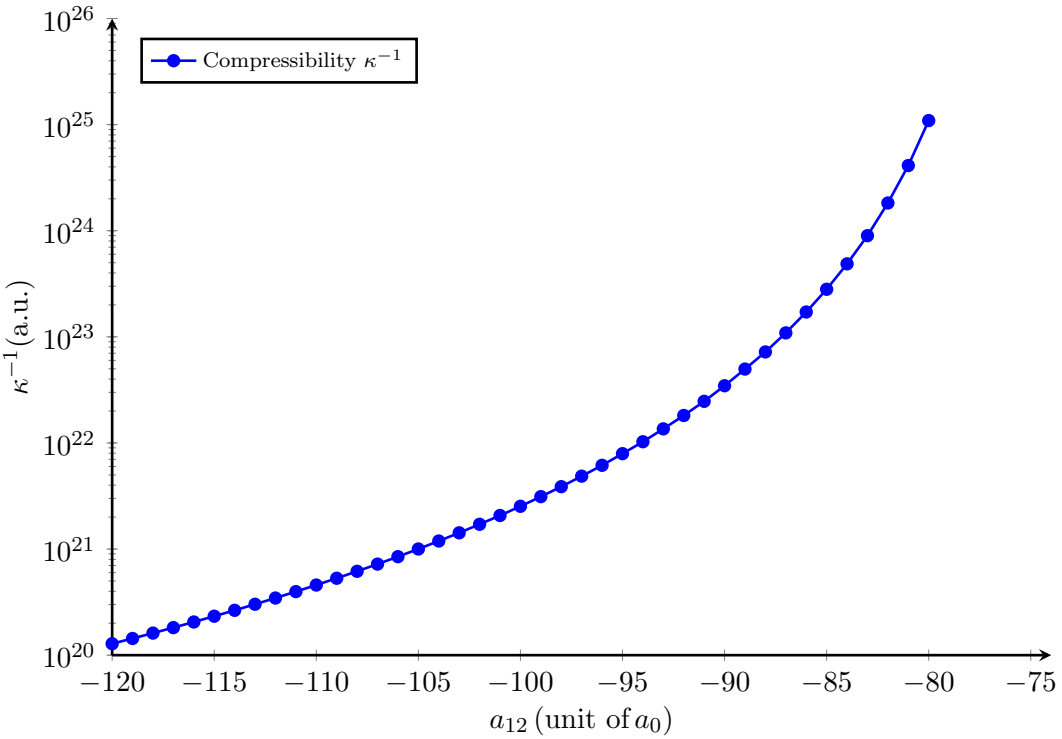

Figure 2.6: Compressibility κ^{-1} as a function of the s-wave scattering length a_{12} in the self-bound droplet regime.

Chapter 3

Surface properties of a self-bound droplet

In this chapter we discuss the surface properties of a ^{41}K-^{87}Rb self-bound droplet. We work with a slab geometry in order to focus the study along the direction to which the liquid-vacuum interface of the droplet belongs. This amounts to neglect curvature effects (which will be investigated in the following chapter), i.e. we consider here droplets with a radius $R \gg \Delta$, with Δ equal to the surface width. The density profile of the liquid-vacuum interface and its thickness along the perpendicular direction is studied with (*i*) a variational method, (*ii*) a numerical method and (*iii*) by directly finding the ground state solution of the two coupled Gross-Pitaevskii equations associated to the two species of the mixture, by means of the numerical imaginary time evolution technique. The critical number of particles over which the droplet is stable is also computed as a function of the interspecies scattering length a_{12}.

3.1 Variational approach

The appearance of self-bound droplets in bosonic mixtures implies the existence of a surface and a surface tension associated to it. For this kind of analysis it is convenient to use a **slab geometry**: we assume an infinite homogeneous system along two of the three directions and we study the density profile along the third axis (z axis), to which the liquid-vacuum interface belongs.
The aim is to simulate the density profile in order to quantify its shape variation as a function of the interspecies scattering length a_{12}. In particular, we expect that the density profile along the z direction of an homogeneous system along x and y has approximately the shape illustrated in figure 3.1. The parameter Δ measures the width between the point at 90% of the bulk density and that one at the 10%, so it quantifies the surface width.
As a first approach to compute surface properties, we can use a variational method: it consists of using a trial parametrization of the density profile depending on one or more parameters and finding the values of these parameters for which the expectation value of the total energy is minimum.
For each value of a_{12}, we can make a parametrization of the density profile of each species using the following analytical function:

$$\rho(z) = \frac{\rho_{\text{bulk}}}{2}\left(1 - \tanh\frac{z}{d}\right) \tag{3.1}$$

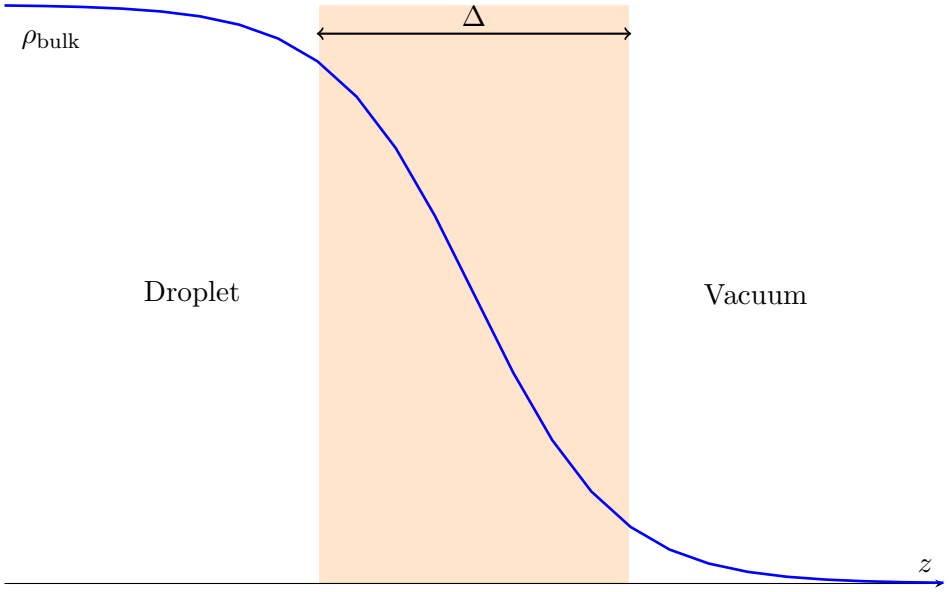

Figure 3.1: Density profile along z direction, Δ is the $10\% - 90\%$ surface width.

where ρ_{bulk} is that one computed from the bulk analysis and d is the unique free parameter which determine the profile's shape. The interface shape according to this model is the one shown in figure 3.1: ρ_{bulk} is the saturated value of the density inside the droplet and the droplet's surface width Δ is proportional to the free parameter d. In fact, from equation 3.1 one has:

$$z = d \tanh^{-1}\left(2\frac{\rho}{\rho_{\text{bulk}}} - 1\right) \tag{3.2}$$

from which

$$\Delta = z\big|_{\rho/\rho_{\text{bulk}}=0.9} - z\big|_{\rho/\rho_{\text{bulk}}=0.1} = 2.2d \tag{3.3}$$

This variational ansatz has to be inserted inside the total energy functional such that the value of the parameter d that minimizes the energy, or equivalently the surface tension, can be found. From thermodynamics, the total energy can be written as:

$$E = \underbrace{TS}_{\text{T}=0} - \underbrace{PV}_{\text{P}=0} + \sigma\mathcal{A} + \mu_1 N_1 + \mu_2 N_2 \tag{3.4}$$

The first and second term are equal to zero because of the low temperature and the mechanical stability condition of the droplet, the third term is different from zero if we have a liquid-vacuum interface of area $\mathcal{A}$ and the last two terms are the chemical potential contributions of the two species of the mixture.
Since the density profile depends only on z, the total energy E for the slab model can be written as:

$$E = \mathcal{A}\int dz \left\{\frac{\hbar^2}{2m_1}|\nabla\sqrt{\rho_1}|^2 + \frac{\hbar^2}{2m_2}|\nabla\sqrt{\rho_2}|^2 + \frac{1}{2}g_{11}\rho_1^2 + \frac{1}{2}g_{22}\rho_2^2 + g_{12}\rho_1\rho_2 + \mathcal{E}_{\text{LHY}}(\rho_1,\rho_2)\right\} \tag{3.5}$$

This is the energy functional (1.30) with the addition of the beyond mean field term $\mathcal{E}_{\text{LHY}}(\rho_1,\rho_2)$ given by (1.44). The prefactor $\mathcal{A}$ is the area of the interface in contact with

the vacuum, m_1 and m_2 are the masses of ^{41}K and ^{87}Rb atoms and the quantities g_{11}, g_{22}, g_{12} are those seen in equations (1.33), (1.34), (1.35). Notice that the dependence on the variable z is inside the densities ρ_1 and ρ_2.
We can assume that the ratio between the two densities is constant everywhere:

$$\frac{\rho_1}{\rho_2} = r \tag{3.6}$$

As seen in figure 2.5, for each interspecies scattering length a_{12} the quantity r can be computed exactly from the ratio of the bulk equilibrium densities: the correctness of this assumption for each z of the slab model will be checked a posteriori.
For simplicity, let's define the following variables:

$$\alpha' = \frac{\hbar^2}{2m_1} + \frac{\hbar^2}{2m_2}\frac{1}{r} \tag{3.7}$$

$$\beta = \frac{1}{2}g_{11} + \frac{1}{2}g_{22}\frac{1}{r^2} + g_{12}\frac{1}{r} \tag{3.8}$$

$$\gamma = \frac{8}{15\pi^2}\left(\frac{m_1}{\hbar^2}\right)^{3/2} g_{11}^{5/2} f\left(\frac{m_2}{m_1}, 1, \frac{g_{22}}{g_{11}r}\right) \tag{3.9}$$

Expanding the kinetic energy derivative as follows

$$|\nabla\sqrt{\rho_1}|^2 = \frac{1}{4}\frac{(\nabla\rho_1)^2}{\rho_1} \tag{3.10}$$

if we call

$$\alpha = \alpha'/4 \tag{3.11}$$

we can write the energy density of the mixture in function of ρ_1 only:

$$\mathcal{E} = \alpha\frac{(\nabla\sqrt{\rho_1})^2}{\rho_1} + \beta\rho_1^2 + \gamma\rho_1^{5/2} \tag{3.12}$$

From (3.4), we can compute the surface tension as:

$$\sigma = \frac{E - \mu_1 N_1 - \mu_2 N_2}{\mathcal{A}} \tag{3.13}$$

Since N_1 and N_2 are not independent because of the fixed ratio between densities, we can write again σ in function of N_1 only:

$$\sigma = \frac{E - \mu_0 N_1}{\mathcal{A}} \tag{3.14}$$

and μ_0 can be interpreted as the chemical potential of a liquid system in equilibrium with the vacuum.
We can find a proper expression for μ_0 by the minimization of the energy functional including the constraint of normalization $\int d\mathbf{r}\rho_1(\mathbf{r}) = N_1$. In this way, also the number of

particle of the second species is fixed because $N_2 = N_1/r$.
The ground state density must satisfy the following condition:

$$\begin{aligned} \frac{\delta}{\delta\rho_1}\left[E - \mu N_1\right] &= 0 \\ \rightarrow \frac{\delta E}{\delta\rho_1} - \mu &= 0 \end{aligned} \tag{3.15}$$

This last passage comes from the property of the integral functionals: the functional derivative of $N_1\left[\rho_1\right] = \int d\mathbf{r}\rho_1(\mathbf{r})$ with respect to ρ_1 coincides with the common derivative of the integrand function with respect to ρ_1.
For the same reason, the derivative of the total energy with respect to ρ_1 is:

$$\frac{\delta E}{\delta\rho_1} = \frac{\partial\mathcal{E}}{\partial\rho_1} - \vec{\nabla}\cdot\left(\frac{\partial\mathcal{E}}{\partial\nabla\rho_1}\right) \tag{3.16}$$

with

$$\frac{\partial\mathcal{E}}{\partial\rho_1} = -\alpha\left(\frac{\nabla\rho_1}{\rho_1}\right)^2 + 2\beta\rho_1 + \frac{5}{2}\gamma\rho_1^{5/2} \tag{3.17}$$

$$\vec{\nabla}\cdot\left(\frac{\partial\mathcal{E}}{\partial\nabla\rho_1}\right) = -2\alpha\frac{\nabla^2\rho_1}{\rho_1} \tag{3.18}$$

Inserting all these results in equation (3.15) and recalling that ρ_1 depends only on z, we find that the density profile along z satisfies the following differential equation:

$$\alpha\left(\frac{1}{\rho_1^2}\left(\frac{\partial\rho_1}{\partial z}\right)^2 - 2\frac{1}{\rho_1}\frac{\partial^2\rho_1}{\partial z^2}\right) + \frac{5}{2}\gamma\rho_1^{3/2} + 2\beta\rho_1 - \mu = 0 \tag{3.19}$$

We can integrate this expression by multiplying each member for $\frac{\partial\rho_1}{\partial z}$: this operation can be done safely since we are interested in the surface profile along z and in this region neither ρ_1 nor $\frac{\partial\rho_1}{\partial z}$ are equal to zero.
We find the following equation:

$$\alpha\left(\frac{1}{\rho_1^2}\left(\frac{\partial\rho_1}{\partial z}\right)^2 - 2\frac{1}{\rho_1}\frac{\partial^2\rho_1}{\partial z^2}\right)\frac{\partial\rho_1}{\partial z} + \frac{5}{2}\gamma\rho_1^{3/2}\frac{\partial\rho_1}{\partial z} + 2\beta\rho_1\frac{\partial\rho_1}{\partial z} - \mu\frac{\partial\rho_1}{\partial z} = 0 \tag{3.20}$$

that is equivalent to

$$\frac{\partial}{\partial z}\left(-\alpha\frac{1}{\rho_1}\left(\frac{\partial\rho_1}{\partial z}\right)^2 + \beta\rho_1^2 + \gamma\rho_1^{5/2} - \mu\rho_1\right) = 0 \tag{3.21}$$

Thus, the density profile along z satisfies:

$$-\alpha\frac{1}{\rho_1}\left(\frac{\partial\rho_1}{\partial z}\right)^2 + \beta\rho_1^2 + \gamma\rho_1^{5/2} - \mu\rho_1 = C \tag{3.22}$$

where the constant C must be equal to zero because the equation must be true for $\rho_1(z)$ which approaches to the vacuum region outside the droplet (where both $\rho_1(z)$ and its derivative with respect to z are equal to zero). Finally, from this last equation (with $C = 0$) we can obtain an expression for the chemical potential μ_0 for a liquid system in equilibrium with the vacuum. It must be constant everywhere and it can be computed by

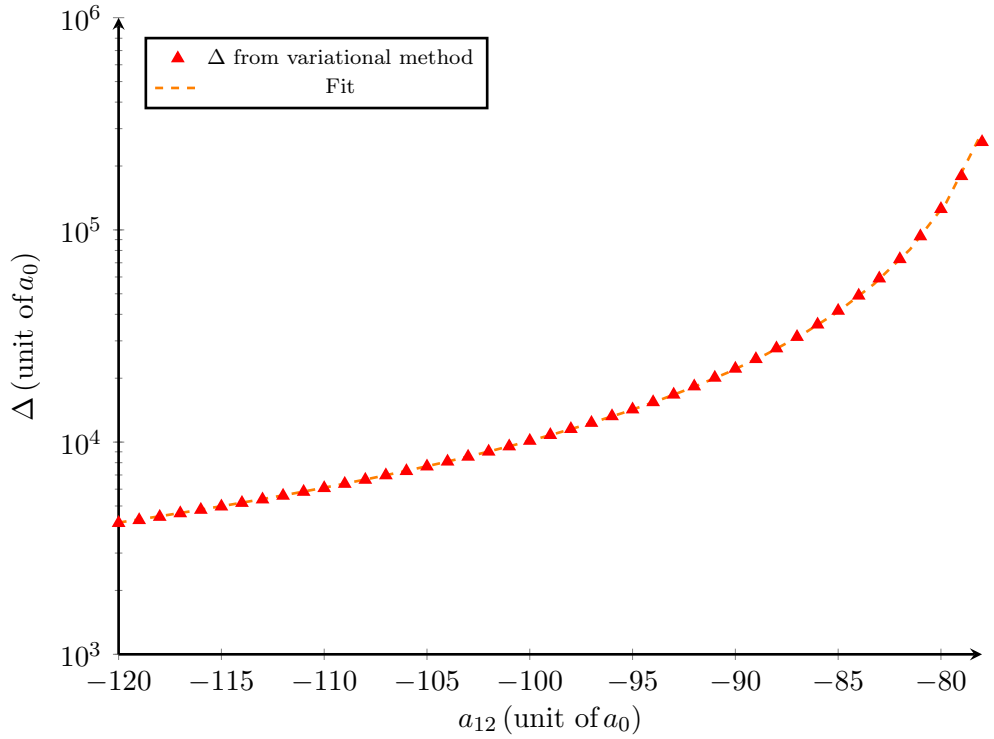

Figure 3.2: Surface width Δ obtained from the variational study as a function of the interspecies s-wave scattering length a_{12}.

replacing the constant particular solution in the bulk region $\rho_1 = \rho_{1,\text{bulk}}$. The result is:

$$\mu_0 = \beta\rho_{1,\text{bulk}} + \gamma\rho_{1,\text{bulk}}^{3/2} \tag{3.23}$$

Once we have all elements to compute the surface tension σ with the expression (3.14), we can use the variational ansatz (3.1) for $\rho_1(z)$ and compute the stationary point of the integral

$$\sigma = \int_{-\infty}^{+\infty} dz\ (\mathcal{E}[\rho_1(z)] - \mu_0\rho_1(z)) \tag{3.24}$$

finding the value of the unique free parameter d for which the surface tension is minimum. This minimization cannot be done analytically but only numerically. The resulting surface width Δ and the resulting surface tension σ as a function of the interspecies scattering length are shown in figure 3.2 and 3.3, respectively.
In particular, the surface width is fitted by the polynomial function:

$$\Delta(a_{12}) = p(a_{12}q + s)^t \tag{3.25}$$

The fitting parameters are:

p	$4.20 \cdot 10^5$ (unit of a_0)
q	-0.50 (unit of $1/a_0$)
s	-37.33
t	-1.49

Table 3.1: Results of the fit of the surface width Δ with the function $\Delta(a_{12}) = p(a_{12}q + s)^t$.

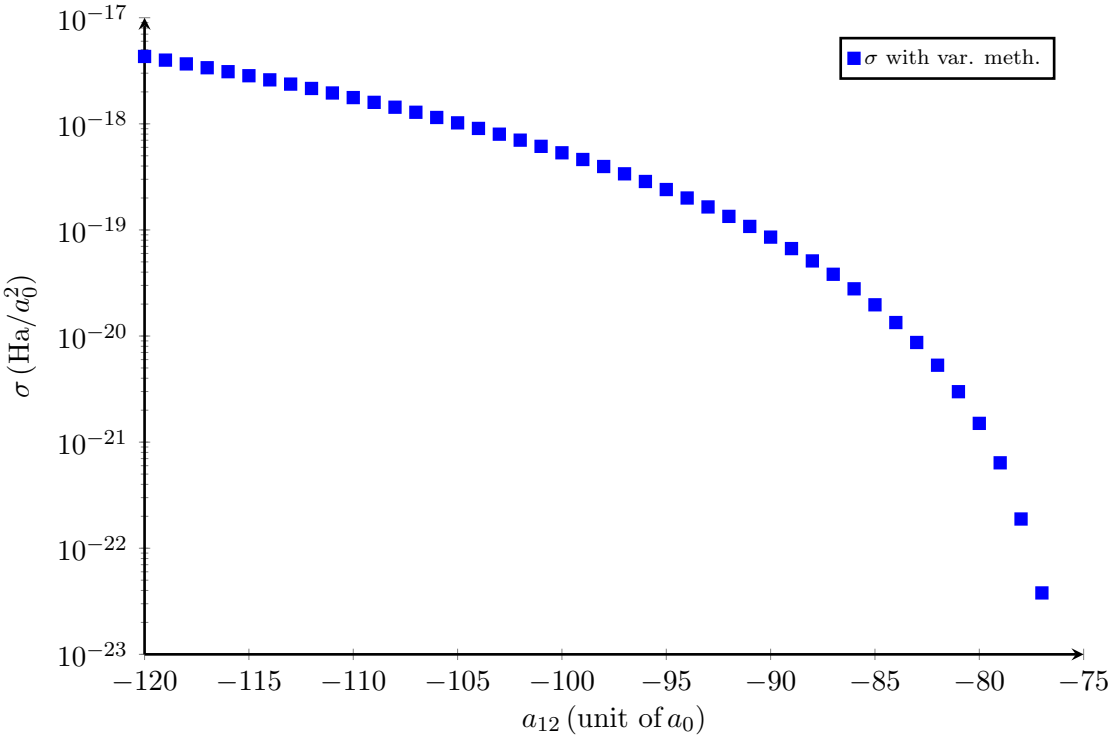

Figure 3.3: Surface tension obtained from the variational study as a function of the interspecies scattering length a_{12}.

Hence, for a fixed value of a_{12}, a complete parametrization of the density profile of the first species of the mixture along the z direction is given by the following expression:

$$\rho_1(z, a_{12}) = \frac{\rho_{1,\mathrm{bulk}}(a_{12})}{2}\left(1 - \tanh\frac{2.2z}{\Delta(a_{12})}\right) \tag{3.26}$$

with $\rho_{1,\mathrm{bulk}}(a_{12})$ obtained from the bulk analysis and $\Delta(a_{12})$ obtained from equation (3.25). Because of the fixed ratio (see (3.6)), the parametrization of the density profile for the second species of the mixture is the same as in (3.26) but multiplied by a factor $1/r$.

3.2 Numerical method

The results obtained from the variational approach are obviously affected by the choice of the selected density profile parametrization.
However, the computations of the previous section has led to a differential equation that must be satisfied by the density profile $\rho_1(z)$. For clarity, this differential equation is written again here:

$$-\alpha\frac{1}{\rho_1}\left(\frac{\partial\rho_1}{\partial z}\right)^2 + \beta\rho_1^2 + \gamma\rho_1^{5/2} - \mu_0\rho_1 = 0 \tag{3.27}$$

Solving with respect to $\frac{\partial\rho_1}{\partial z}$:

$$\frac{\partial\rho_1}{\partial z} = \pm\sqrt{\left(\frac{\rho_1}{\alpha}\right)\left[\beta\rho_1^2 + \gamma\rho_1^{5/2} - \mu_0\rho_1\right]} \tag{3.28}$$

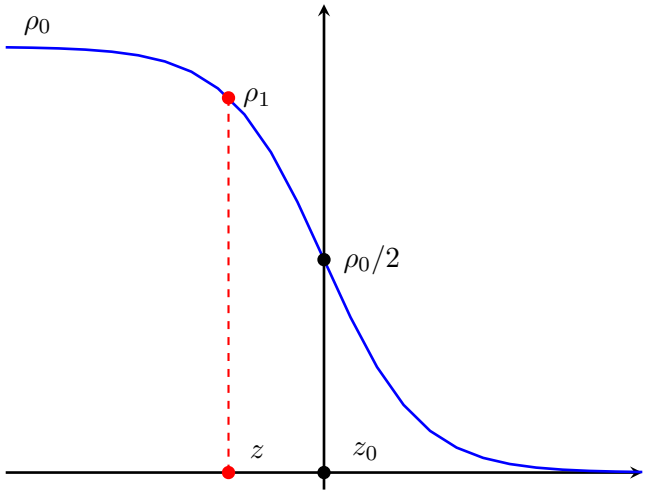

Figure 3.4: Density profile along z direction, enhanced points are useful to solve the numerical integral.

The density profile we are looking for is decreasing from bulk to vacuum (see figure 3.1), so we can safely choose the minus sign in (3.28).
To simplify the notation we define the function $h(\rho_1)$:

$$\frac{\partial \rho_1}{\partial z} = -\sqrt{\left(\frac{\rho_1}{\alpha}\right)\left[\beta\rho_1^2 + \gamma\rho_1^{5/2} - \mu_0\rho_1\right]} \equiv h(\rho_1) \tag{3.29}$$

From (3.29) one has:

$$dz = \frac{d\rho_1}{h(\rho_1)} \tag{3.30}$$

Let's define some useful points along the density profile, as shown in figure 3.4:

- $(z_0,\ \rho_0/2)$ is the central point of the density profile. For simplicity, we can choose $z_0 = 0$.
- $(z,\ \rho_1)$ is a generic point which belongs to the density profile, with $\rho_1 \in [0 : \rho_0]$.

By integrating both members of (3.30) from $(z_0,\ \rho_0/2)$ to $(z,\ \rho_1)$ we obtain:

$$z = z_0 + \int_{\rho_0/2}^{\rho_1} d\rho\, \frac{1}{h(\rho)} \tag{3.31}$$

In practice, we have to scan all the density values in the interval $[0 : \rho_0]$ and by solving numerically the integral we can find the corresponding z position. In this way, it is possible to determine the profile $\rho_1(z)$ of the liquid-vacuum interface.
In figure 3.5 and 3.6 we show the results for $a_{12} = -85\,a_0$ and $a_{12} = -96\,a_0$: the points are the numerical results while the dashed lines are the variational ones discussed in the previous section. In both cases the agreement is very good, so the variational ansatz provides a good parametrization of the density profile even if it is not an exact solution of the differential equation (3.27).
Looking at the interfaces profiled computed for different values of the scattering length, one sees that the droplet surface width becomes smaller as the absolute value of a_{12} increases. This sounds reasonable: the stronger interspecies attraction makes the droplet

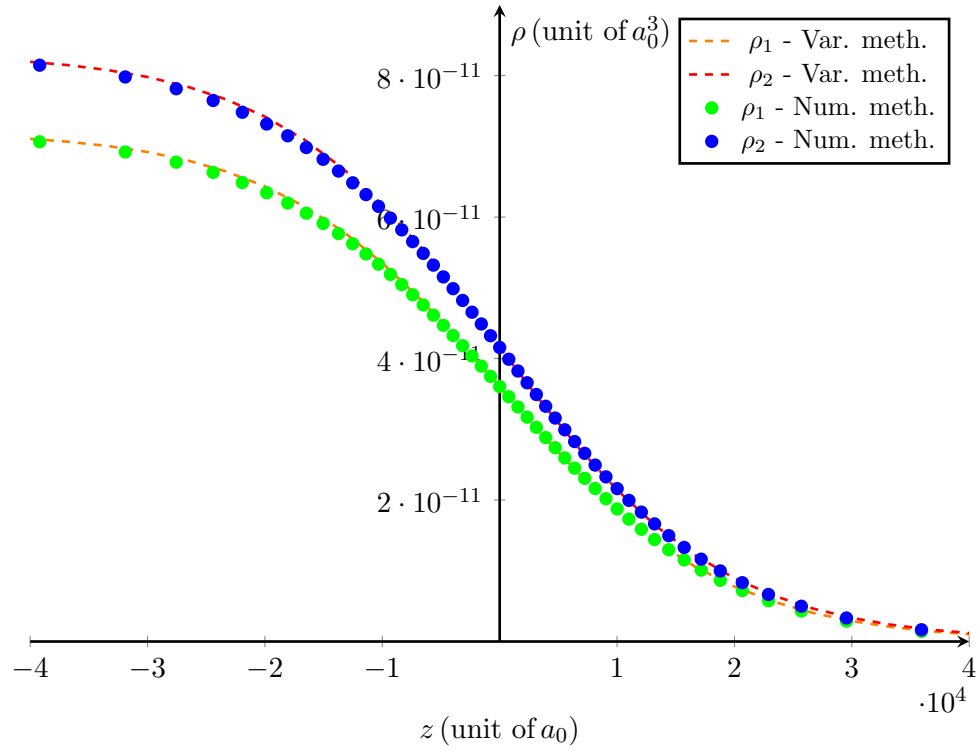

Figure 3.5: Density profiles ρ_1 and ρ_2 of the two species of the mixtures computed with the variational and numerical method for $a_{12} = -85a_0$.

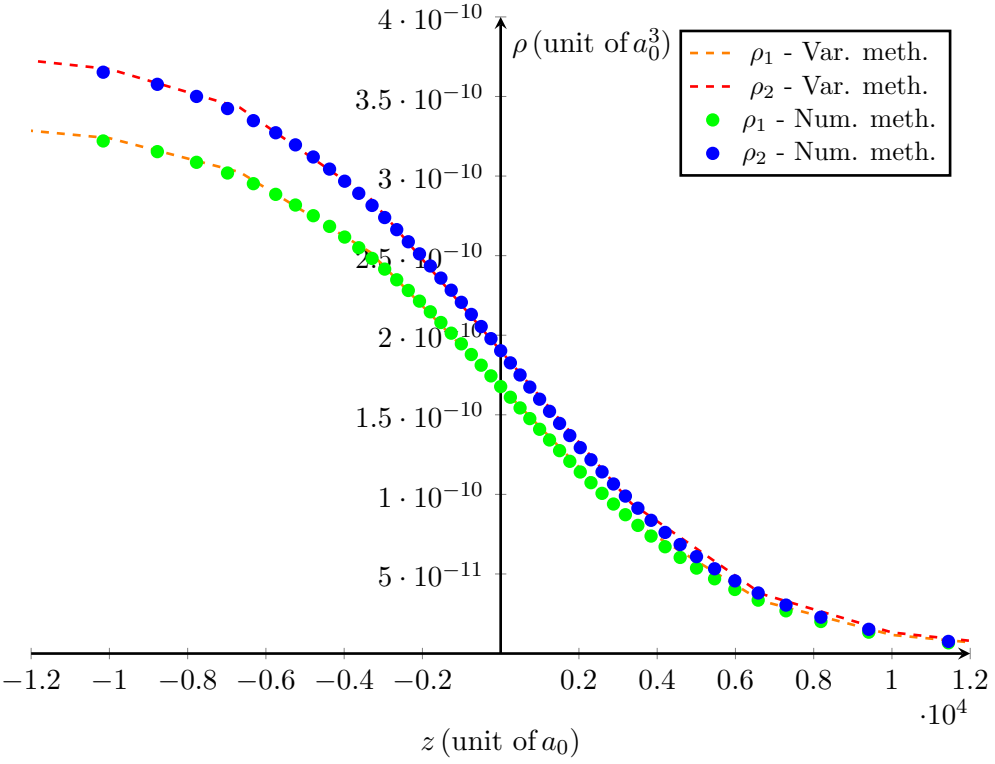

Figure 3.6: Density profiles ρ_1 and ρ_2 of the two species of the mixtures computed with the variational and numerical method for $a_{12} = -96a_0$.

more compact. In figure 3.7 some density profiles and the corresponding value of a_{12} are reported to highlight these differences.

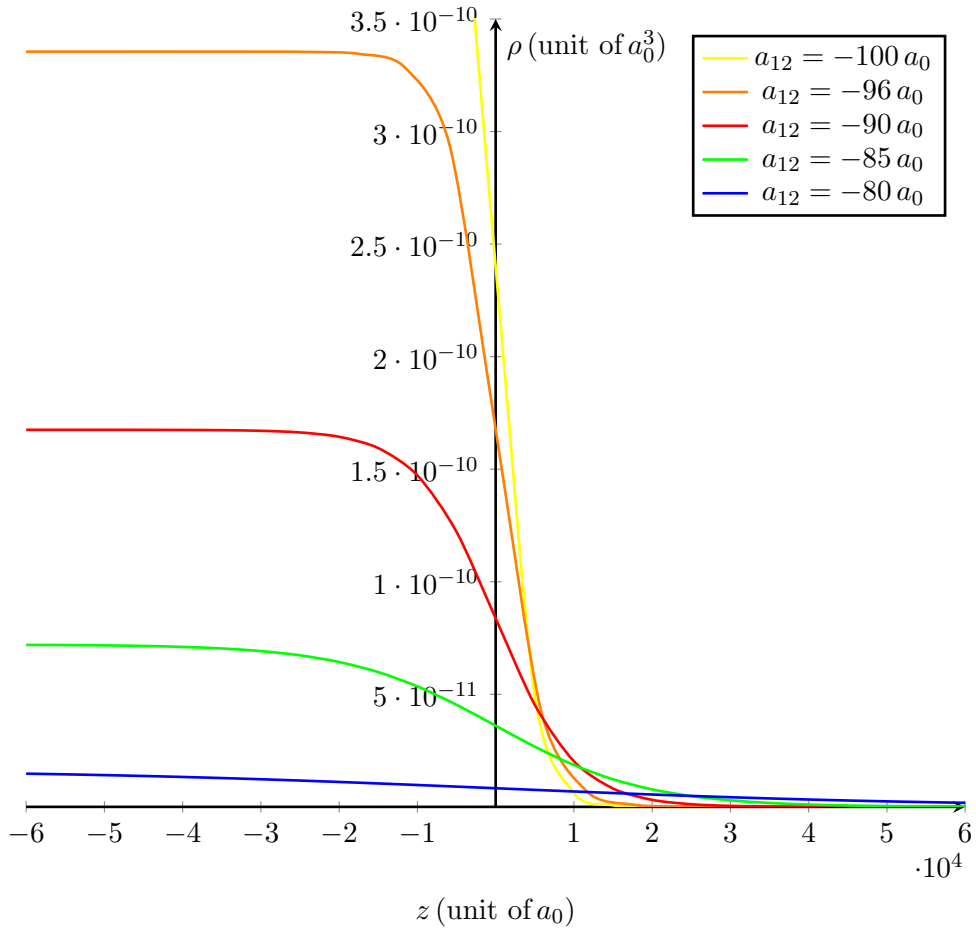

Figure 3.7: Density profiles $\rho_1(z)$ for different values of the scattering length a_{12}.

We can also use equation (3.29) to compute directly the surface tension. In fact, recalling that σ can be computed with the expression (3.24), we can make a change of variable in the integral thanks to the relation (3.30) so that:

$$\sigma = \int_0^{\rho_0} \frac{d\rho_1}{h(\rho_1)} \left(\mathcal{E}[\rho_1(z)] - \mu_0 \rho_1(z)\right) \tag{3.32}$$

Recalling the expression of the energy density functional $\mathcal{E}[\rho_1(z)]$ seen in (3.12) and the expression of $h(\rho_1)$ seen in (3.29) we finally get the expression:

$$\sigma = \int_0^{\rho_0} d\rho_1 \, 2\sqrt{\alpha \left(\beta\rho_1 + \gamma\rho_1^{3/2} - \mu_0\right)} \tag{3.33}$$

Notice that the above equation allows to compute σ without prior knowledge of the density profile. Results of the surface tension from the integral (3.33) are illustrated in figure 3.8 and compared with those ones from variational methods.
The values of σ from the two methods are in agreement but it is important to stress the fact that with the second method we obtained results without any initial hypothesis about the shape of the density profile. The dashed line is a polynomial fit of the numerical results

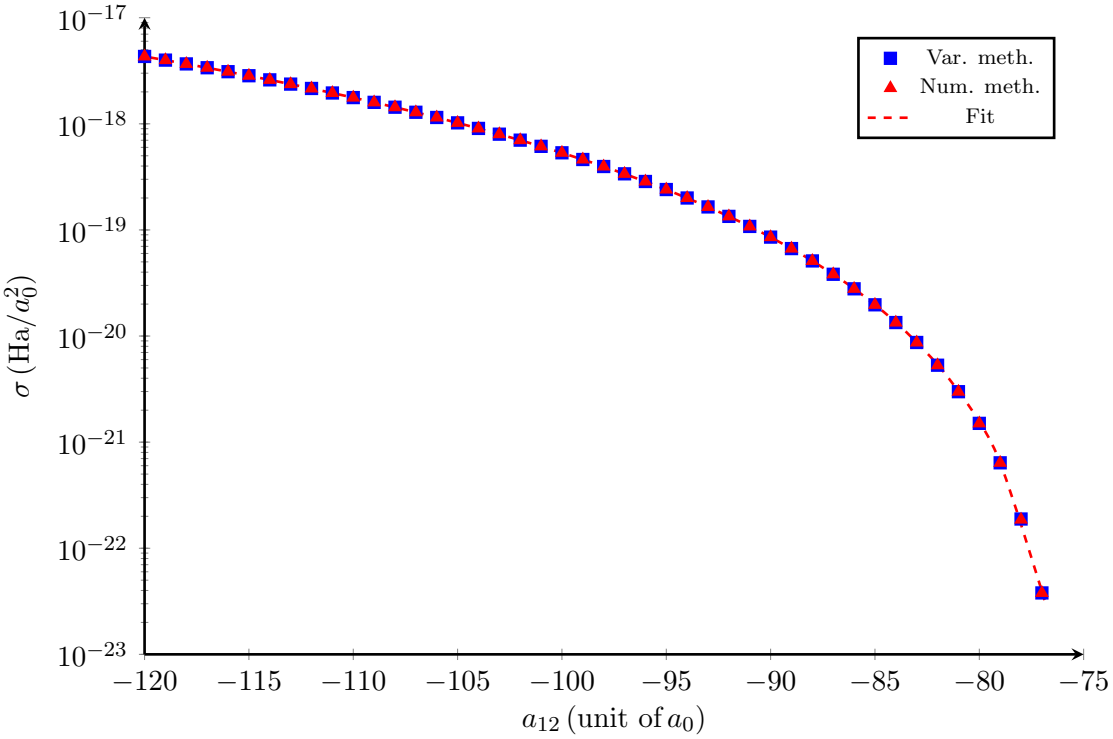

Figure 3.8: Surface tension as a function of the interspecies scattering length a_{12}.

with the function

$$\sigma(a_{12}) = p(a_{12}q + s)^t \tag{3.34}$$

to have a complete parametrization of the surface tension. The fitting parameters are reported in table 3.2.

p	$1.39 \cdot 10^{-25}$ (unit of a_0)
q	-2.99 (unit of $1/a_0$)
s	-225.14
t	3.52

Table 3.2: Results of the fit of the surface tension with the function $\sigma(a_{12}) = p(a_{12}q + s)^t$.

Notice that the surface tension spans several orders of magnitude and it is positive as expected, since breaking a bulk system has an energy cost.

3.3 Ground state solution of the two coupled Gross-Pitaevskii equations

Results from variational and numerical methods seems to be reasonable and they are in agreement with each other. We can check the correctness of the previous results by performing a simulation which solves directly the two coupled Gross-Pitaevskii equations associate to the two species of the mixtures.
The **imaginary time evolution** technique allows to find the ground state condensate wave function of the system and so the ground state density profile. Let's suppose to know the Hamiltonian of the system and let's consider the time dependent Schrödinger equation

associated to it:

$$-i\hbar\frac{\partial}{\partial t}\left|\psi\right\rangle = \left(\hat{H} - E_0\right)\left|\psi\right\rangle \tag{3.35}$$

The quantity E_0 is simply an energy offset equal to the ground state energy, its use will be clear in the next steps. By performing a Wick rotation from real time t to imaginary time $i\tau$, the time dependent Schrödinger equation becomes:

$$-\hbar\frac{\partial}{\partial \tau}\left|\psi\right\rangle = \left(\hat{H} - E_0\right)\left|\psi\right\rangle \tag{3.36}$$

and its solution is

$$\left|\psi\right\rangle = e^{-\frac{(\hat{H}-E_0)}{\hbar}\tau}\left|\psi_0\right\rangle \tag{3.37}$$

with $\left|\psi\right\rangle$ the state of the system at time τ and $\left|\psi_0\right\rangle$ the its initial state. The decomposition of the initial state in the basis of eigenstates of the Hamiltonian is always possible, such that:

$$\left|\psi_0\right\rangle = \sum_i a_i \left|\phi_i\right\rangle \qquad a_i \in \mathbb{C} \tag{3.38}$$

If we insert this decomposition of $\left|\psi_0\right\rangle$ in equation (3.37) we obtain:

$$\left|\psi\right\rangle = \sum_i a_i e^{-\frac{E_i-E_0}{\hbar}\tau}\left|\phi_i\right\rangle \tag{3.39}$$

where E_i is the eigenvalue of the Hamiltonian associated to the eigenstate $\left|\phi_i\right\rangle$. In the limit of $\tau \to +\infty$, only the term with $i = 0$ would contribute to the sum and so:

$$\left|\psi\right\rangle = \lim_{\tau\to+\infty} e^{-\frac{(\hat{H}-E_0)}{\hbar}\tau}\left|\psi_0\right\rangle = a_0\left|\phi_0\right\rangle \tag{3.40}$$

which is the exact ground state of the system, a part from a multiplicative factor.
In a numerical simulation the ground state wave function is computed iteratively performing the following steps:

- Choose an initial trial wave function $\left|\psi_0\right\rangle$ normalized to the total number of particles N of the system and a time interval $\Delta\tau$ to discretize the time evolution.

- Compute the initial ground state energy E_0 as

$$E_0 = \frac{\left\langle\psi_0\right|\hat{H}\left|\psi_0\right\rangle}{\left\langle\psi_0|\psi_0\right\rangle} \tag{3.41}$$

- For small values of $\Delta\tau$ we can use the approximation $e^{-\frac{(\hat{H}-E_0)}{\hbar}\Delta\tau} \sim \left(1 - \frac{\hat{H}-E_0}{\hbar}\Delta\tau\right)$ and update the wave function as follows:

$$\left|\psi_{n+1}\right\rangle = \left(1 - \frac{\hat{H} - E_0}{\hbar}\Delta\tau\right)\left|\psi_n\right\rangle \qquad n = 0, 1, 2, ... \tag{3.42}$$

- Update the ground state energy value as follows:

$$E_0 = \frac{\left\langle\psi_n\right|\hat{H}\left|\psi_n\right\rangle}{\left\langle\psi_n|\psi_n\right\rangle} \tag{3.43}$$

- Normalize the temporary wave function $|\psi_n\rangle$ to the total number of particles N.
- Repeat the last three steps until convergence is reached and stop the procedure when E_0 remains almost constant for many consecutive steps.

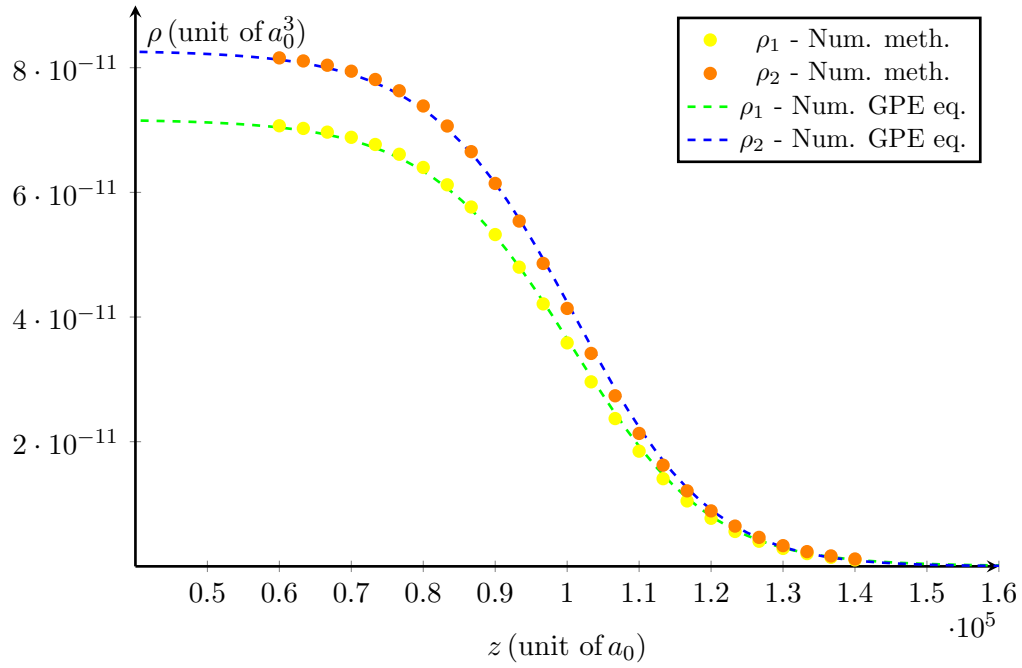

Figure 3.9: Density profiles ρ_1 and ρ_2 of the two species of the mixtures: dots represent the density profile obtained from the numerical method of section 3.2 and dashed lines represent results computed by solving numerically the GPE equation $a_{12} = -85a_0$.

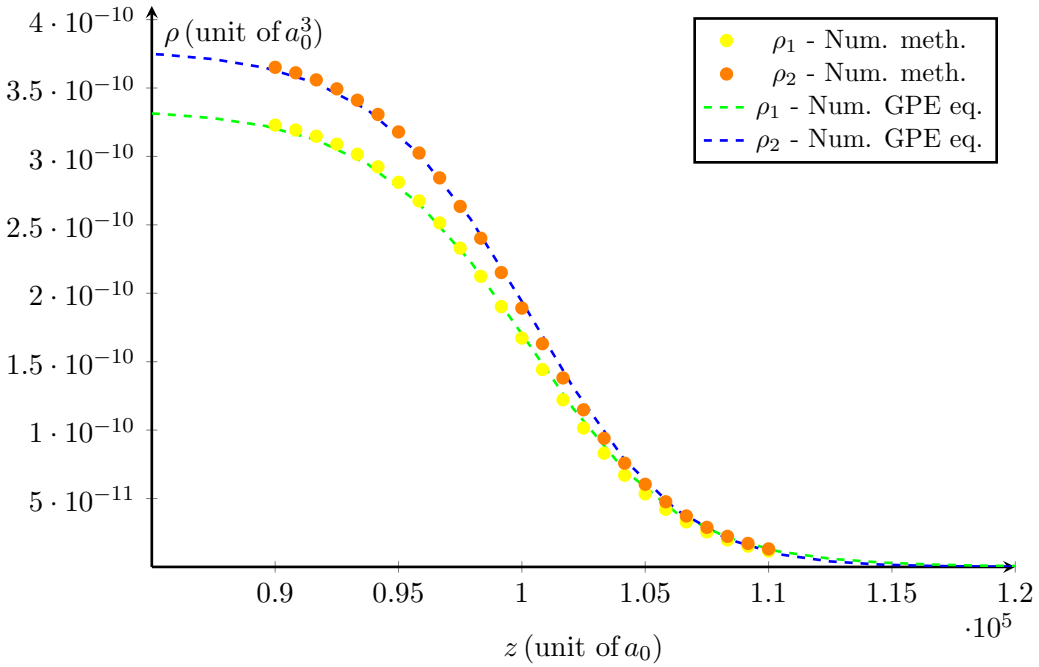

Figure 3.10: Density profiles ρ_1 and ρ_2 of the two species of the mixtures: dots represent the density profile obtained from the numerical method of section 3.2 and dashed lines represent results computed by solving numerically the GPE equation $a_{12} = -96a_0$.

Applying the imaginary time evolution technique to our system, we want to find the ground state solutions of the two coupled stationary Gross-Pitaevskii equations with the LHY corrections [19]:

$$\begin{cases} \left(-\frac{\hbar^2}{2m_1}\nabla^2 + V_1\left(\rho_1, \rho_2\right)\right)\psi_1 = \mu_1\psi_1 \\ \left(-\frac{\hbar^2}{2m_2}\nabla^2 + V_2\left(\rho_1, \rho_2\right)\right)\psi_2 = \mu_2\psi_2 \end{cases} \tag{3.44}$$

where μ_i is the chemical potential of the i species and

$$V_1 = g_{11}\rho_1 + g_{12}\rho_2 + \frac{\delta E_{\mathrm{LHY}}}{\delta\rho_1} \tag{3.45}$$

$$V_2 = g_{22}\rho_2 + g_{12}\rho_1 + \frac{\delta E_{\mathrm{LHY}}}{\delta\rho_2} \tag{3.46}$$

that are the effective potentials felt by each species of the mixture. Since $\frac{\delta E_{\mathrm{LHY}}}{\delta\rho_i} = \frac{\partial\mathcal{E}_{\mathrm{LHY}}}{\partial\rho_i}$ for the property of the integral functionals, an explicit expression for the derivatives of the LHY correction with respect to the densities of the two species was already given in the previous chapter with equations (2.5) and (2.6). Recall that the density profile is linked to the wave function by relation 1.25 but, unlike the numerical method seen in the previous section, the ratio between the two densities here are not fixed a priori.
Notice that in the two GPE equations the chemical potentials μ_1 and μ_2 play the role of E_0 in the general description of the method explained above.
Simulations are performed by choosing a proper mesh in the real space and periodic boundary conditions (PBC) are selected. This is possible because, due to our use of a slab geometry, the system is periodic in space. The use of PBC is also convenient because it allows to easily switch from real to momentum space and viceversa, a useful trick that allows to save computational cost especially when the system has long-range interaction terms (for example in presence of dipolar interaction). In that case, the Fourier transform and its inverse are computed by means of Fast Fourier Transform algorithms (FFT). In any case, the simulation cell size must be big enough to assure that each repetition of the system does not interact with the periodic replicas.
In figure 3.9 and 3.10 the resulting density profiles for $a_{12} = -85a_0$ and $a_{12} = -96a_0$ are reported and compared to results obtained with the numerical method seen in section 3.2. The agreement is again very good: stressing the fact that by performing the numerical simulation to solve the GPE equation we obtain a discretized but exact ground state density of the system, we can conclude that the numerical method seen in section 3.2 is the simplest one, it does not require any prior knowledge about the density profile and it provides results in perfect agreement with the correct solution from the GPE equation.
The unique assumption made in section 3.2 for the numerical method is that, for a fixed value of a_{12}, the ratio between ρ_1 and ρ_2 along the density profile is constant everywhere and equal to the one between the two corresponding bulk equilibrium densities. We can check the validity of this assumptions in the figures 3.11 and 3.12: the ratio between $\rho_1(z)$ and $\rho_2(z)$ (blue points) is indeed constant and equal to the bulk ratio nearly everywhere in the range of the system extension. Only in the very outer portion of the surface (red points) it deviates from the expected value but this small variation is negligible as proved by the nearly perfect agreement between the two methods.

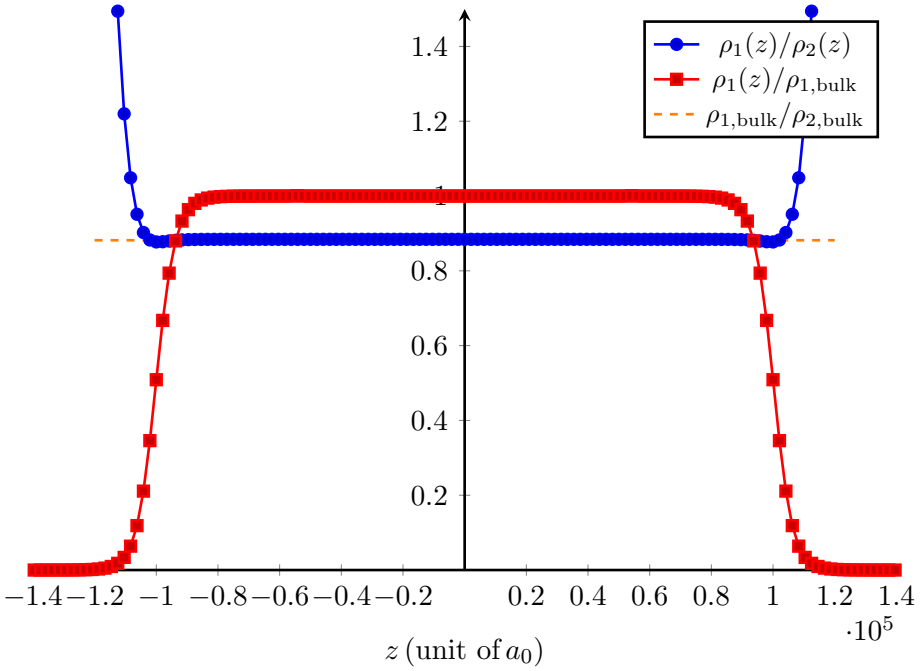

Figure 3.11: Blue points represent the ratio between ρ_1 and ρ_2 as a function of z along the complete density profile, red points represent the density profile ρ_1 normalized to the bulk density $\rho_{1,\text{bulk}}$ and the orange dashed line is the expected ratio between bulk densities for $a_{12} = -96\, a_0$.

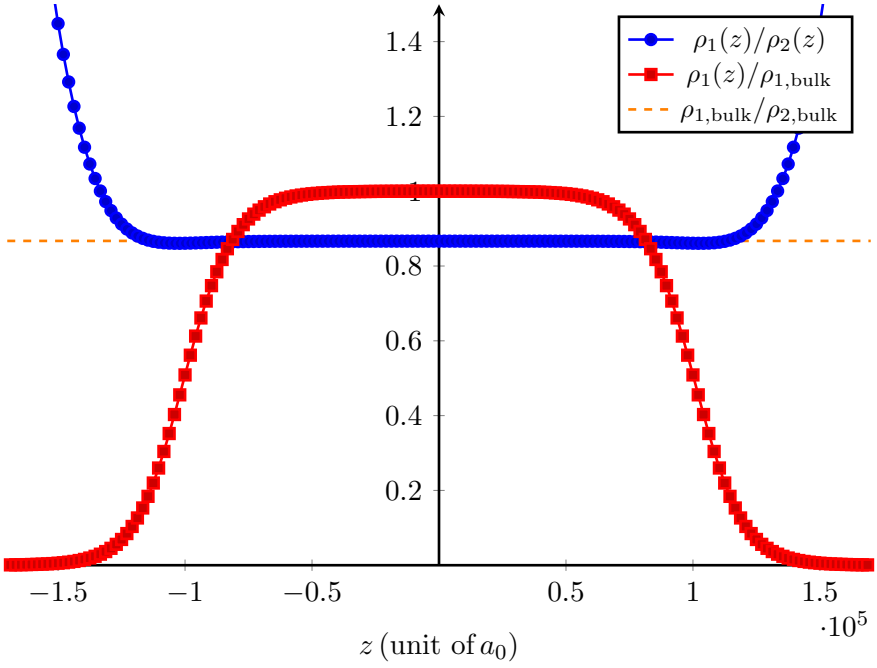

Figure 3.12: Blue points represent the ratio between ρ_1 and ρ_2 as a function of z along the complete density profile, red points represent the density profile ρ_1 normalized to the bulk density $\rho_{1,\text{bulk}}$ and the orange dashed line is the expected ratio between bulk densities for $a_{12} = -85\, a_0$.

3.4 The critical number of particles for droplet stability

It is useful to collect all the informations about surface properties obtained so far and, in particular, to understand how the shape of the droplet's radial density profile changes

with the interspecies scattering length a_{12} and the total number of particles N. According to the shape of its radial density profile, a droplet can be loosely classified as:

- A "true" droplet composed of a central region of fairly uniform density ("bulk") and an external surface region where the density drops more or less rapidly to zero with distance. If we define the radius of the droplet as

$$R = \sqrt[3]{\frac{3N}{4\pi\rho_{\text{bulk}}}} \tag{3.47}$$

that comes from the relation $\frac{4}{3}\pi R^3 \rho_{\text{bulk}} = N$, a "true" droplet is such that the ratio between the surface width Δ and the radius R is very small:

$$\frac{\Delta}{R} \ll 1 \tag{3.48}$$

An example of this kind of density profile is schematically illustrated in the following.

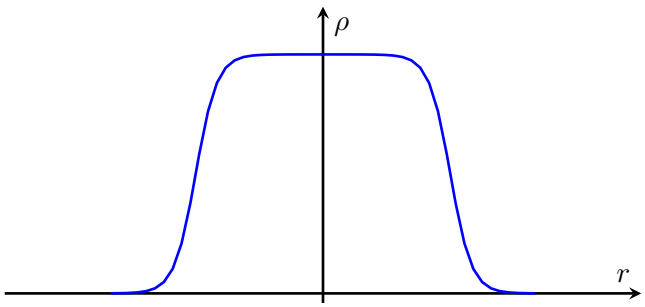

Figure 3.13: Density profile of a droplet with a central bulk region and a thin surface region.

- An "all surface" droplet, where the central bulk portion is almost absent, the density profile is gaussian-like and the surface width Δ is comparable to the radius R of the droplet:

$$\frac{\Delta}{R} \sim 1 \tag{3.49}$$

An example of this kind of density profile is illustrated schematically in the following.

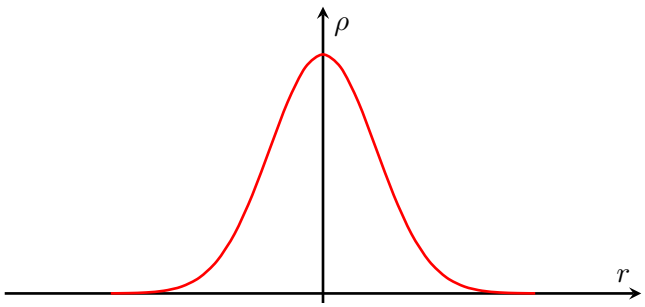

Figure 3.14: Density profile of an "all surface" droplet without a central bulk region.

We will study in the following how the ratio $\frac{\Delta}{R}$ changes as a function of N and a_{12}. We must notice, however, that not all values of N are allowed for a droplet formation. In fact,

small droplets with a number of particle N under a critical value N_c are unstable: this is due to the dominating kinetic term over interaction energy that leads to the evaporation process.
An easy way to see this and have an estimate of the critical number of atoms for a given value of a_{12} is to perform a variational study. Let's assume that in the critical region the droplet has a gaussian-like density profile: this is reasonable since near the evaporation droplets would not have a compact central bulk (this assumption will be confirmed a posteriori).
The density profile of the first species of the mixture is:

$$\rho_1(r) = \frac{N_1}{\pi^{3/2}\sigma^3} e^{-\frac{r^2}{\sigma^2}} \tag{3.50}$$

where N_1 is the total number of particles of the selected species, the prefactor $\frac{N_1}{\pi^{3/2}\sigma^3}$ comes from normalization and σ is the variance of the gaussian. Again, the ratio $\rho_1/\rho_2 = r$ is assumed to be fixed everywhere. The total energy functional is thus a functional of ρ_1 only:

$$\begin{aligned} E &= \int d\mathbf{r} \left\{ \frac{\hbar^2}{2m_1} |\nabla\sqrt{\rho_1}|^2 + \frac{\hbar^2}{2m_2} |\nabla\sqrt{\rho_2}|^2 + \frac{1}{2} g_{11}\rho_1^2 + \frac{1}{2} g_{22}\rho_2^2 + g_{12}\rho_1\rho_2 + \mathcal{E}_{\text{LHY}} \right\} = \\ &= \int d\mathbf{r} \left\{ 4\alpha \left(\frac{\partial\sqrt{\rho_1}}{\partial r} \right)^2 + \beta\rho_1^2 + \gamma\rho_1^{5/2} \right\} \end{aligned} \tag{3.51}$$

where the term $\mathcal{E}_{\text{LHY}}$ is given by (1.44) and, in the last passage, coefficients α, β and γ are those ones defined in equations (3.11), (3.8), (3.9) respectively.
Inserting $\rho_1(r)$ as given in (3.50) in the total energy functional, the three contributions to the integral are:

- The kinetic term E_{kin}

$$\begin{aligned} E_{\text{kin}} &= \int d\mathbf{r}\, 4\alpha \left(\frac{\partial\sqrt{\rho_1(r)}}{\partial r} \right)^2 = \\ &= \int_0^{+\infty} dr\, 4\pi r^2 4\alpha \left(\frac{\partial\sqrt{\rho_1(r)}}{\partial r} \right)^2 = \\ &= \frac{6\alpha N_1}{\sigma^2} \end{aligned} \tag{3.52}$$

- The MF interaction term

$$\begin{aligned} E_{\text{int}} &= \int d\mathbf{r}\, \beta\rho_1(r)^2 = \\ &= \int_0^{+\infty} dr\, 4\pi r^2 \beta\rho_1(r)^2 = \\ &= \frac{\beta N_1^2}{(2\pi)^{3/2}\sigma^3} \end{aligned} \tag{3.53}$$

- The LHY term

$$\begin{aligned} E_{\text{LHY}} &= \int d\mathbf{r}\, \beta \rho_1(r)^{5/2} = \\ &= \int_0^{+\infty} dr\, 4\pi r^2 \beta \rho_1(r)^{5/2} = \\ &= \frac{4\gamma N_1^{5/2}}{5\sqrt{10}\pi^{9/4}\sigma^{9/2}} \end{aligned} \tag{3.54}$$

To simplify the notation, let's call:

$$a = 6\alpha > 0 \tag{3.55}$$

$$b = \frac{\beta}{(2\pi)^{3/2}} < 0 \tag{3.56}$$

$$c = \frac{4\gamma}{5\sqrt{10}\pi^{9/4}} > 0 \tag{3.57}$$

such that the effective single-component energy per particle reads:

$$\frac{E}{N_1} = \frac{a}{\sigma^2} + \frac{bN_1}{\sigma^3} + \frac{cN_1^{3/2}}{\sigma^{9/2}} \tag{3.58}$$

For a fixed value of a_{12}, we are interested in the pair of parameters $(\sigma_0, N_{1,\text{c}})$ for which energy per particle is minimum and equal to zero, hence the point which separates stable droplets with negative total energy from unstable ones with positive energy. Solving the system

$$\begin{cases} \frac{\partial(E/N_1)}{\partial\sigma} = 0 \\ \\ \frac{E}{N_1} = 0 \end{cases} \tag{3.59}$$

with respect to σ, we find that

$$\sigma_0 = -\frac{3b}{5a} N_1 \tag{3.60}$$

Notice that σ_0 is a variance and it is a positive quantity ($b < 0$) as it must be. Inserting this solution in the second equation of the system we found that

$$N_{1,\text{c}} = -\frac{c}{\delta^{9/2}\left(\frac{a}{\delta^2} + \frac{b}{\delta^3}\right)} \tag{3.61}$$

where $\delta = -\frac{3b}{5a}$.
This is the critical threshold for the number of atoms of the first component (^{41}K) of the mixture, under which the energy of the droplet is no longer negative and the evaporation process occurs.
Since the ratio between the densities of the two species is fixed $\rho_1/\rho_2 = r$, also the ratio between the number of particles N_1 and N_2 is. Thus, the critical total number of atoms N_c is:

$$\begin{aligned} N_c &= N_{1,\text{c}} + N_{2,\text{c}} = \\ &= N_{1,\text{c}} \left(1 + \frac{1}{r}\right) \end{aligned} \tag{3.62}$$

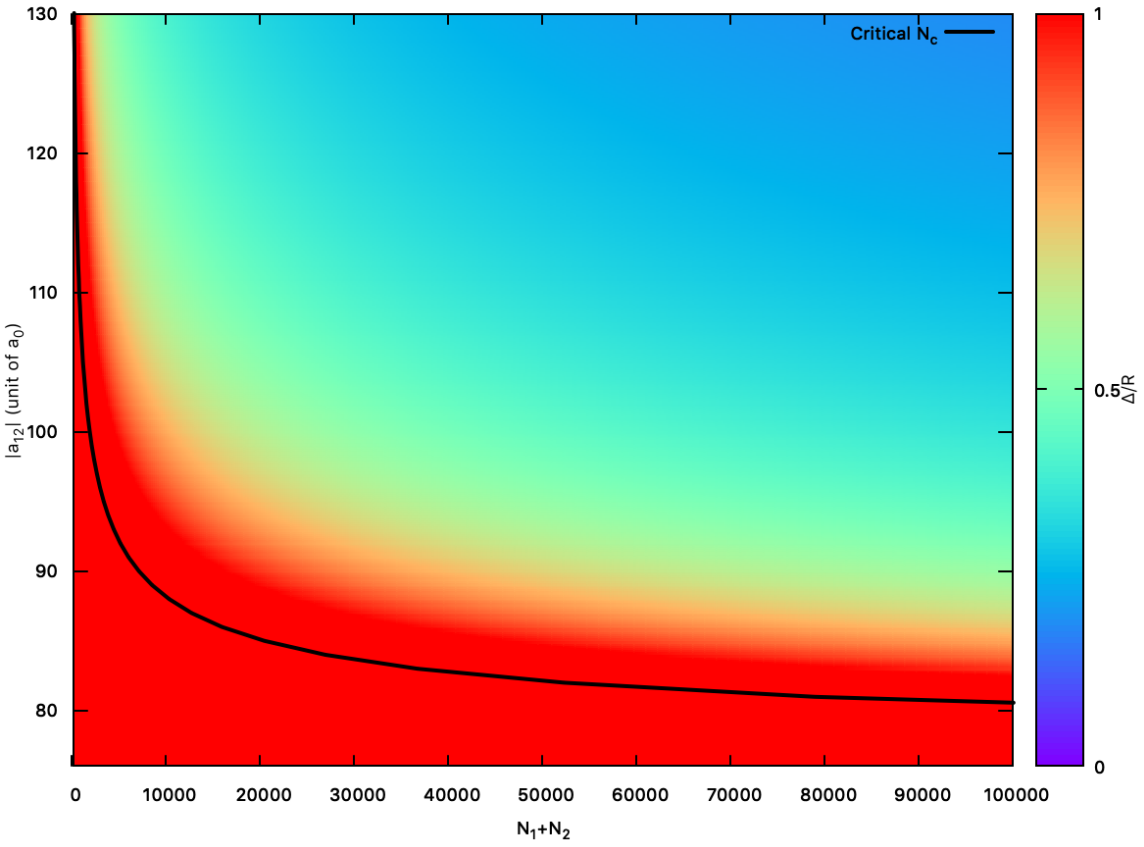

Figure 3.15: Summarizing the results about droplets' surface: the color scales like the ratio between the surface width Δ and the radius R of the droplet. The red region identifies gaussian-like radial density profiles (see figure 3.14) while the green and blue region identifies droplets with a central bulk region (see figure 3.13). The black solid line marks the total critical number of particles N_c below which the droplet evaporates.

At this point, we can collect all the information about the shape of the droplet in figure 3.15: in the plane $(N, |a_{12}|)$ with $N = N_1 + N_2$ equal to the total number of particles, the color scales like the ratio $\frac{\Delta}{R}$ and the solid black line delimits the critical number of particles N_c under which the droplet is unstable, for each value of $|a_{12}|$. The red region identifies gaussian-like radial density profiles (see figure 3.14) while the green and blue region identifies "true" droplets with a central bulk region (see figure 3.13). Notice that the assumption of gaussian density profile in the critical region made at the beginning of the computation is true since the black line belongs to the red region for each $|a_{12}|$.

Chapter 4

The liquid-drop model

In this chapter we solve numerically the two coupled Gross-Pitaevskii equations associated to the two species ^{41}K and ^{87}Rb of the Bose-Bose mixture, for a fixed number of particles, in the regime where formation of self-bound droplets is expected. The total energy is computed as a function of the total number of particles and the validity of the liquid drop model for this kind of system is verified. From the parameters of this model the Tolman length is computed, which allow us to calculate a curvature correction to the surface tension.

4.1 The total energy model for a liquid droplet

After the analysis of the surface properties, the microscopic characterization of a ^{41}K-^{87}Rb droplet is not complete without the knowledge of the total energy. From past computations on liquid ^{4}He droplets [24–26] we know that the **liquid-drop model** (LDM) accurately predicts the behaviour of the energy as a function of the total number of particles. According to this model the total energy E of a droplet made of N particles is well represented by the following semi-empirical formula [27]:

$$E(N) = E_v N + E_s N^{2/3} + E_c N^{1/3} \tag{4.1}$$

- The first term is the **volume energy**: the coefficient E_v describes the bulk energy per particle of the droplet.
- The second term is the **surface energy**: the coefficient E_s is linked to the surface tension σ by the following relation

  $$\sigma = \frac{E_s}{4\pi r_0^2} \tag{4.2}$$

  where r_0 is the unit radius of the droplet computed from

  $$\frac{4\pi r_0^3 \rho_{\text{bulk}}}{3} = 1 \tag{4.3}$$

  A detailed explanation of relation (4.2) will be given in section 4.2.
- The third term is the **curvature energy**: the coefficient E_c is linked to the Tolman length, which describes curvature effects on the surface tension [23].

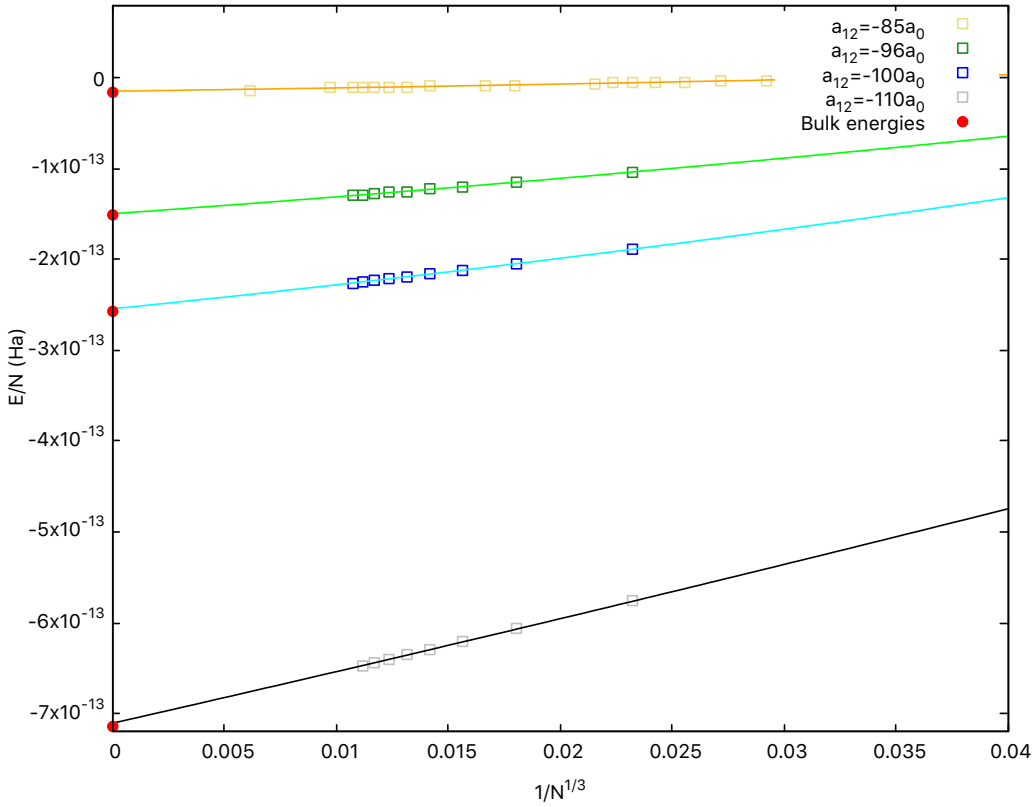

Figure 4.1: Total energy of a droplet as a function of $1/N^{1/3}$ for a set of four different a_{12} values. Square points are ground state energies per particle obtained from the imaginary time evolution of a droplet with a fixed number of particles N, solid lines are the fitting curves according to the semi-empirical liquid-drop model and red points at zero x-axis are energies per particle of an infinitely large drop (bulk energies).

With the same technique explained in section 3.3, we perform a numerical imaginary time evolution in a three dimensional mesh to find the ground state structure of a droplet and compute its total energy. In figure 4.1 we report total energies as a function of $1/N^{1/3}$ for a set of four different values of a_{12} while in figures 4.2 and 4.3 the densities of the droplet in the $x-y$ plane are illustrated for $a_{12} = -85a_0$ and $a_{12} = -96a_0$, respectively. By decreasing the scattering length, i.e. by making the system more attractive, we can observe that the central bulk density increases, the size of the drop squeezes and the surface width becomes visibly smaller.

The ground state energies per particle of the droplet obtained from the imaginary time evolution (square points) are fitted with the semi-empirical formula (4.1) of the liquid-drop model (solid lines) written in the following way:

$$\frac{E(N)}{N} = E_v + E_s x + E_c x^2 \tag{4.4}$$

with $x = N^{-1/3}$. The bulk energies per particle computed in chapter 2.2 (see figure 2.2) are the red points at zero x-axis to enhance at first sight their compatibility with the constant parameters E_v of the fitting curves. In table 4.1 fitting parameters are reported.

As a proof of the accuracy of the fit, in table 4.2 some comparisons are reported:

- The correspondence between the fitting parameter E_v and the bulk energy per parti-

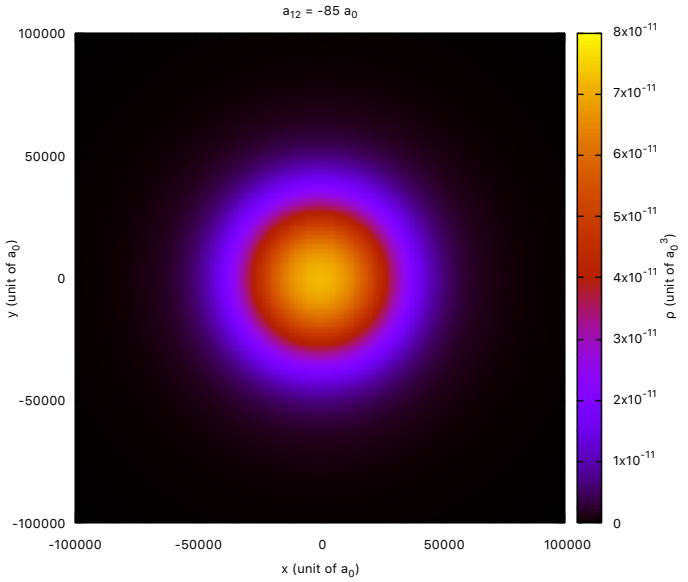

Figure 4.2: Density in atomic units in the $x - y$ plane passing through the droplet center for a droplet in free space with $a_{12} = -85\, a_0$.

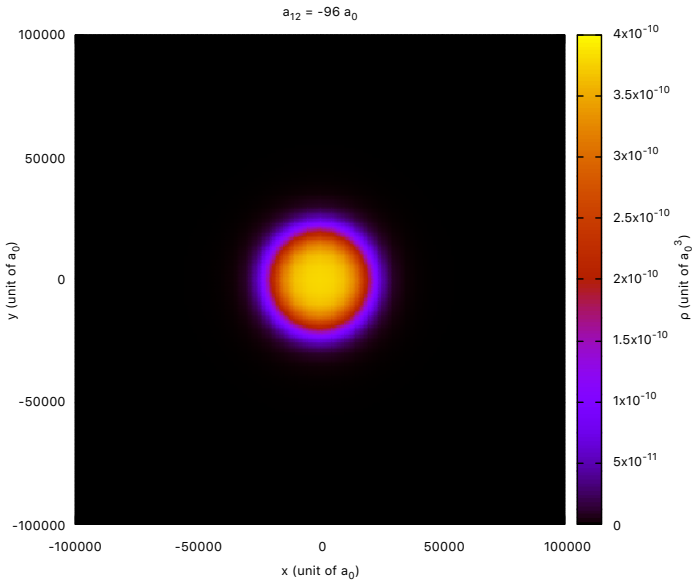

Figure 4.3: Density in atomic units in the $x - y$ plane passing through the droplet center for a droplet in free space with $a_{12} = -96\, a_0$.

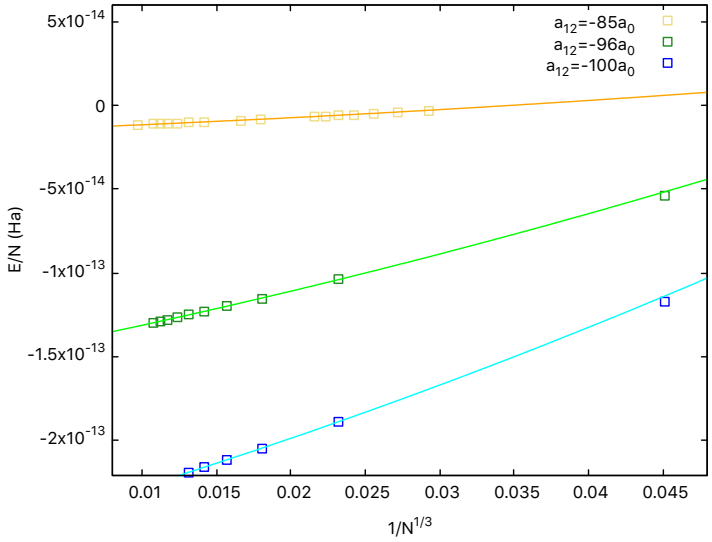

Figure 4.4: Zoom of the total energy of a droplet in a 3D mesh as a function of $1/N^{1/3}$ for a set of a_{12} values in the region of big N, to focus on the deviations from the LDM.

a_{12} (units of a_0)	E_v (Ha)	E_s (Ha)	E_c (Ha)
-85	$-1.50 \cdot 10^{-14}$	$3.26 \cdot 10^{-13}$	$3.17 \cdot 10^{-12}$
-96	$-1.50 \cdot 10^{-13}$	$1.76 \cdot 10^{-12}$	$9.39 \cdot 10^{-12}$
-100	$-2.55 \cdot 10^{-13}$	$2.52 \cdot 10^{-12}$	$1.32 \cdot 10^{-11}$
-110	$-7.09 \cdot 10^{-13}$	$5.24 \cdot 10^{-12}$	$2.15 \cdot 10^{-11}$

Table 4.1: Fitting parameters of the energy per particle with the liquid-drop model.

a_{12} (units of a_0)	E_v (Ha)	E_{bulk} (Ha)	σ_{fit} (Ha/a_0^2)	σ_{bulk} (Ha/a_0^2)
-85	$-1.50 \cdot 10^{-14}$	$-1.53 \cdot 10^{-14}$	$1.95 \cdot 10^{-20}$	$1.97 \cdot 10^{-20}$
-96	$-1.50 \cdot 10^{-13}$	$-1.51 \cdot 10^{-13}$	$2.91 \cdot 10^{-19}$	$2.86 \cdot 10^{-19}$
-100	$-2.55 \cdot 10^{-13}$	$-2.57 \cdot 10^{-13}$	$5.29 \cdot 10^{-19}$	$5.32 \cdot 10^{-19}$
-110	$-7.08 \cdot 10^{-13}$	$-7.18 \cdot 10^{-13}$	$1.74 \cdot 10^{-18}$	$1.76 \cdot 10^{-18}$

Table 4.2: Comparison between E_v and the bulk energy per particle and comparison between the surface tension σ_{fit} obtained from E_s and σ_{num} obtained from the numerical method discussed in the previous chapter (see figure 3.8).

cle of an infinitely large drop in the equilibrium configuration, computed numerically in chapter 2.

- The correspondence between the surface tension σ_{fit} obtained from the fitting parameter according to relation (4.2) and the one σ_{num} obtained by the numerical method as seen in section 3.2.

The evident agreement is a test of validity of the liquid-drop model on a BECs mixture system in the self-bound regime.
By the way, focusing on the region of small N we observed some deviations from the model (see figure 4.4): this can lead back to the fact that under a certain value of N the bulk portion of the droplet vanishes and so energy contributions are no more distributed according to the liquid-drop model. Explicitly, for $a_{12} = -96a_0$ and $a_{12} = -100a_0$ deviations around $1/N^{1/3} \sim 0.045$ correspond to droplets with $N \sim 10000$ particles. For these cases, the absence of the bulk region is confirmed by the map in figure 3.15: the points $(96, 10000)$ and $(100, 10000)$ belong to the red region which marks droplets with gaussian-like radial density profile.
Assuming the reliability of this model, the third fitting parameter E_c connected to the curvature of the liquid-vacuum interface allows to make a correction of the surface tension σ computed before, as discussed in the following sections.

4.2 The Tolman length

In 1949, Tolman studied the dependence of the surface tension on the size of a droplet [28]. The so-called Tolman length δ, a small quantity, independent on the droplet size, conveniently defined in terms of an expansion in $1/R$ of the pressure difference across the droplets surface, where R is the radius of the droplet:

$$\Delta P = \frac{2\sigma_0}{R}\left(1 - \frac{\delta}{R}\right) \tag{4.5}$$

with ΔP the difference between the bulk pressure inside the liquid and the one of the vapor outside and σ_0 the surface tension of a planar interface. The Tolman length is also useful to define the size-dependent surface tension $\sigma(R)$ [23, 29, 30]:

$$\sigma(R) = \sigma_0\left(1 - \frac{2\delta}{R}\right) \tag{4.6}$$

obtained from an expansion at first order on $1/R$.
So far, the surface tension computed in chapter 3 for a ^{41}K - ^{87}Rb droplet was that one of a planar interface (that from now we call σ_0 to distinguish it from the size-dependent one), though in real droplets an interfacial curvature of the surface in contact with the vacuum is present (see figure 4.5).
As illustrated in figures 4.6 and 4.7, the Tolman length δ is negative for interfaces that tend to curve towards the liquid and positive for those that tend to curve towards the vacuum. For this reason, we expect a negative Tolman length for ^{41}K - ^{87}Rb droplets and, as a consequence, the corrected surface tension would be greater than the planar one and it would approach to it for $R \to +\infty$.
The Tolman length can be computed from the third fitting parameter of the liquid-drop

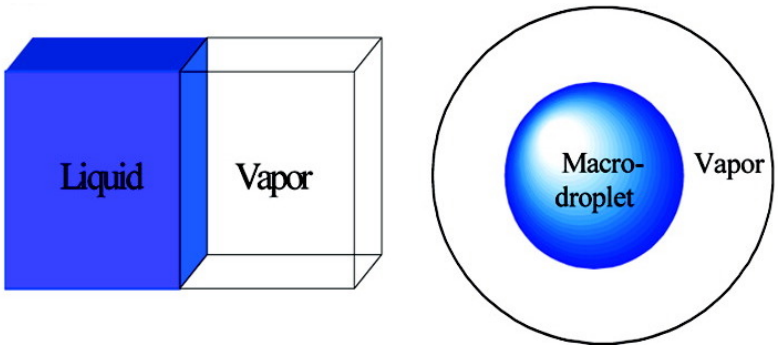

Figure 4.5: On the left: planar liquid-vapor interface with surface tension σ_0. On the right: droplet's liquid-vapor interface with surface tension $\sigma(R)$ affected by the interfacial curvature. Images taken from [31].

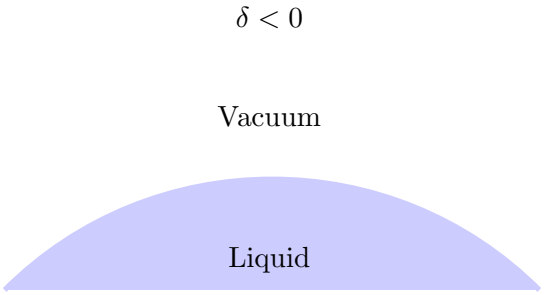

Figure 4.6: The Tolman length δ is negative for interfaces that tend to curve towards the liquid.

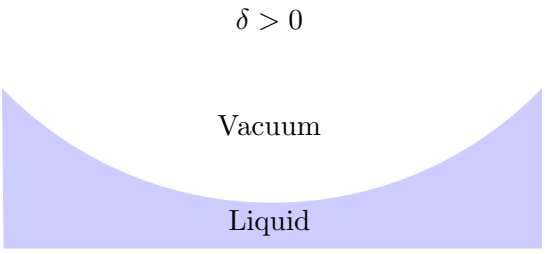

Figure 4.7: The Tolman length δ is positive for interfaces that tend to curve towards the vacuum.

model E_c. In fact, for a free droplet:

$$E_{tot} = E_{\text{bulk}} + E_{\text{sc}} \tag{4.7}$$

where E_{sc} is the energy contribution given by a curved surface. This last term can be written as:

$$E_{\text{sc}} = 4\pi R^2 \sigma \tag{4.8}$$

with σ given by equation (4.6).
Since the liquid-drop model and equation (4.7) describe the same system, we can write:

$$E_{\text{bulk}} + 4\pi r^2 \sigma = E_v N + E_s N^{2/3} + E_c N^{1/3} \tag{4.9}$$

The one to one correspondence between E_{bulk}/N and E_v was already discussed, we can conclude that the surface and curvature terms of the liquid-drop model are both contained in $E_{\text{sc}} = 4\pi R^2 \sigma$. The explicit form of E_{sc} is:

$$\begin{aligned} E_{\text{sc}} &= 4\pi R^2 \sigma_0 \left(1 - \frac{2\delta}{R}\right) = \\ &= 4\pi R^2 \sigma_0 - 4\pi R^2 \sigma_0 \frac{2\delta}{R} \end{aligned} \tag{4.10}$$

Recalling that from the relation $\frac{4}{3}\pi R^3 \rho_{\text{bluk}} = N$, the radius R of the droplet can be written as:

$$R = \left(\frac{3N}{4\pi\rho_{\text{bulk}}}\right)^{1/3} = r_0 N^{1/3} \tag{4.11}$$

where r_0 is the unit radius previously defined in (4.3). Using this relation, we find:

$$E_{\text{sc}} = \underbrace{4\pi r_0^2 \sigma_0}_{E_s} N^{2/3} \underbrace{- 8\pi r_0^2 \sigma_0 \delta}_{E_c} N^{1/3} \tag{4.12}$$

where the association with the liquid-drop model coefficients is immediate according to the powers of N. In this way, we demonstrated the connection between E_s and σ_0 given by equation (4.2) and we found a direct relation between the coefficient E_c and the Tolman length δ:

$$E_c = 8\pi r_0^2 \sigma_0 \delta \tag{4.13}$$

More recently, by a thermodynamic treatment Bartell derived an approximated expression for the Tolman length in terms of the isothermal compressibility κ^{-1} [32], in particular:

$$\delta \approx -\kappa^{-1} \sigma_0 \tag{4.14}$$

where σ_0 is the surface tension of the planar interface. Previously, some studies have noticed that the product $\kappa^{-1}\sigma_0$ is a fundamental characteristic length in liquid droplets [33–37] though the connection with the Tolman δ was never explicitly made. It is quite interesting to observe how the Tolman length, a physical quantity linked to the curvature of an interface, can be computed as a product of a purely bulk property with a purely surface one. This approximation reflects a the origin of the interfacial curvature, that can be seen as the mutual combination of a self-bound state's bulk region and an interrupting surface region of finite size.
Figure 4.8 shows δ values computed with the two methods: the approximated expression connected to the isothermal compressibility predicts correctly the sign and the order of

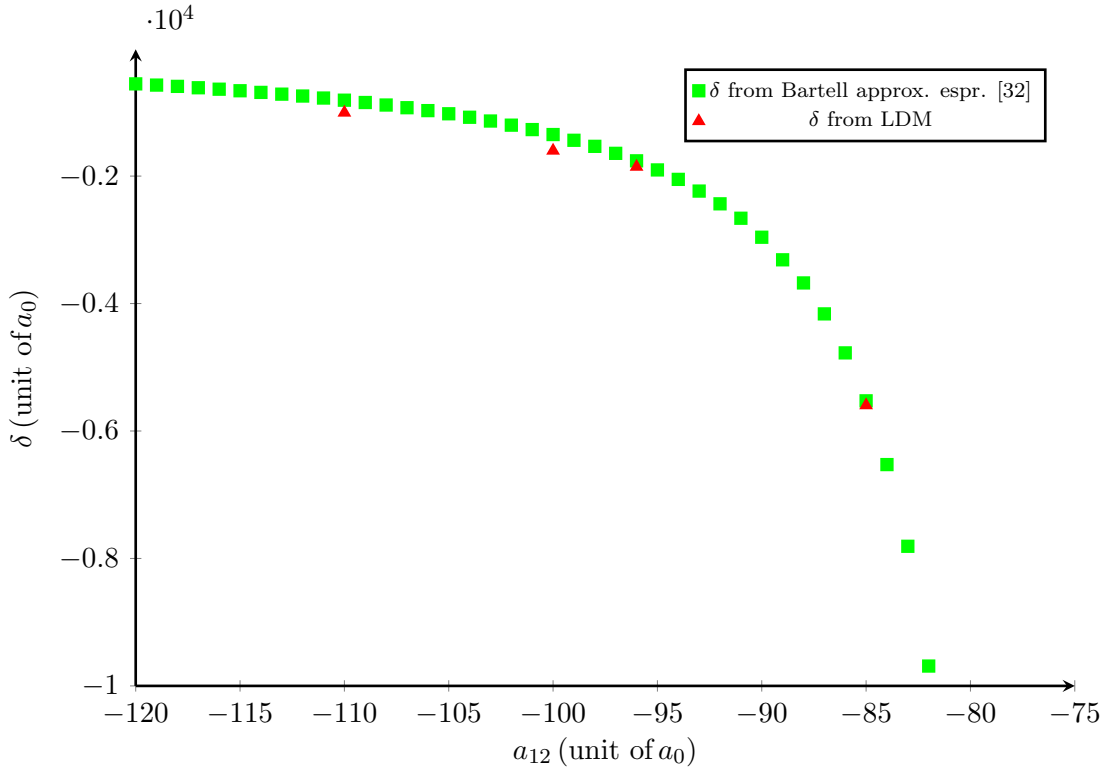

Figure 4.8: Tolman length δ as a function of the interspecies scattering length a_{12}.

magnitude of δ and, near the critical point, it is in good agreement with the Tolman length obtained from the liquid-drop model. This is reasonable: the approximated expression was obtained in the limit of large droplet radius R [32], that is a valid hypothesis if we approach to the critical point of the ^{41}K - ^{87}Rb droplet.

4.3 The surface tension correction

Once the Tolman length for a given a_{12} in the self-bound regime has been calculated, the magnitude of the size-dependent surface tension affected by the finite size R of the droplet and its interfacial curvature can be computed by the equation (4.6):

$$\sigma(R) = \sigma_0 \left(1 - \frac{2\delta}{R}\right)$$

In figure 4.9 we show the dependence of the corrected surface tension σ as a function of the droplet's total number of particles N.
As a consequence of the negative sign of the Tolman length, the corrected size-dependent σ is greater than the planar surface tension and it decreases monotonically with increasing droplet size. With this last correction the analysis of the surface tension is complete and, from an experimental point of view, this quantity can be helpful to study collisions between self-bound droplets. In fact, when two drops approach each other with a certain relative velocity, after the collision they can merge in a single final drop or divide in two or more drops, depending on whether or not the surface tension is sufficient to resist against the kinetic energy of the colliding pair [38–41]. Collisions between self-bound quantum

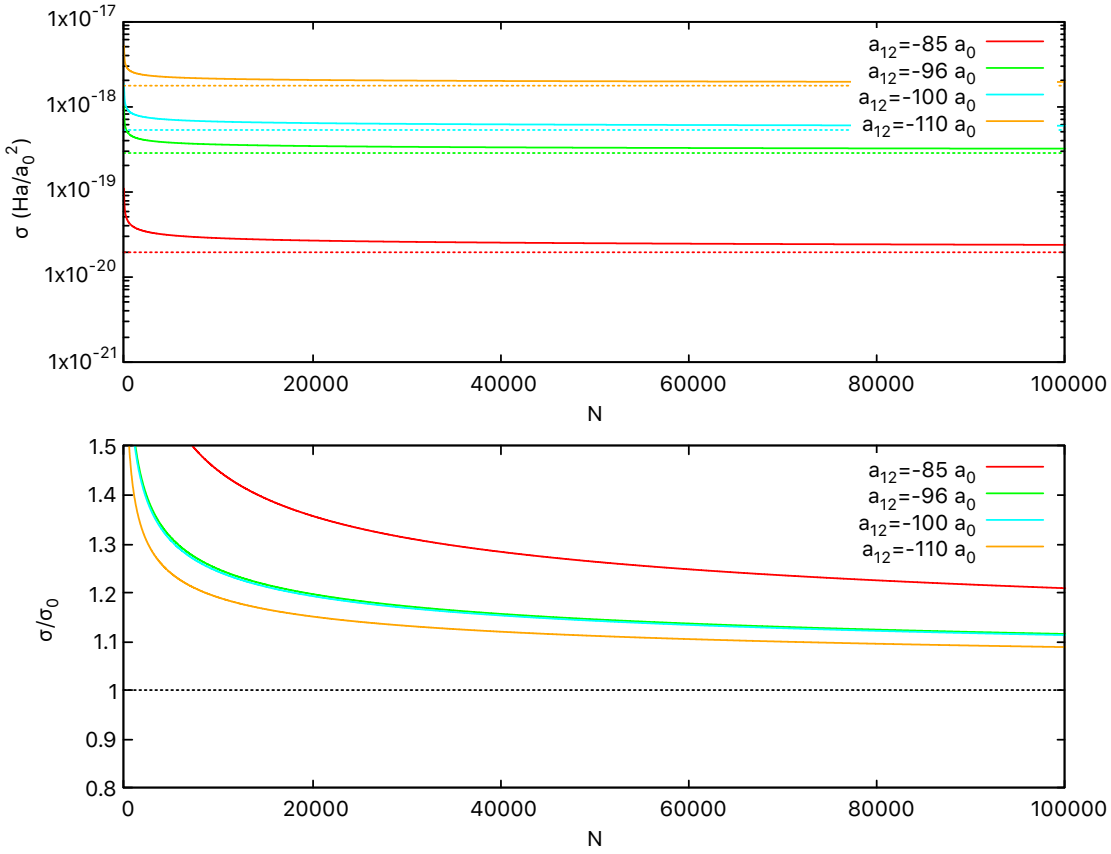

Figure 4.9: Corrected surface tension σ as a function of the droplet total number of particles N for a set of four values of a_{12}. The upper panel shows σ that approaches to the planar surface tension in the limit $N \to +\infty$. The lower panel shows the ratio σ/σ_0 as a function of N.

droplets formed by a mixture of ^{39}K atoms were studied experimentally at LENS: firstly, two separated quantum droplets are created using a repulsive barrier, then, by releasing it, they acquire a certain tunable velocity towards the center of the system. According to the value of the relative velocity v, there are two different outcomes of the collision: if the colliding velocity is smaller than a critical value v_c, the droplets merge in a single final one, while for velocities larger than v_c they remain separate and they keep moving in opposite directions after the collisional event, as shown in figure 4.10.

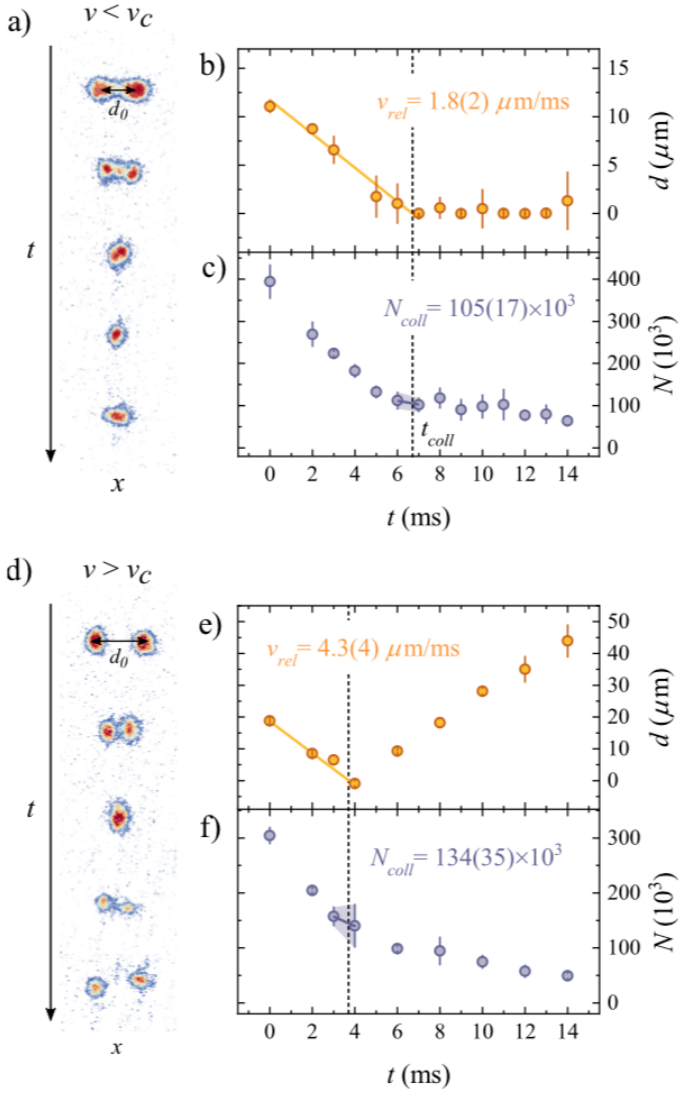

Figure 4.10: Examples of two collisional events resulting in merging (a) and separation (d) of the droplets. In b) and e) there are the time evolution of the distance d in μm between the two droplets and in c) and f) of the total atom number N.

The possibility to have single merged droplet after the collision is related to the capability to absorb the excess kinetic energy $E_{\text{kin}} \propto v^2 N$. For a big number of particles N, the relevant energy contribution which can host excitations to absorb the collision kinetic energy, is the surface energy provided by the second term of the liquid-drop model proportional to $N^{2/3}$: in fact, the bulk term is conserved during the collision and the curvature energy

term is negligible for large values of N [38]. Thus, in analogy to the Weber criterion for classical liquid droplets [42], the condition for merging is given by $E_{\text{kin}} \lesssim E_s N^{2/3}$.
Instead, in the case of a small number of particles N (the region where deviations from the liquid drop model have been observed) there is no longer distinction between bulk and surface regions and one would expect the whole binding energy of the droplet to be the relevant energy scale.
In conclusion, it is clear that surface tension plays a crucial role in probing the dynamical properties droplets made of a bosonic binary mixture with a large number of particles (the so-called "true" droplets) and, in particular, the study of collisions with the ^{41}K-^{87}Rb mixture could be interesting to better investigate this dynamics since these mixture droplets have the advantage of a longer lifetime, due to a lower three-body recombination rate, as explained in the introduction.

Chapter 5

Bright solitons in mixtures of Bose-Einstein condensates

In this chapter we study Bose-condensed bright soliton states of a system in a quasi-1D configuration. The origin of this localized and non-dispersive wave packet is first investigated in a single-species BEC made of ultracold and ultradilute atoms with attractive interaction. Then, the study is extended to the heteronuclear ^{41}K - ^{87}Rb mixture in an optical waveguide: we develop a variational model to show the transition between solitons and droplets, according to the atom number and interspecies interaction strength, and the presence of a bistable region in which both states coexist. Finally, we perform a numerical simulation to show the soliton evaporation when releasing the external trap.

5.1 The bright soliton state in a BEC

In a Bose-Einstein condensate, solitons are localized wave packets that can propagate without distortion as a result of the balance between non-linearity and dispersion [43]. In a BEC of ultracold and dilute atoms, the non-linearity originates from the atomic interactions, as manifested by the nonlinear term in the Gross-Pitaevskii equation which describes the system at a mean field level. Depending on attractive and repulsive interatomic interactions, these localized solutions of the GPE are called bright or dark solitons, respectively, and in the last year they have been studied extensively both theoretically [44–46] and experimentally [47–49].
The simplest way to see the origin of a localized state for a Bose gas with attractive interaction between atoms in an external trapping potential, is to consider the expression of the total energy E for a D-dimensional BEC (characterized by a contact interaction and treated at the mean-field level) with a fixed total number of atoms N:

$$E = \int d^D\mathbf{r} \left(\frac{\hbar^2}{2m} |\nabla \Psi(\mathbf{r})|^2 + U|\Psi(\mathbf{r})|^2 + \frac{g}{2}|\Psi(\mathbf{r})|^4 \right) \tag{5.1}$$

$$N = \int d^D\mathbf{r}\, |\Psi(\mathbf{r})|^2 \tag{5.2}$$

with U external harmonic trap ($U \sim r^2$), $g = \frac{4\pi\hbar^2 a_s}{m} < 0$ the coupling constant of the interatomic interaction and $\Psi(\mathbf{r})$ is the normalized condensate wave function.

Assuming that L is the typical system size, from the normalization condition:

$$[\Psi] \sim \frac{\sqrt{N}}{L^{D/2}} \tag{5.3}$$

For example, using a Gaussian ansatz the condensate wave function reads:

$$\Psi(\mathbf{r}) \propto \frac{\sqrt{N}}{\sigma^{D/2}} e^{-\frac{\mathbf{r}^2}{2\sigma^2}} \tag{5.4}$$

where the variance σ has the role of characteristic size of the state.
From the dimensional analysis of each term of the total energy expression (the kinetic, the external potential and the interaction term, respectively) one gets:

$$E_{kin} \sim \frac{N}{L^2} \qquad E_{pot} \sim NL^2 \qquad E_{int} \sim \frac{N^2}{L^D} \tag{5.5}$$

Thus, the total energy reads:

$$E \sim \frac{aN}{L^2} + bNL^2 - \frac{cN^2}{L^D} \tag{5.6}$$

with $a, b, c > 0$ constants related to the physical quantities of the system.
We can distinguish the three cases:

- If $D = 1$, the total energy

  $$E \sim \frac{aN}{L^2} + bNL^2 - \frac{cN^2}{L} \tag{5.7}$$

  has always a minimum for a finite value of L and without any restriction for N, i.e. a localized, stable state exists and the collapse of the system is avoided (see figure 5.1).

- If $D = 2$ the total energy

  $$E \sim \frac{aN}{L^2} + bNL^2 - \frac{cN^2}{L^2} = \frac{N(a - cN)}{L^2} + bNL^2 \tag{5.8}$$

  has a minimum for a finite value of L only if $(a - cN) > 0$, or equivalently only if the total number of particles N is under a certain threshold $N_c = a/c$ (see figure 5.2). This restriction on the number of particles N is limited to BEC with short-range attractive potential, in the case of long-range interaction (for example dipolar interaction) stable 2D bright solitons can exist [50].

- If $D = 3$ the total energy is

  $$E \sim \frac{aN}{L^2} + bNL^2 - \frac{cN^2}{L^3} \tag{5.9}$$

  and a metastable state, result of the balance between the kinetic energy, the trap potential energy and the interaction energy, can exist in a 3D BEC with trapping potential if the number of atoms is below a critical one N_c (see figure 5.3). In this case, the critical number of atoms must be computed numerically.

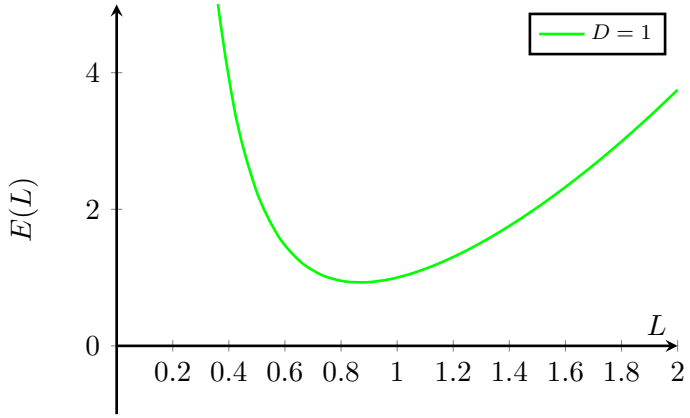

Figure 5.1: Total energy E as a function of the typical system size L for a 1D BEC (numerical constants a, b and c are put equal to 1).

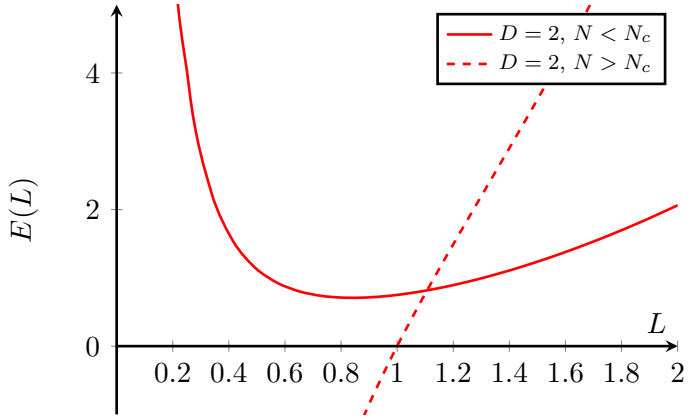

Figure 5.2: Total energy E as a function of the typical system size L for a 2D BEC (numerical constants a, b and c are put equal to 1, so also $N_c = 1$). Solid line represent the case in which the soliton state is stable ($N = 0.2 < N_c$), the dashed line represents the case for which a self-bound state does not exist ($N = 2 > N_c$) .

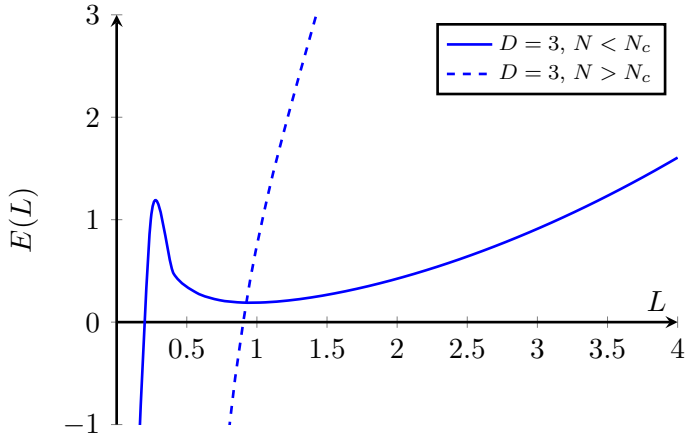

Figure 5.3: Total energy E as a function of the typical system size L for a 3D BEC (numerical constants a, b and c are put equal to 1). In this case, the critical number of particles is computed graphically $N_c \sim 0.35$ (see image 5.4), solid line represent a case in which the soliton state is stable ($N = 0.1 < N_c$), the dashed line represents a case for which a self-bound state does not exist ($N = 1.5 > N_c$).

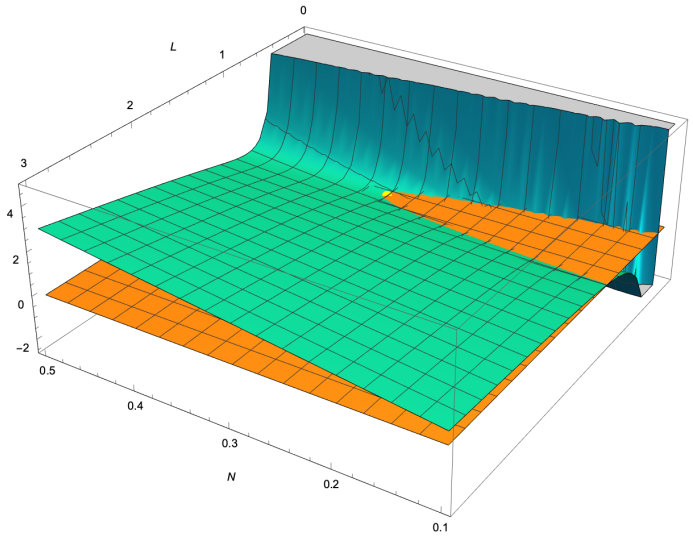

Figure 5.4: Graphic solution of $\frac{\partial E}{\partial L} = 0$ to find approximately the critical number of atoms for which the confined state exists for this simple toy model in 3D with $a, b, c = 1$: the green surface is the derivative of the total energy with respect to L as a function of L and N, the orange surface is the plane $\frac{\partial E}{\partial L} = 0$. These two surfaces intersect (so the the total energy has a metastable minimum for a finite value of L) only if N is less then $N_c \sim 0.35$.

This simple model predicts the existence of a stable, localized state state for each value of N for a system in a 1D configuration, but a more detailed description allows to find the exactly solution of the bright soliton state.
Static and dynamical properties of a pure Bose-Einstein condensate made of dilute and ultracold atoms are very well described by the time-dependent Gross-Pitaevskii equation:

$$i\hbar\frac{\partial}{\partial t}\Psi(\mathbf{r},t) = \left[\frac{\hbar^2}{2m}\nabla^2 + U(\mathbf{r}) + \frac{4\pi\hbar^2 a_s}{m}|\Psi(\mathbf{r},t)|^2\right]\Psi(\mathbf{r},t) \tag{5.10}$$

where $\Psi(\mathbf{r},t)$ is the condensate wavefunction defined in chapter 1, m is the mass of the species of atoms that composes the BEC and a_s is the s-wave scattering length. It is the time-dependent version of the GPE seen in equation (1.24), obtained starting from the time-dependent many-particle Schrödinger equation in the mean field approximation. We are interested in a dimensional reduced system in a quasi-1D configuration, so let us consider a very strong harmonic confinement only along x and y axis such that the total external trap is:

$$U(\mathbf{r}) = \frac{1}{2}m\omega_\perp^2(x^2+y^2) \tag{5.11}$$

From this choice, we can guess the following ansatz for the condensate wave function $\Psi(\mathbf{r},t)$ [51]:

$$\Psi(\mathbf{r},t) = f(z,t)\frac{\sqrt{N}}{\pi^{1/2}a_\perp}\exp\left(\frac{x^2+y^2}{2a_\perp^2}\right) \tag{5.12}$$

The quantity $a_\perp = \sqrt{\frac{\hbar}{m\omega_\perp}}$ is the characteristic length of the harmonic confinement along x and y axis while the function $f(z,t)$ is the condensate wave function along the free z axis. In other words, one can decouple the total wave function in a general function along z (longitudinal direction) and a gaussian wave packet along the directions with the harmonic confinement (transverse direction).

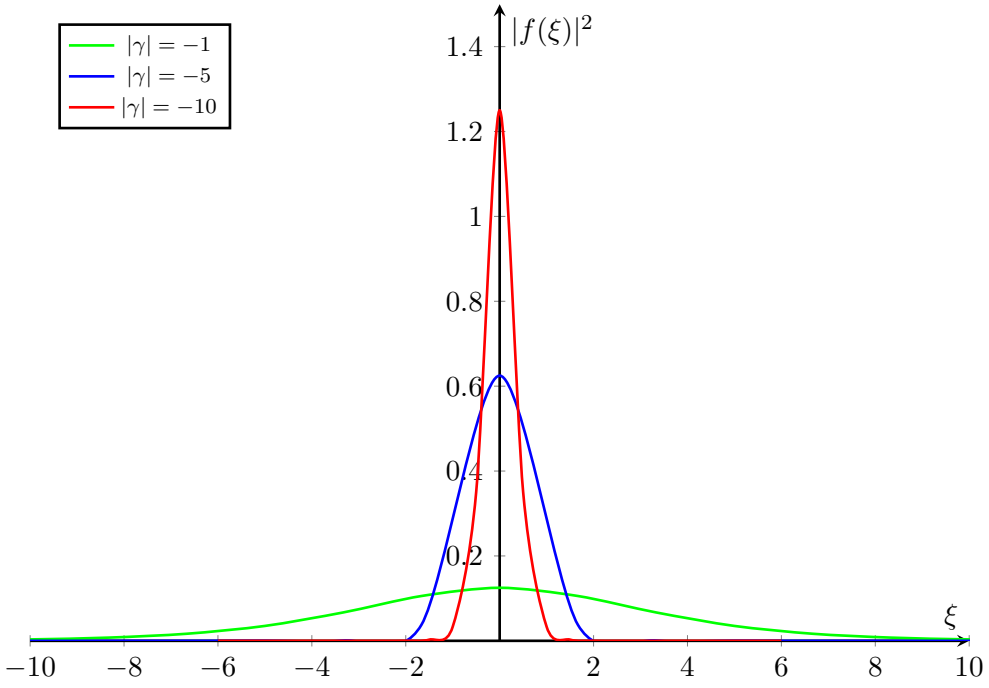

Figure 5.5: Density profile of the bright soliton state along z in the moving frame of reference with velocity v three values of the effective one-dimensional interaction strength γ (for semplicity, m and $\hbar$ are set to 1).

By inserting this ansatz in equation (5.10) and integrating along the confined directions, the effective dimensional reduced time-dependent GPE along the free direction z is:

$$i\hbar\frac{\partial}{\partial t}f(z,t) = \left[\frac{\hbar^2}{2m}\frac{\partial^2}{\partial z^2} + \gamma|f(z,t)|^2\right] f(z,t) \tag{5.13}$$

where $\gamma = \frac{2\hbar^2 a_s}{m a_\perp^2}$ is the effective one-dimensional interaction strength.
Equation (5.13) is a time-dependent 1D non-linear Schrödinger equation and in 1972 it was demonstrated that, for attractive interatomic interaction ($\gamma < 0$), an exact solution is the **bright soliton** wave packet of the form [15, 51, 52]

$$f(z,t) = \sqrt{\frac{m|\gamma|}{8\hbar^2}}\, sech\left[\frac{m|\gamma|}{4\hbar^2}(z - vt)\right] e^{iv(z-vt)} e^{\left(i\frac{mv^2/2-\mu}{\hbar}t\right)} \tag{5.14}$$

where v is the velocity of propagation, $\mu = -\frac{m\gamma^2}{16\hbar^2}$ and $sech[x] = \frac{2}{e^x + e^{-x}}$ is the hyperbolic secant function. A detailed derivation of the analytical form of this solution is in Appendix A.
The shape invariant density profile along z is:

$$n(z,t) = |f(z,t)|^2 = \left|\sqrt{\frac{m|\gamma|}{8\hbar^2}}\, sech\left[\frac{m|\gamma|}{4\hbar^2}(z - vt)\right]\right|^2 \tag{5.15}$$

Setting the new variable $\xi = z - vt$, so operating in the moving frame of reference, the density profile along ξ is illustrated in figure 5.5 for some values of the parameter γ.
Even if in the following sections we are interested in the attractive interatomic interaction case, for completeness, we report here also the case of repulsive interaction ($\gamma > 0$). In

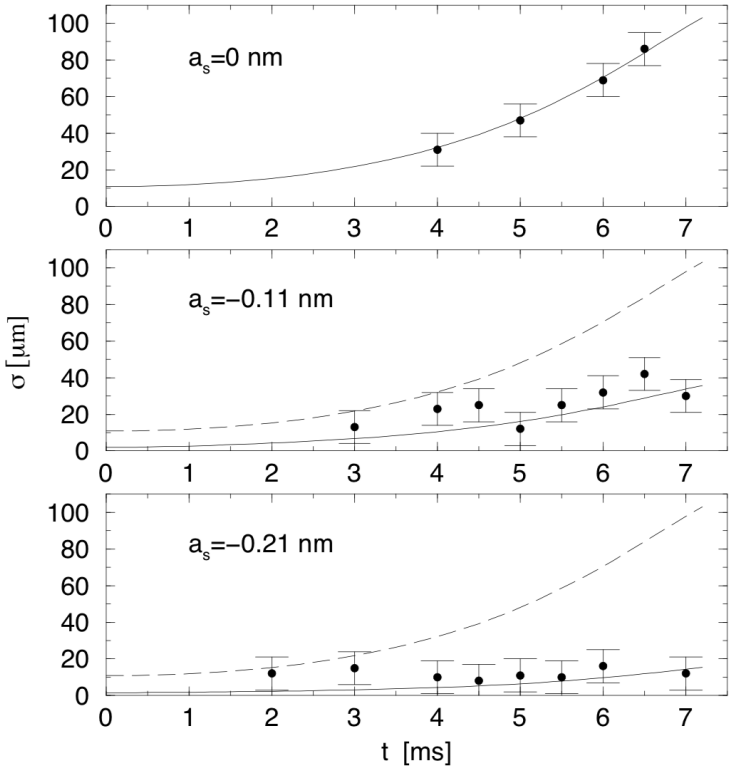

Figure 5.6: Root mean square size σ of the BEC state width along the longitudinal direction vs propagation time t for different values of the s-wave scattering length a_s. The solid line represents the numerical solution of the time-dependent GPE, the dashed line is the ideal gas solution of the GPE and black points are experimental data from [48]. Figures taken from [51].

this regard, an exact solution is the **dark soliton** wave packet [13, 15]:

$$f(z,t) = \sqrt{\frac{\gamma\phi_\infty^2 - mv^2}{\gamma}} \left(tanh\left[(z-vt)\sqrt{\gamma\phi_\infty^2 - v^2}\right] + i\sqrt{\frac{mv^2}{\gamma\phi_\infty^2 - mv^2}} \right) e^{-i\mu t/\hbar} \quad (5.16)$$

where ϕ_∞ is the asymptotic constant value of $|f(z,t)|$, v is again the velocity of propagation and $\mu = \gamma\phi_\infty^2$. At variance with the bright soliton solution (5.14), where the density reaches a maximum at the center of the soliton, the dark soliton solution is instead characterized by a central region which is void of atoms.
In 2002 two relevant studies about bright solitons in Bose-Einstein condensates with ^{7}Li [47, 48] atoms were made. In their experiment, Khaykovich et al. [48] measured the root mean square size σ of the longitudinal width of the self-bound state at different time for three values of the scattering length a_s, tuned by means of Feshbach resonances technique: $a_s = 0$ nm, $a_s = 0.11$ nm, and $a_s = 0.21$ nm. In figure 5.6 there are experimental data compared to the numerical solution of the 1D time dependent GPE: the MF interaction term (thus the non-linear term in the GPE) makes the soliton move without dispersion, as highlighted by the constant variance σ, while an ideal Bose gas without interaction moves spreading along the longitudinal axis.
Strecker et al. [47], instead, reported the experimental formation of a train of bright solitons in a quasi-1D BEC system of ^{7}Li atoms by a sudden change in the sign of the scattering length from positive to negative. As shown in figure 5.7, the condensate spreads

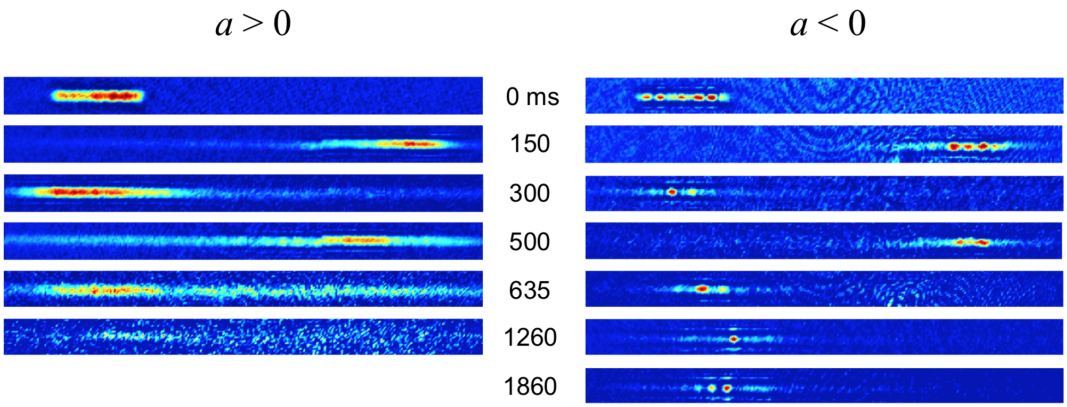

Figure 5.7: On the left: experimental observation of a spreading condensate for $a > 0$. On the right: experimental observation of a soliton train for $a < 0$. In both cases, the condensate state is set in motion by offsetting the optical potential and it is observed to propagate in the potential for many oscillatory cycles. Figures taken from [51].

for positive scattering length $a > 0$, while for $a < 0$ the solitonic non-dispersive and localized structures are formed. In the second case, once the scattering length have changed from positive to negative at $t = 0$, the number of solitons produced is the result of modulational instability of the time-dependent macroscopic wave function of the Bose condensate and it depends on the absolute value of the final negative scattering length $|a|$, on the characteristic length of transverse harmonic confinement $a_\perp$ and on the initial longitudinal length of the quasi-1D BEC L (see [53] for more details).
The experimental study of bright solitons in ultracold atoms is an hot topic in this field and it is interesting the application on bosonic binary mixtures, as discussed in the following.

5.2 Variational study of the soliton-droplet transition in a ^{41}K - ^{87}Rb mixture in an optical waveguide

In this section we study a system which can host both bright solitons and quantum droplets, two different localized states that exist in different regimes. We consider a system made of a bosonic ^{41}K - ^{87}Rb mixture with attractive interspecies interaction in an optical waveguide: this system can host quantum droplets as discussed in previous chapters but the optical waveguide confers a quasi-1D configuration which favours the soliton appearance. A variational approach allows to study the nature of the localized state in this kind of system, focusing on the transition from soliton to quantum droplet upon increasing the atom number.
The system is exactly the same described in the previous chapters but it is confined along x-axis and y-axis by an harmonic trap (transverse directions) while it is free along the z-axis (longitudinal direction).
We can perform a variational study using a gaussian ansatz for the wavefunction of ^{41}K, the first component of the mixture:

$$\phi_1 = \mathcal{A}\, e^{-\frac{R^2}{2\sigma_R^2}} e^{-\frac{z^2}{2\sigma_z^2}} \tag{5.17}$$

where σ_z is the typical longitudinal extension of the system, σ_R is the typical extension of the system along the transverse confined direction and $R = \sqrt{\mathbf{x}^2 + \mathbf{y}^2}$ is the modulus of a vector that belongs to the transverse radial direction. The factor $\mathcal{A}$ is the normalization constant that can be found by imposing the normalization to the fix number of particles of the first component N_1:

$$N_1 = \int d^3\mathbf{r}\, |\phi_1(\mathbf{r})|^2 = \mathcal{A}^2\, 2\pi \int_0^{+\infty} dR\, R \int_{-\infty}^{+\infty} dz\, e^{-\frac{R^2}{\sigma_R^2}} e^{-\frac{z^2}{\sigma_z^2}} = \mathcal{A}^2\, \pi^{3/2} \sigma_z \sigma_R^2 \tag{5.18}$$

from which

$$\mathcal{A} = \left(\frac{N_1}{\pi^{3/2} \sigma_z \sigma_R^2} \right)^{1/2} \tag{5.19}$$

Hence, the wave functions of the two components of the mixture are:

$$\phi_1(z, R) = \left(\frac{N_1}{\pi^{3/2} \sigma_z \sigma_R^2} \right)^{1/2} e^{-\frac{R^2}{2\sigma_R^2}} e^{-\frac{z^2}{2\sigma_z^2}} \tag{5.20}$$

$$\phi_2(z, R) = \left(\frac{N_1}{\pi^{3/2} \sigma_z \sigma_R^2} \sqrt{\frac{g_{11}}{g_{22}}} \right)^{1/2} e^{-\frac{R^2}{2\sigma_R^2}} e^{-\frac{z^2}{2\sigma_z^2}} \tag{5.21}$$

where, recalling the computations in chapter 3, we used again the assumption that the ratio between densities (and thus between the number of particles) is fixed everywhere and equal to:

$$\frac{\rho_1}{\rho_2} = \frac{|\phi_1|^2}{|\phi_2|^2} = \sqrt{\frac{g_{22}}{g_{11}}} \tag{5.22}$$

Assuming an external transverse harmonic potential with characteristic frequency ω_1 for the ^{41}K component and ω_2 for the ^{87}Rb component, the total energy expression for this heteronuclear mixture is:

$$\begin{aligned} E = \int d\mathbf{r} \Bigg[& \frac{\hbar^2}{2m_1} |\nabla \phi_1|^2 + \frac{\hbar^2}{2m_2} |\nabla \phi_2|^2 + \frac{1}{2} g_{11} |\phi_1|^4 + \frac{1}{2} g_{22} |\phi_2|^4 + g_{12} |\phi_1|^2 |\phi_2|^2 + \\ & + \frac{1}{2} m_1 \omega_1 R^2 |\phi_1|^2 + + \frac{1}{2} m_2 \omega_2 R^2 |\phi_2|^2 + \mathcal{E}_{\mathrm{LHY}} \left(|\phi_1|^2, |\phi_2|^2 \right) \Bigg] \end{aligned} \tag{5.23}$$

It is the same energy functional for a bosonic mixture seen in chapter 3, with the addition of the harmonic potential terms for the two species, that are the fundamental tool for the dimensional reduction of the system.
By inserting $\phi_1(z, R)$ and $\phi_2(z, R)$ given by equations (B.1) and (B.2), we compute all the energy contributions as a function of the free parameters of the wave functions σ_z and σ_R (for a detailed description of all computations see Appendix B). To simplify the notation we define the following coefficients:

$$a = \frac{\hbar^2}{2} \frac{N_1}{2} \left(\frac{1}{m_1} + \frac{1}{m_2} \sqrt{\frac{g_{11}}{g_{22}}} \right) \tag{5.24}$$

$$b = \frac{1}{2^{5/2}} \frac{N_1^2}{\pi^{3/2}} \left(2 g_{11} + 2 g_{12} \sqrt{g_{11} g_{22}} \right) = \frac{1}{2^{3/2}} \frac{N_1^2}{\pi^{3/2}} \sqrt{\frac{g_{11}}{g_{22}}} \delta g \tag{5.25}$$

$$c = \frac{N_1}{2} \left(m_1 \omega_1^2 + m_2 \omega_2^2 \sqrt{\frac{g_{11}}{g_{22}}} \right) \tag{5.26}$$

$$d = \frac{16}{15\sqrt{\pi}} \bar{f} \sqrt{2} \left(\frac{g_{11} N_1}{\pi^{3/2}} \right)^{5/2} \left(\frac{m_1}{5\hbar^2} \right)^{3/2} \tag{5.27}$$

where δg is the parameter defined in equation (1.37) and $\bar{f}$ is the constant value of the function f defined in section for a fixed ratio between densities.
With this notation, the total energy for the bosonic mixture under a transverse harmonic confinement as a function of the free variational parameters σ_R and σ_z reads:

$$E = a \left(\frac{2\sigma_z^2 + \sigma_R^2}{\sigma_z^2 \sigma_R^2} \right) + b \left(\frac{1}{\sigma_z \sigma_R^2} \right) + c\, \sigma_R^2 + d \left(\frac{1}{\sigma_z \sigma_R^2} \right)^{3/2} \tag{5.28}$$

A numerical simulation is performed to find the values of parameters σ_z and σ_R that minimize the total energy for a fixed value of particles N and for a given interspecies scattering length a_{12}.
In particular, simulation are performed using the following parameters:

$$\omega_1 = 100\, Hz \tag{5.29}$$

$$\omega_2 = 80\, Hz \tag{5.30}$$

$$\omega_m = \sqrt{\omega_1 \omega_2} \approx 90\, Hz \tag{5.31}$$

$$a_{\mathrm{ho}} = \sqrt{\frac{\hbar}{m_r \omega_m}} \approx 9.5 \cdot 10^5\, a_0 \tag{5.32}$$

where ω_m is the geometrical average of the two frequencies, a_{ho} the characteristic size along the transverse directions and m_r the reduced mass. Notice that in the total energy expression we are taking into account quantum fluctuations embodied in the Lee-Huang-Yang term so the droplets formation is possible above a critical number of atoms. We expect that for small values of N the energy has a single minimum corresponding to a dilute and elongated bright soliton state and that for large values of N the energy minimum corresponds to a dense solution with a spatial extension $\sigma_z \sim \sigma_R \ll a_{\mathrm{ho}}$, that is a quantum self-bound droplet [8].
Figures 5.8, 5.9 and 5.10 show some results:

- For the given scattering length $a_{12} = -90\, a_0$, the nature of the self-bound state changes from soliton-like to droplet-like by increasing the number of particles N, as expected. The soliton state has a longitudinal size σ_z larger then the transverse size σ_R, instead for the droplet they are comparable and smaller than the characteristic harmonic length ($\sigma_z \sim \sigma_R \ll a_{\mathrm{ho}}$), as expected. The crossover between soliton and droplet state is continuous, as proved by the fact that the total energy (computed for variational parameters selected by the minimization) is a continuous function of the total number of particles N (see figure 5.10(a)). Figures 5.8 show the energy as a function of the radial σ_R and longitudinal σ_z size for $N = 2000$ (soliton), $N = 4000$ (crossover region) and $N = 6000$ (droplet).

- For the given scattering length $a_{12} = -98\, a_0$, again the nature of the self-bound state changes from soliton-like to droplet-like by increasing the number of particles N but a bistable region exists. For a certain number of particle range, both solutions coexist as proved by the fact that the total energy computed for variational parameters selected by the minimization can have two minima (see figure 5.10(b)). Figures 5.9 show the energy as a function of the radial σ_R and longitudinal σ_z size for $N = 1500$ (soliton), $N = 1900$ (bistable region) and $N = 3000$ (droplet).

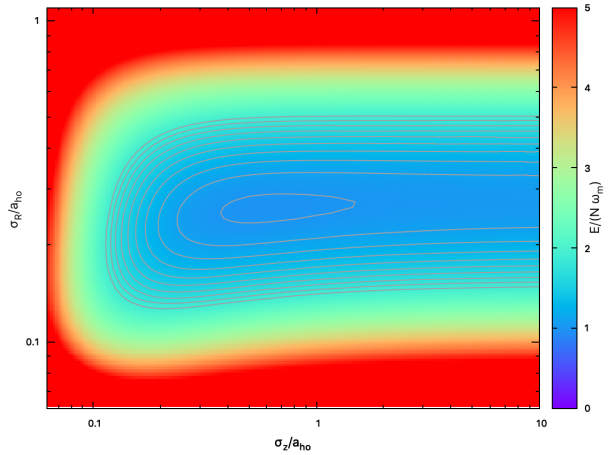

(a) $N = 2000$, soliton state.

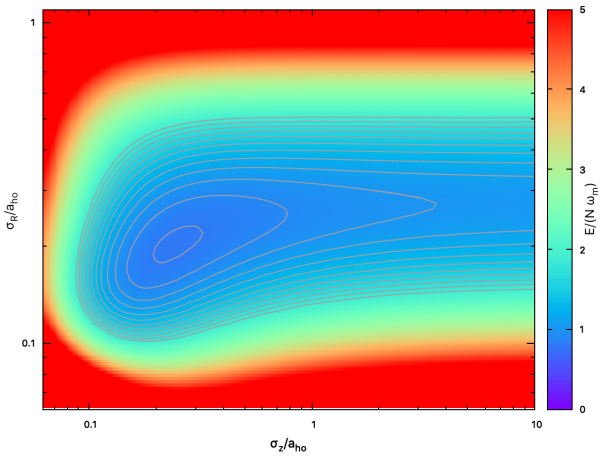

(b) $N = 4000$, crossover region.

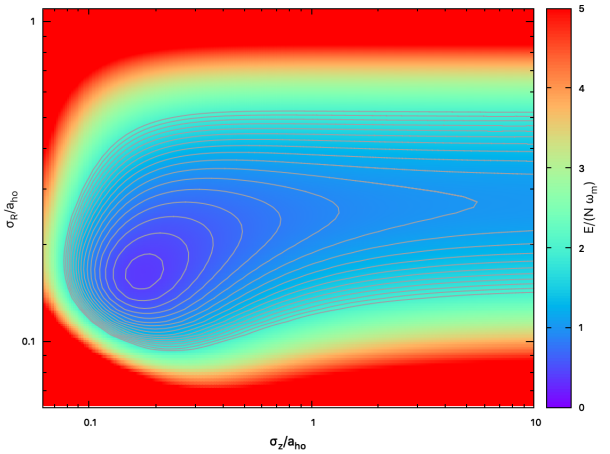

(c) $N = 6000$, quantum droplet.

Figure 5.8: The maps show the energy of the self-bound state for $a_{12} = -90\,a_0$ as a function of the radial σ_R and longitudinal σ_z size for $N = 2000$ (soliton), $N = 4000$ (crossover region) ans $N = 4000$ (droplet).

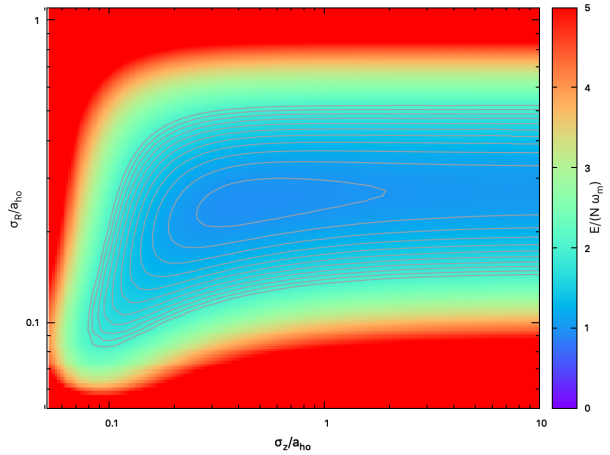

(a) $N = 1500$, soliton state.

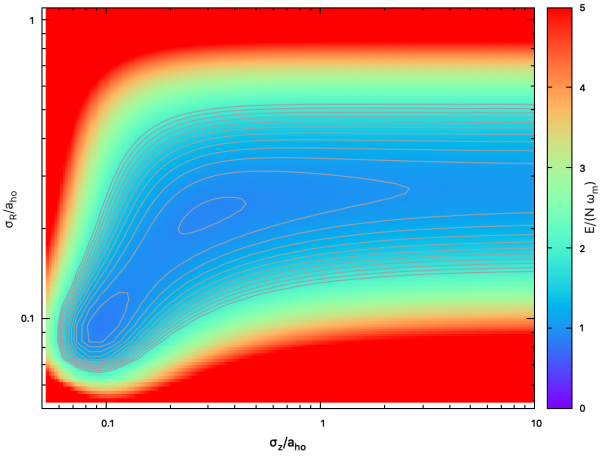

(b) $N = 1900$, bistable region.

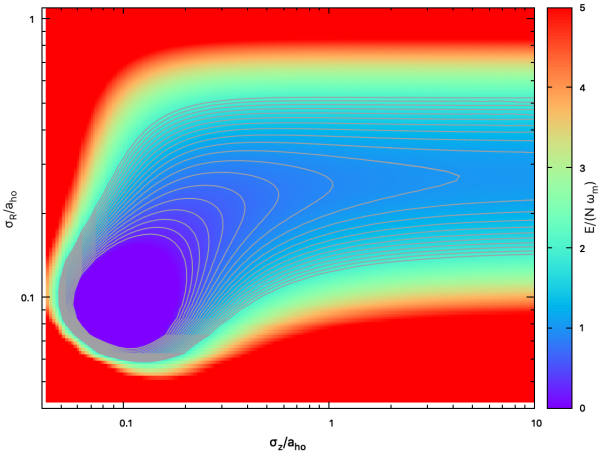

(c) $N = 3000$, quantum droplet.

Figure 5.9: The maps show the energy of the self-bound state for $a_{12} = -98\,a_0$ as a function of the radial σ_R and longitudinal σ_z size for $N = 1500$ (soliton), $N = 1900$ (bistable region) ans $N = 3000$ (droplet).

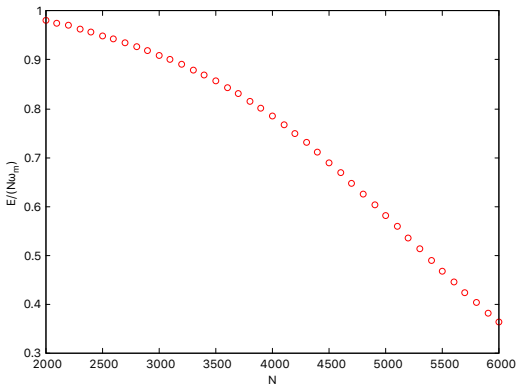

(a) $a_{12} = -90\,a_0$

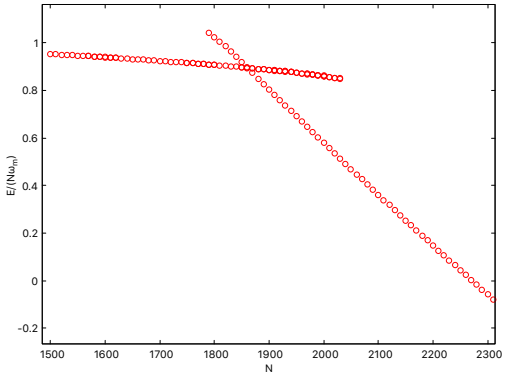

(b) $a_{12} = -98\,a_0$

Figure 5.10: Total energy computed for the variational parameters selected by the minimization as function of the total number of particles N: (a) for $a_{12} = -90\,a_0$ the continuous trend confirms the absence of a bistable region in which both bright soliton states and droplets coexist while (b) for $a_{12} = -98\,a_0$ in the range $1800 \lesssim N \lesssim 2050$ both bright soliton states and droplets coexist.

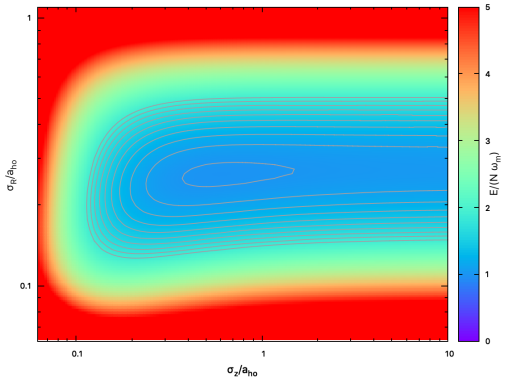

(a) $a_{12} = -90\,a_0$, soliton.

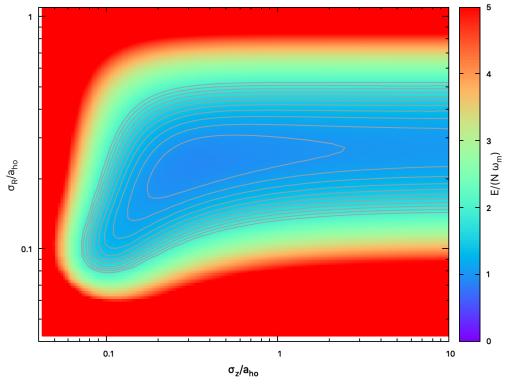

(b) $a_{12} = -96\,a_0$, soliton.

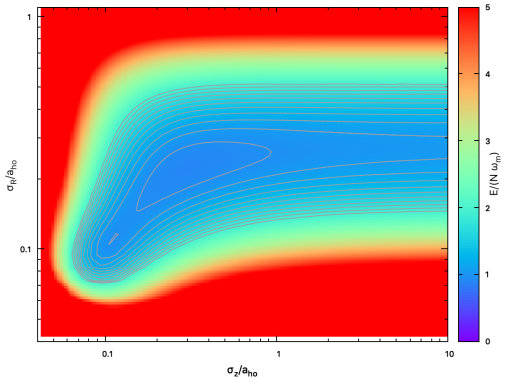

(c) $a_{12} = -97\,a_0$, bistable region.

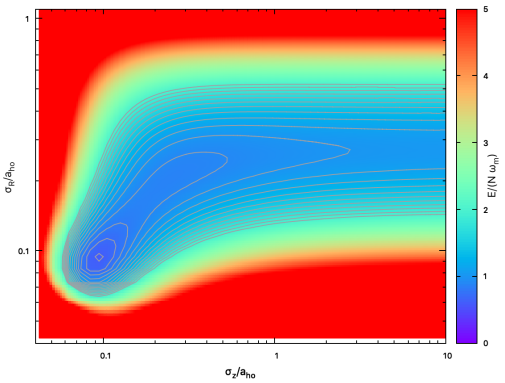

(d) $a_{12} = -98\,a_0$, droplet.

Figure 5.11: By keeping constant the total number of particles to $N = 2000$, the self-bound state moves from soliton-like to droplet-like when a_s decreases from $a_s = -90\,a_0$ to $a_s = -98\,a_0$ passing through the bistable region.

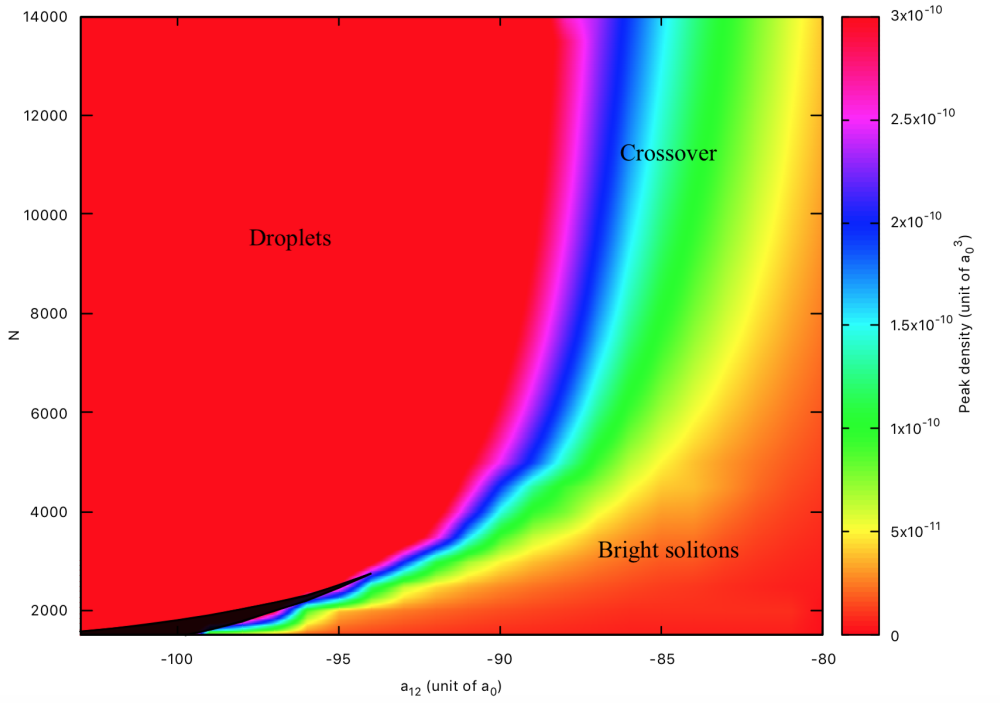

Figure 5.12: Soliton-to-droplet diagram: ground state peak density as a function of the total number of particles N and the scattering length a_{12}. The red region (top left) identifies the droplet regime, the orange region (bottom right) identifies the bright solitons solutions, the the black area (bottom left) is the bistable region where both the bright soliton state and the quantum droplet can exist.

Figure 5.11 shows how the self-bound ground state moves from soliton-like to droplet-like when a_s decreases from $a_s = -90\,a_0$ to $a_s = -98\,a_0$ passing through the bistable region, this time for a fixed number of particles $N = 2000$.
All these information can be summed in the final **soliton-to-droplet diagram** in figure 5.12, obtained by computing the ground state peak density of the the mixture in a quasi-1D system from the numerical solution of the two coupled Gross-Pitaevskii equations. The two condensate wave functions ψ_1 and ψ_2 associated to the mixture components are again connected to the numerical density as $\rho_i = |\psi_i|^2$ for $i = 1, 2$. The imaginary time technique is used again to solve:

$$\begin{cases} \left(-\frac{\hbar^2}{2m_1}\nabla^2 + V_1\left(\rho_1, \rho_2\right)\right)\psi_1 = \mu_1\psi_1 \\ \left(-\frac{\hbar^2}{2m_2}\nabla^2 + V_2\left(\rho_1, \rho_2\right)\right)\psi_2 = \mu_2\psi_2 \end{cases} \tag{5.33}$$

where μ_i is the chemical potential of the i species and

$$V_1 = g_{11}\rho_1 + g_{12}\rho_2 + \frac{1}{2}\,m_1\omega_1^2\,(x^2 + y^2) + \frac{\delta E_{\mathrm{LHY}}}{\delta\rho_1} \tag{5.34}$$

$$V_2 = g_{22}\rho_2 + g_{12}\rho_1 + \frac{1}{2}\,m_2\omega_2^2\,(x^2 + y^2) + \frac{\delta E_{\mathrm{LHY}}}{\delta\rho_2} \tag{5.35}$$

that are the effective potentials felt by each species of the mixture in presence of an external harmonic confinement along x-axis and y-axis. In figure 5.12, the color scales like

the ground state peak density represented in function of the interspecies scattering length a_{12} and the total number of particles N. The black area is the bistable region computed from the variational method by selecting the range in which energy has two minima, for a given a_{12}: it becomes smoothly connected in the crossover region around $a_{12} \sim -94\,a_0$. The red region (top left) identifies the droplet regime, where the solution of the GPE is a dense and isotropic self-bound state with $\sigma_R \sim \sigma_z \ll a_{\text{ho}}$, while the orange region (bottom right) identifies the bright solitons solutions of the GPE, more diluted and elongated along the longitudinal axis.

5.3 Real time evolution of the soliton state

One of the fundamental features of the bright soliton state is that it is linked to the quasi-1D configuration of the system, i.e., once the trap is released, it evaporates, while a quantum droplet remains stable also in free-space, as discussed in the previous chapters. Starting from the solitonic ground state of the ^{41}K-^{87}Rb bosonic mixture affected by the harmonic confinement along y and z, a numerical simulation is performed to study the real-time evolution of the system. At time $t = 0$ the external trap is released and the evolution is made by solving numerically the two coupled time-dependent Gross-Pitaevskii equation in free-space:

$$\begin{cases} \left(-\frac{\hbar^2}{2m_1}\nabla^2 + V_1\left(\rho_1, \rho_2\right)\right)\psi_1 = i\hbar\frac{\partial\psi_1}{\partial t} \\ \left(-\frac{\hbar^2}{2m_2}\nabla^2 + V_2\left(\rho_1, \rho_2\right)\right)\psi_2 = i\hbar\frac{\partial\psi_2}{\partial t} \end{cases} \tag{5.36}$$

where

$$V_1 = g_{11}\rho_1 + g_{12}\rho_2 + \frac{\delta E_{\text{LHY}}}{\delta\rho_1} \tag{5.37}$$

$$V_2 = g_{22}\rho_2 + g_{12}\rho_1 + \frac{\delta E_{\text{LHY}}}{\delta\rho_2} \tag{5.38}$$

The initial condition of the system is given by the ground state density of the trapped system, computed by an imaginary time evolution. In figure 5.13 some ground states are represented in the plane $x - y$ with $N \approx 33000$, $\omega_{z,1} = \omega_{y,1} = 120\,Hz$ and $\omega_{z,2} = \omega_{y,2} = 80\,Hz$ for a set of a_{12} values. For $a_{12} = -80\,a_0$ the system has an elongated and dilute solitonic state, by increasing the absolute value of a_{12} it approaches more and more to a dense localized droplet. Since we want to study a soliton evaporation, the real-time evolution will be done for a system with $a_{12} = -80\,a_0$ with the initial condition given by the ground state density shown in figure 5.13(a).
The numerical method used to solve these GP equations is the **Predictor-Modifier-Corrector** method that is a variation of the predictor-corrector method for the solution of ordinary differential equations [54]. In general, given a differential equation

$$\frac{dy}{dx} = f(x, y) \qquad y_i^{'} = \frac{dy}{dx}\Big|_{x=x_i} \tag{5.39}$$

a predictor-corrector algorithm performs the following steps:

- Predict the value of y at $x = x_{n+1}$, called $\bar{y}_{n+1}$ (prediction).
- Using the differential equation, calculate $\bar{y}_{n+1}^{'} = f(x_{n+1}, \bar{y}_{n+1})$.
- Calculate again a new y_{n+1}, using an iterative formula (correction).
- Repeat these two last steps until y_{n+1} reaches convergence.

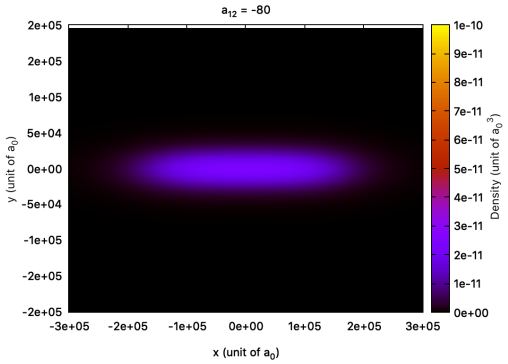

(a) $a_{12} = -80\, a_0$.

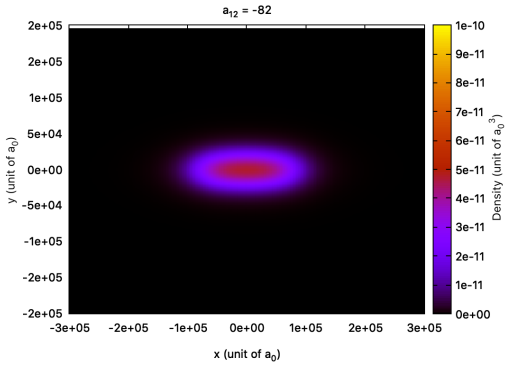

(b) $a_{12} = -82\, a_0$.

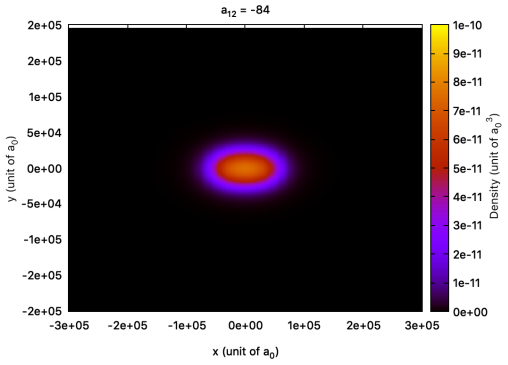

(c) $a_{12} = -84\, a_0$.

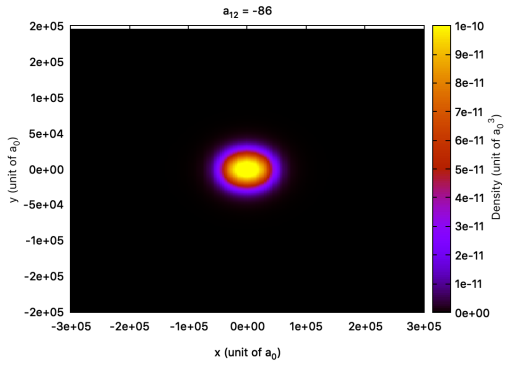

(d) $a_{12} = -86\, a_0$.

Figure 5.13: Ground state densities of ^{41}K-^{87}Rb bosonic mixture in a quasi-1D configuration in the plane $x - y$ for a set of four values of the scattering length a_{12}.

The advantage of the iterative integration formula is the high accuracy they achieve at each step, however the successive recalculations of $f(x, y)$ at each step until convergence is reached could be a disadvantage for the large computational cost. One way of avoiding the iteration is to accept the first value of the corrector as y_{n+1} or, a more sophisticated non-iterative variation is the Predictor-Modifier-Corrector method given by the following set of equations:

- The value of y_{n+1} is predicted with p_{n+1}:

$$p_{n+1} = y_{n-3} + \frac{4h}{3}(2y_n^{'} - y_{n-1}^{'} + 2y_{n-2}^{'}) \tag{5.40}$$

  where $h = x_{i+1} - x_i$ is the space step.

- The predictor is modified by m_{n+1}:

$$m_{n+1} = p_{n+1} - \frac{28}{29}(p_n - c_n) \tag{5.41}$$

  with

$$m_{n+1}^{'} = f(x_{n+1}, m_{n+1}) \tag{5.42}$$

- The corrector c_{n+1} is computed:

$$c_{n+1} = y_{n-1} + \frac{h}{3}\left(m_{n+1}^{'} + 4y_n^{'} + y_{n-1}^{'}\right) \tag{5.43}$$

- The final value of y_{n+1} is:

$$y_{n+1} = c_{n+1} + \frac{1}{29}(p_{n+1} - c_{n+1}) \tag{5.44}$$

Due to the absence of iteration, since only two values of $f(x, y)$ are computed at each step, this method is optimized for this kind of time evolution and it is also stable.
In figure 5.14 there is the real time evolution of the solitonic state in the $x - y$ plane with the corresponding time evolution of the density along the transverse direction y integrated along x and z. The density range in the figures is kept constant and, as expected, the soliton evaporates in a few milliseconds and, in particular, it expands isotropically along the directions where it was previously confined.
In conclusion, the optical waveguide plays a crucial role for a bosonic binary mixture, which can host both bright solitons and quantum droplets in this configuration. The releasing of the external trap clearly reveals the nature of the two self-bound state: while a droplet is stable in free-space, the soliton evaporates and the absence of the trapping potential leads to a complete dissipation of the localised wave packet. Another interesting experimental possibility for the future could be the study of collisions between bright solitons in mixture of Bose-Einstein condensates in comparison to droplets collisions, for a deeper investigation of dynamical properties of the localized quantum states in BECs [55, 56].

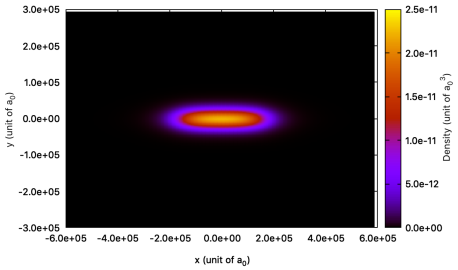

(a) $t = 0.35\,ms$.

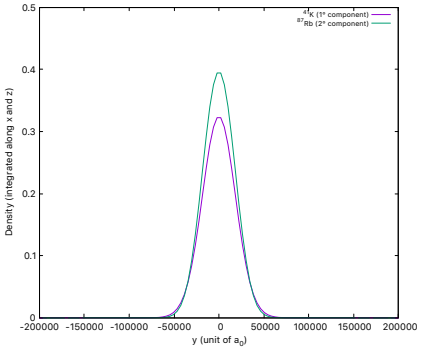

(b) $t = 0.35\,ms$.

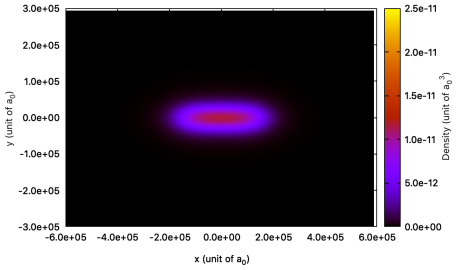

(c) $t = 1.78\,ms$.

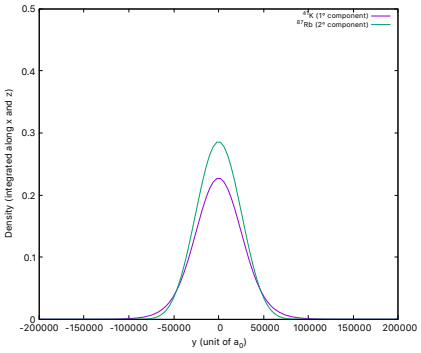

(d) $t = 1.78\,ms$.

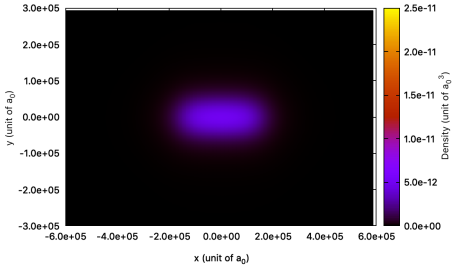

(e) $t = 3.55\,ms$.

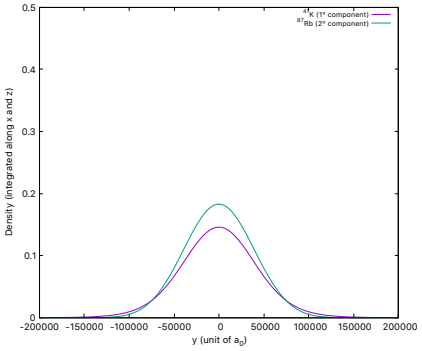

(f) $t = 3.55\,ms$.

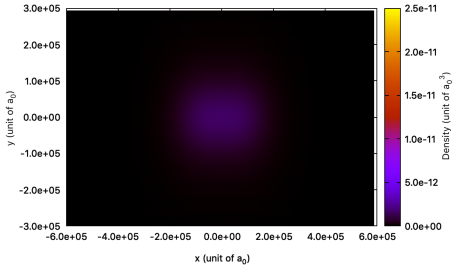

(g) $t = 7.12\,ms$.

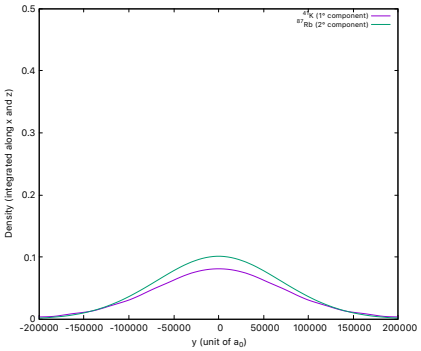

(h) $t = 7.12\,ms$.

Figure 5.14: Left column: real time evolution of the soliton state in the $x-y$ plane. Right column: real time evolution of the density along y integrated along x and z.

Conclusions

In this thesis we studied a bosonic ^{41}K-^{87}Rb mixture of Bose–Einstein condensates with tunable interspecies interaction in the self-bound regime by means of numerical simulations based on the Density Functional Theory. The competition between the mean-field interspecies attraction and the Lee-Huang-Yang beyond mean-field repulsion leads to the droplet formation with numerical densities of an order of magnitude of $10^{14} - 10^{15}$ atoms/cm^3, an extremely low density compared to any other existing liquids. Among the three methods used to study surface properties of the self-bound droplets in free space, the numerical method reveals to be the simplest, it allows to compute the radial density profile and the surface tension of the droplet easily and all the results are in agreement with the correct solution obtained by directly solving the two coupled Gross-Pitaevskii equation associated to the two components of the ^{41}K-^{87}Rb mixture. The energy of the droplets is well accounted for by the liquid-drop model and the Tolman length, obtained from the fitting coefficients of this model, allows to apply a curvature correction to the surface tension. By confining the bosonic binary mixture in a quasi-1D configuration with an optical waveguide, the transition between bright solitons and self-bound droplets is studied, highlighting the presence of a bistable region in which both localized states coexist.

Appendices

Appendix A

Derivation of the bright soliton's analytical solution

Here we derive the analytical formula of the bright soliton state, an exact solution of the dimensional reduced 1D time-dependent Gross-Pitaevskii equation along the non-confined direction z seen in chapter 5:

$$i\hbar\frac{\partial}{\partial t}f(z,t)=\left[\frac{\hbar^2}{2m}\frac{\partial^2}{\partial z^2}+\gamma|f(z,t)|^2\right]f(z,t) \tag{A.1}$$

The solution of the GP equation reads [51]

$$f(z,t)=\phi\left(z-vt\right)e^{iv(z-vt)}e^{\left(i\frac{mv^2/2-\mu}{\hbar}t\right)} \tag{A.2}$$

with $\mu=-\frac{m\gamma^2}{16\hbar^2}<0$ and γ the effective one-dimensional interaction strength defined in section 5.1. The aim is to find the correct form for the function $\phi\left(z-vt\right)$. We can work in the moving reference frame by changing variable $z\rightarrow z-vt=\xi$ (in this way the function ϕ is time-independent and centred in $\xi=0$). Inserting the function $f(\xi)$ in equation (A.1) one finds the 1D stationary GP equation for $\phi\left(\xi\right)$:

$$\left[\frac{\hbar^2}{2m}\frac{\partial^2}{\partial\xi^2}+\gamma|\phi\left(\xi\right)|^2\right]\phi\left(\xi\right)=\mu\phi\left(\xi\right) \tag{A.3}$$

Assuming that $\phi\left(\xi\right)$ is real and defining the function

$$W\left(\phi\right)=\frac{1}{2}\frac{m|\gamma|}{\hbar^2}\phi^4+\frac{m\mu}{\hbar^2}\phi^2 \tag{A.4}$$

equation (A.3) can be rewritten as

$$\frac{\partial^2\phi}{\partial\xi^2}=-\frac{\partial W\left(\phi\right)}{\partial\phi} \tag{A.5}$$

Written in this form, the GPE is the equation of motion of the quantity ϕ in function of the variable ξ. In analogy to the unidimensional Newton equation and the consequent conservation of total energy [57], the correspondent conserved quantity for this dynamical

system is:

$$E = \frac{1}{2}\frac{\partial \phi}{\partial \xi} + W(\phi) \tag{A.6}$$

from which

$$\frac{\partial \phi}{\partial \xi} = \sqrt{2(E - W(\phi))} \tag{A.7}$$

Recalling that $|\phi|$ is the modulus of the condensate wave function of the system along z in the moving reference frame along z direction, we can impose that $\phi(\xi) \to 0$ and $\frac{\partial \phi}{\partial \xi} \to 0$ as $|\xi| = |z - vt| \to \infty$. This is reasonable since the system is finite and at a finite time at long distance the wave function must approach asymptotically to zero.
Computing equation (A.6) in these limiting conditions, it is clear that the conserved quantity must be zero $E = 0$.
As direct a consequence, one gets:

$$d\xi = \frac{d\phi}{\sqrt{-2W(\phi)}} \tag{A.8}$$

Integrating both members from $\xi = 0$ to a general $\xi = \xi^{'}$ one finds:

$$\begin{aligned} \int_0^{\xi^{'}} d\xi &= \int_{\phi(0)}^{\phi(\xi^{'})} \frac{d\phi}{\sqrt{-\frac{m|\gamma|}{\hbar^2}\phi^4 - \frac{2m\mu}{\hbar^2}\phi^2}} = \\ &= \int_{\phi(0)}^{\phi(\xi^{'})} \frac{d\phi}{\sqrt{-\frac{m|\gamma|}{\hbar^2}\phi^4 + \frac{2m|\mu|}{\hbar^2}\phi^2}} \end{aligned} \tag{A.9}$$

We can set $\frac{\partial \phi}{\partial \xi}\big|_{\xi=0} = 0$: the wave function we are looking for is centered in $\xi = 0$ (we moved to the new reference frame for this reason) and it is symmetric so it is quite reasonable to assume the presence of a maximum in the central point. Hence, from the computation of equation (A.6) for $\xi = 0$ one finds the result:

$$\phi(0) = \sqrt{\frac{2|\mu|}{\gamma}} \tag{A.10}$$

Performing the integration of equation (A.9), making a final substitution $\xi^{'} \to \xi$ and by reversing the function, the result is:

$$\phi(\xi) = \sqrt{\frac{2|\mu|}{|\gamma|}} sech\left[\sqrt{\frac{m|\mu|}{\hbar^2}}\xi\right] \tag{A.11}$$

Taking into account that $\mu = -\frac{m\gamma^2}{16\hbar^2}$, one gets the final form seen in (5.14). This is a solitonic solution: in the moving reference frame the profile does not spread in time and it remain always the same. This observation concludes the complete derivation of the analytical bright soliton solution of the 1D GP equation, obtained from a dimensional reduction of the 3D GP equation of a system in a transverse confinement.

Appendix B

Total energy expression for a mixture of BECs in a quasi-1D configuration

Here we derive the total energy expression of a binary bosonic mixture, assuming a fixed ratio between the densities of the two components. The normalized wave functions of the two components of the mixture are:

$$\phi_1(z,R) = \left(\frac{N_1}{\pi^{3/2}\sigma_z\sigma_R^2}\right)^{1/2} e^{-\frac{R^2}{2\sigma_R^2}} e^{-\frac{z^2}{2\sigma_z^2}} \tag{B.1}$$

$$\phi_2(z,R) = \left(\frac{N_1}{\pi^{3/2}\sigma_z\sigma_R^2}\sqrt{\frac{g_{11}}{g_{22}}}\right)^{1/2} e^{-\frac{R^2}{2\sigma_R^2}} e^{-\frac{z^2}{2\sigma_z^2}} \tag{B.2}$$

The total energy expression to be computed is:

$$\begin{aligned} E = \int d\mathbf{r} \Bigg[&\frac{\hbar^2}{2m_1}|\nabla\phi_1|^2 + \frac{\hbar^2}{2m_2}|\nabla\phi_2|^2 + \frac{1}{2}g_{11}|\phi_1|^4 + \frac{1}{2}g_{22}|\phi_2|^4 + g_{12}|\phi_1|^2|\phi_2|^2 + \\ &+ \frac{1}{2}m_1\omega_1 R^2|\phi_1|^2 + + \frac{1}{2}m_2\omega_2 R^2|\phi_2|^2 + \mathcal{E}_{\mathrm{LHY}}\left(|\phi_1|^2, |\phi_2|^2\right) \Bigg] \end{aligned} \tag{B.3}$$

The two wave functions are decomposed in two directions:

- The radial direction $\vec{R}$ in the $x-y$ plane, where the harmonic confinement is present.
- The $\vec{z}$ direction in absence of any confinement.

For this reason, cylindrical coordinates are a convenient choice to solve the integral (see figure B.1). Since the wave functions do not depend on θ, one has

$$\int d\mathbf{r} = 2\pi \int_0^{+\infty} dR\, R \int_{-\infty}^{+\infty} dz \tag{B.4}$$

We can compute the total energy term by term:

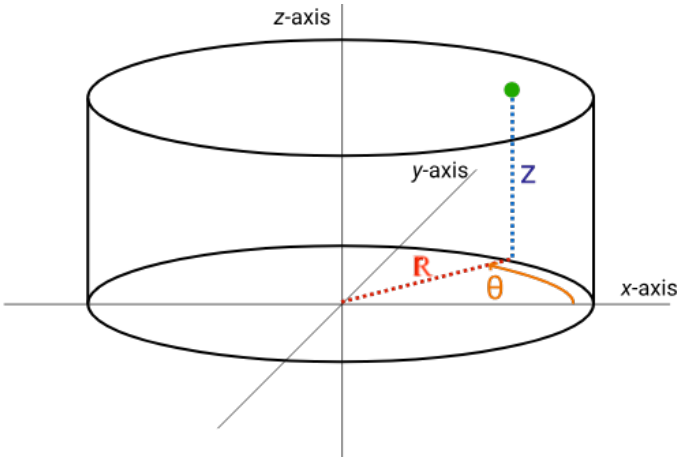

Figure B.1: A generic cylindrical coordinate system: R is the distance of the projection of the green generic point in the $x-y$ plane from the origin, θ is the angle between the x-axis and that same projection of the green point in the $x-y$ plane and z is the height of the green point.

- The kinetic term for the first mixture component $E_{\text{kin},1}$:

$$\begin{aligned} E_{\text{kin},1} &= \int d\mathbf{r}\, \frac{\hbar^2}{2m_1} |\nabla \phi_1|^2 = \\ &= 2\pi \int_0^{+\infty} dR\, R \int_{-\infty}^{+\infty} dz\, \frac{\hbar^2}{2m_1} \left| \frac{\partial \phi_1}{\partial R} \cdot \mathbf{R} + \frac{\partial \phi_1}{\partial z} \cdot \mathbf{z} \right|^2 = \\ &= \frac{\hbar^2}{m_1} \frac{N_1}{\sqrt{\pi}\sigma_z \sigma_R^2} \left[\frac{1}{2}\sqrt{\pi}\sigma_z + \frac{\sigma_R^2 \sqrt{\pi}}{4\sigma_z} \right] = \\ &= \frac{\hbar^2}{2m_1} \frac{N_1}{2} \left(\frac{2\sigma_z^2 + \sigma_R^2}{\sigma_z^2 \sigma_R^2} \right) \end{aligned} \tag{B.5}$$

- The kinetic term for the second mixture component $E_{\text{kin},2}$:

$$\begin{aligned} E_{\text{kin},2} &= \int d\mathbf{r}\, \frac{\hbar^2}{2m_2} |\nabla \phi_2|^2 = \\ &= 2\pi \int_0^{+\infty} dR\, R \int_{-\infty}^{+\infty} dz\, \frac{\hbar^2}{2m_2} \left| \frac{\partial \phi_2}{\partial R} \cdot \mathbf{R} + \frac{\partial \phi_2}{\partial z} \cdot \mathbf{z} \right|^2 = \\ &= \frac{\hbar^2}{m_2} \frac{N_1}{\sqrt{\pi}\sigma_z \sigma_R^2} \sqrt{g_{11} g_{22}} \left[\frac{1}{2}\sqrt{\pi}\sigma_z + \frac{\sigma_R^2 \sqrt{\pi}}{4\sigma_z} \right] = \\ &= \frac{\hbar^2}{2m_1} \frac{N_1}{2} \sqrt{\frac{g_{11}}{g_{22}}} \left(\frac{2\sigma_z^2 + \sigma_R^2}{\sigma_z^2 \sigma_R^2} \right) \end{aligned} \tag{B.6}$$

- The MF intraspecies interaction term for the first mixture component $E_{\mathrm{MF},1}$:

$$\begin{aligned} E_{\mathrm{MF},1} &= \int d\mathbf{r}\, \frac{1}{2} g_{11} |\phi_1|^4 \\ &= \frac{1}{2} g_{11}\, 2\pi \int_0^{+\infty} dR\, R \int_{-\infty}^{+\infty} dz\, |\phi_1|^4 = \\ &= \frac{1}{2} g_{11}\, 2\pi \int_0^{+\infty} dR\, R\, e^{-\frac{2R^2}{\sigma_R^2}} \int_{-\infty}^{+\infty} dz\, e^{-\frac{2z^2}{\sigma_z^2}} \left(\frac{N_1}{\pi^{3/2} \sigma_z \sigma_R^2} \right)^2 = \\ &= \frac{1}{2^{5/2}} g_{11} \frac{N_1^2}{\pi^{3/2} \sigma_z \sigma_R^2} \end{aligned} \tag{B.7}$$

- The MF intraspecies interaction term for the second mixture component $E_{\mathrm{MF},2}$:

$$\begin{aligned} E_{\mathrm{MF},2} &= \int d\mathbf{r}\, \frac{1}{2} g_{22} |\phi_2|^4 \\ &= \frac{1}{2} g_{22}\, 2\pi \int_0^{+\infty} dR\, R \int_{-\infty}^{+\infty} dz\, |\phi_2|^4 = \\ &= \frac{1}{2} g_{22} \frac{g_{11}}{g_{22}}\, 2\pi \int_0^{+\infty} dR\, R\, e^{-\frac{2R^2}{\sigma_R^2}} \int_{-\infty}^{+\infty} dz\, e^{-\frac{2z^2}{\sigma_z^2}} \left(\frac{N_1}{\pi^{3/2} \sigma_z \sigma_R^2} \right)^2 = \\ &= \frac{1}{2^{5/2}} g_{11} \frac{N_1^2}{\pi^{3/2} \sigma_z \sigma_R^2} \end{aligned} \tag{B.8}$$

- The MF interspecies interaction term $E_{\mathrm{MF},12}$:

$$\begin{aligned} E_{\mathrm{MF},12} &= \int d\mathbf{r}\, g_{12} |\phi_1|^2 |\phi_2|^2 \\ &= g_{12}\, 2\pi \int_0^{+\infty} dR\, R \int_{-\infty}^{+\infty} dz\, |\phi_1|^4 \sqrt{\frac{g_{11}}{g_{22}}} = \\ &= \frac{1}{2^{3/2}} g_{12} \sqrt{\frac{g_{11}}{g_{22}}} \frac{N_1^2}{\pi^{3/2} \sigma_z \sigma_R^2} \end{aligned} \tag{B.9}$$

- The external energy for the first mixture component $E_{\mathrm{ext},1}$:

$$\begin{aligned} E_{\mathrm{ext},1} &= \int d\mathbf{r}\, \frac{1}{2} m_1 \omega_1^2 R^2 |\phi_1|^2 \\ &= m_1 \omega_1^2 \pi \int_0^{+\infty} dR\, R^3\, e^{-\frac{R^2}{\sigma_R^2}} \int_{-\infty}^{+\infty} dz\, e^{-\frac{z^2}{\sigma_z^2}} \left(\frac{N_1}{\pi^{3/2} \sigma_z \sigma_R^2} \right) = \\ &= \frac{N_1 m_1 \omega_1^2}{2} \sigma_R^2 \end{aligned} \tag{B.10}$$

- The external energy for the second mixture component $E_{\text{ext},2}$:

$$\begin{aligned} E_{\text{ext},2} &= \int d\mathbf{r}\, \frac{1}{2} m_2 \omega_2^2 R^2 |\phi_2|^2 \\ &= m_2 \omega_2^2 \pi \int_0^{+\infty} dR\, R^3\, e^{-\frac{R^2}{\sigma_R^2}} \int_{-\infty}^{+\infty} dz\, e^{-\frac{z^2}{\sigma_z^2}} \left(\frac{N_1}{\pi^{3/2}\sigma_z \sigma_R^2} \sqrt{g_{11}} g_{22} \right) = \\ &= \frac{N_1 m_2 \omega_2^2}{2} \sqrt{\frac{g_{11}}{g_{22}}} \sigma_R^2 \end{aligned} \tag{B.11}$$

- The LHY term E_{LHY}:

$$\begin{aligned} E_{\text{LHY}} &= \int d\mathbf{r}\, \mathcal{E}_{\text{LHY}} \left(|\phi_1|^2, |\phi_2|^2 \right) = \\ &= 2\pi \int_0^{+\infty} dR\, R \int_{-\infty}^{+\infty} dz\, \frac{8}{15\pi^2} \left(\frac{m_1}{\hbar^2} \right)^{3/2} g_{11}^{5/2} |\phi_1|^5\, \bar{f} = \\ &= \frac{16}{15\pi} \left(\frac{m_1}{\hbar^2} \right)^{3/2} g_{11}^{5/2} \bar{f} \left(\frac{N_1}{\pi^{3/2}\sigma_R^2 \sigma_z} \right)^{5/2} \int_0^{+\infty} dR\, R\, e^{-\frac{5R^2}{2\sigma_R^2}} \int_{-\infty}^{+\infty} dz\, e^{-\frac{5z^2}{2\sigma_z^2}} = \\ &= \frac{16}{15\sqrt{\pi}} \bar{f} \sqrt{2} \left(\frac{g_{11} N_1}{\pi^{3/2}} \right)^{5/2} \left(\frac{m_1}{5\hbar^2 \sigma_R^2 \sigma_z} \right)^{3/2} \end{aligned} \tag{B.12}$$

  where $\bar{f}$ is the constant value of the function f for a fixed ratio between densities (as seen in section 5.2).

Thus, the total energy expression for mixture of BECs in a quasi-1D configuration is:

$$\begin{aligned} E = {} & \frac{\hbar^2}{2m_1} \frac{N_1}{2} \left(\frac{2\sigma_z^2 + \sigma_R^2}{\sigma_z^2 \sigma_R^2} \right) + \frac{\hbar^2}{2m_1} \frac{N_1}{2} \sqrt{\frac{g_{11}}{g_{22}}} \left(\frac{2\sigma_z^2 + \sigma_R^2}{\sigma_z^2 \sigma_R^2} \right) + \frac{1}{2^{3/2}} g_{11} \frac{N_1^2}{\pi^{3/2}\sigma_z \sigma_R^2} + \\ & + \frac{1}{2^{3/2}} g_{12} \sqrt{\frac{g_{11}}{g_{22}}} \frac{N_1^2}{\pi^{3/2}\sigma_z \sigma_R^2} + \frac{N_1 m_1 \omega_1^2}{2} \sigma_R^2 + \frac{N_1 m_2 \omega_2^2}{2} \sqrt{\frac{g_{11}}{g_{22}}} \sigma_R^2 + \\ & + \frac{16}{15\sqrt{\pi}} \bar{f} \sqrt{2} \left(\frac{g_{11} N_1}{\pi^{3/2}} \right)^{5/2} \left(\frac{m_1}{5\hbar^2 \sigma_R^2 \sigma_z} \right)^{3/2} \end{aligned} \tag{B.13}$$

Bibliography

[1] D. S. Petrov. "Quantum Mechanical Stabilization of a Collapsing Bose-Bose Mixture". In: *Physical Review Letters* 115.15 (Oct. 2015). ISSN: 1079-7114. DOI: 10.1103/physrevlett.115.155302.

[2] Bose. "Plancks Gesetz und Lichtquantenhypothese". In: *Zeitschrift fur Physik* 26.1 (Dec. 1924), pp. 178–181. DOI: 10.1007/BF01327326.

[3] Enric Pérez and Tilman Sauer. "Einstein's quantum theory of the monatomic ideal gas: Non-statistical arguments for a new statistics". In: *Archive for History of Exact Sciences* 64 (Sept. 2010), pp. 561–612. DOI: 10.1007/s00407-010-0066-x.

[4] F. LONDON. "The λ-Phenomenon of Liquid Helium and the Bose-Einstein Degeneracy". In: *Nature* 141.3571 (1938), pp. 643–644.

[5] M. H. Anderson et al. "Observation of Bose-Einstein Condensation in a Dilute Atomic Vapor". In: *Science* 269.5221 (1995), pp. 198–201. ISSN: 0036-8075. DOI: 10.1126/science.269.5221.198. eprint: https://science.sciencemag.org/content/269/5221/198.full.pdf. URL: https://science.sciencemag.org/content/269/5221/198.

[6] K. B. Davis et al. "Bose-Einstein Condensation in a Gas of Sodium Atoms". In: *Phys. Rev. Lett.* 75 (22 Nov. 1995), pp. 3969–3973. DOI: 10.1103/PhysRevLett.75.3969. URL: https://link.aps.org/doi/10.1103/PhysRevLett.75.3969.

[7] G. Semeghini et al. "Self-Bound Quantum Droplets of Atomic Mixtures in Free Space". In: *Phys. Rev. Lett.* 120 (23 June 2018), p. 235301. DOI: 10.1103/PhysRevLett.120.235301. URL: https://link.aps.org/doi/10.1103/PhysRevLett.120.235301.

[8] P. Cheiney et al. "Bright Soliton to Quantum Droplet Transition in a Mixture of Bose-Einstein Condensates". In: *Phys. Rev. Lett.* 120 (13 Mar. 2018), p. 135301. DOI: 10.1103/PhysRevLett.120.135301. URL: https://link.aps.org/doi/10.1103/PhysRevLett.120.135301.

[9] C. R. Cabrera et al. "Quantum liquid droplets in a mixture of Bose-Einstein condensates". In: *Science* 359.6373 (2018), pp. 301–304. ISSN: 0036-8075. DOI: 10.1126/science.aao5686. eprint: https://science.sciencemag.org/content/359/6373/301.full.pdf. URL: https://science.sciencemag.org/content/359/6373/301.

[10] Fatkhulla Abdullaev and Josselin Garnier. "Bright Solitons in Bose-Einstein Condensates: Theory". In: vol. 45. Dec. 2008, pp. 25–43. DOI: 10.1007/978-3-540-73591-5_2.

[11] C. D'Errico et al. "Observation of quantum droplets in a heteronuclear bosonic mixture". In: *Phys. Rev. Research* 1 (3 Dec. 2019), p. 033155. DOI: 10.1103/PhysRevResearch.1.033155. URL: https://link.aps.org/doi/10.1103/PhysRevResearch.1.033155.

[12] Kerson Huang. *Statistical Mechanics*. 2nd ed. Wiley, 1987.

[13] Lev Pitaevskii and Sandro Stringari. *Bose-Einstein condensation and superfluidity*. Vol. 164. Oxford University Press, 2016.

[14] N. Bogoliubov. "On the theory of superfluidity". In: *Journal of Physics* 19.4 (), p. 7.

[15] Luca Salasnich. *Quantum Physics of Light and Matter*. Jan. 2017. DOI: 10.1007/978-3-319-52998-1.

[16] Cheng Chin et al. "Feshbach resonances in ultracold gases". In: *Reviews of Modern Physics* 82.2 (Apr. 2010), pp. 1225–1286. ISSN: 1539-0756. DOI: 10.1103/revmodphys.82.1225. URL: http://dx.doi.org/10.1103/RevModPhys.82.1225.

[17] Kerson Huang and C. N. Yang. "Quantum-Mechanical Many-Body Problem with Hard-Sphere Interaction". In: *Phys. Rev.* 105 (3 Feb. 1957), pp. 767–775. DOI: 10.1103/PhysRev.105.767. URL: https://link.aps.org/doi/10.1103/PhysRev.105.767.

[18] T. D. Lee, Kerson Huang, and C. N. Yang. "Eigenvalues and Eigenfunctions of a Bose System of Hard Spheres and Its Low-Temperature Properties". In: *Phys. Rev.* 106 (6 June 1957), pp. 1135–1145. DOI: 10.1103/PhysRev.106.1135. URL: https://link.aps.org/doi/10.1103/PhysRev.106.1135.

[19] Francesco Ancilotto et al. "Self-bound ultradilute Bose mixtures within local density approximation". In: *Physical Review A* 98.5 (Nov. 2018). ISSN: 2469-9934. DOI: 10.1103/physreva.98.053623. URL: http://dx.doi.org/10.1103/PhysRevA.98.053623.

[20] David M Larsen. "Binary mixtures of dilute bose gases with repulsive interactions at low temperature". In: *Annals of Physics (New York)(US)* 24 (1963).

[21] F Minardi et al. "Effective expression of the Lee-Huang-Yang energy functional for heteronuclear mixtures". In: *Physical Review A* 100.6 (2019), p. 063636.

[22] G.E. Volovik. *The Universe in a Helium Droplet*. International Series of Monographs on Physics. OUP Oxford, 2009. ISBN: 9780199564842. URL: https://books.google.it/books?id=6uj76kFJOHEC.

[23] Edgar Blokhuis and Joris Kuipers. "Thermodynamic expressions for the Tolman length". In: *The Journal of chemical physics* 124 (Mar. 2006), p. 74701. DOI: 10.1063/1.2167642.

[24] V. R. Pandharipande et al. "Calculations of Ground-State Properties of Liquid ^{4}He Droplets". In: *Phys. Rev. Lett.* 50 (21 May 1983), pp. 1676–1679. DOI: 10.1103/

PhysRevLett.50.1676. URL: https://link.aps.org/doi/10.1103/PhysRevLett.50.1676.

[25] Siu A Chin and E Krotscheck. "Structure and collective excitations of He 4 clusters". In: *Physical Review B* 45.2 (1992), p. 852.

[26] F. Dalfovo et al. "Structural and dynamical properties of superfluid helium: A density-functional approach". In: *Phys. Rev. B* 52 (2 July 1995), pp. 1193–1209. DOI: 10.1103/PhysRevB.52.1193. URL: https://link.aps.org/doi/10.1103/PhysRevB.52.1193.

[27] V. Cikojević et al. "Ultradilute quantum liquid drops". In: *Physical Review B* 97.14 (Apr. 2018). ISSN: 2469-9969. DOI: 10.1103/physrevb.97.140502. URL: http://dx.doi.org/10.1103/PhysRevB.97.140502.

[28] Richard C Tolman. "The effect of droplet size on surface tension". In: *The journal of chemical physics* 17.3 (1949), pp. 333–337.

[29] Philipp Rehner and Joachim Gross. "Surface tension of droplets and Tolman lengths of real substances and mixtures from density functional theory". In: *The Journal of Chemical Physics* 148.16 (2018), p. 164703. DOI: 10.1063/1.5020421. eprint: https://doi.org/10.1063/1.5020421. URL: https://doi.org/10.1063/1.5020421.

[30] Hai Ming Lu and Qing Jiang. "Size-dependent surface tension and Tolman's length of droplets". In: *Langmuir* 21.2 (2005), pp. 779–781.

[31] Y. Lei et al. "The Tolman Length: Is It Positive or Negative?" In: *Journal of the American Chemical Society* 127 (Dec. 2005), pp. 15346–7. DOI: 10.1021/ja054297i.

[32] Lawrence S Bartell. "Tolman's δ, surface curvature, compressibility effects, and the free energy of drops". In: *The Journal of Physical Chemistry B* 105.47 (2001), pp. 11615–11618.

[33] SW Mayer. "A molecular parameter relationship between surface tension and liquid compressibility". In: *The Journal of Physical Chemistry* 67.10 (1963), pp. 2160–2164.

[34] Wolfgang Helfrich. "Elastic properties of lipid bilayers: theory and possible experiments". In: *Zeitschrift für Naturforschung C* 28.11-12 (1973), pp. 693–703.

[35] S Fisk and B Widom. "Structure and free energy of the interface between fluid phases in equilibrium near the critical point". In: *The Journal of Chemical Physics* 50.8 (1969), pp. 3219–3227.

[36] PA Egelstaff and B Widom. "Liquid surface tension near the triple point". In: *The Journal of Chemical Physics* 53.7 (1970), pp. 2667–2669.

[37] KK Mon and D Stroud. "Surface widths of simple liquids and an empirical law of freezing". In: *The Journal of Chemical Physics* 74.3 (1981), pp. 2078–2080.

[38] Giovanni Ferioli et al. "Collisions of self-bound quantum droplets". In: *Physical review letters* 122.9 (2019), p. 090401.

[39] N Ashgriz and JY Poo. "Coalescence and separation in binary collisions of liquid drops". In: *Journal of Fluid Mechanics* 221 (1990), pp. 183–204.

[40] J Qian and Chung King Law. "Regimes of coalescence and separation in droplet collision". In: *Journal of fluid mechanics* 331 (1997), pp. 59–80.

[41] Yu Pan and Kazuhiko Suga. "Numerical simulation of binary liquid droplet collision". In: *Physics of Fluids* 17.8 (2005), p. 082105.

[42] J Qian and Chung King Law. "Regimes of coalescence and separation in droplet collision". In: *Journal of fluid mechanics* 331 (1997), pp. 59–80.

[43] Fatkhulla Abdullaev and Josselin Garnier. "Bright Solitons in Bose-Einstein Condensates: Theory". In: vol. 45. Dec. 2008, pp. 25–43. DOI: 10.1007/978-3-540-73591-5_2.

[44] Lincoln D Carr, Mary Ann Leung, and William P Reinhardt. "Dynamics of the Bose-Einstein condensate: quasi-one-dimension and beyond". In: *Journal of Physics B: Atomic, Molecular and Optical Physics* 33.19 (2000), p. 3983.

[45] A. D. Jackson, G. M. Kavoulakis, and C. J. Pethick. "Solitary waves in clouds of Bose-Einstein condensed atoms". In: *Physical Review A* 58.3 (Sept. 1998), pp. 2417–2422. ISSN: 1094-1622. DOI: 10.1103/physreva.58.2417. URL: http://dx.doi.org/10.1103/PhysRevA.58.2417.

[46] Victor M Perez-Garcia, Humberto Michinel, and Henar Herrero. "Bose-Einstein solitons in highly asymmetric traps". In: *Physical Review A* 57.5 (1998), p. 3837.

[47] Kevin E. Strecker et al. "Formation and propagation of matter-wave soliton trains". In: *Nature* 417.6885 (May 2002), pp. 150–153. ISSN: 1476-4687. DOI: 10.1038/nature747. URL: http://dx.doi.org/10.1038/nature747.

[48] L. Khaykovich. "Formation of a Matter-Wave Bright Soliton". In: *Science* 296.5571 (May 2002), pp. 1290–1293. ISSN: 1095-9203. DOI: 10.1126/science.1071021. URL: http://dx.doi.org/10.1126/science.1071021.

[49] Simon L. Cornish, Sarah T. Thompson, and Carl E. Wieman. "Formation of Bright Matter-Wave Solitons during the Collapse of Attractive Bose-Einstein Condensates". In: *Phys. Rev. Lett.* 96 (17 May 2006), p. 170401. DOI: 10.1103/PhysRevLett.96.170401. URL: https://link.aps.org/doi/10.1103/PhysRevLett.96.170401.

[50] Axel Griesmaier et al. "Bose-Einstein condensation of chromium". In: *Physical Review Letters* 94.16 (2005), p. 160401.

[51] L. Salasnich. "Bright solitons in ultracold atoms". In: *Optical and Quantum Electronics* 49.12 (Nov. 2017). ISSN: 1572-817X. DOI: 10.1007/s11082-017-1247-5. URL: http://dx.doi.org/10.1007/s11082-017-1247-5.

[52] A Shabat and V Zakharov. "Exact theory of two-dimensional self-focusing and one-dimensional self-modulation of waves in nonlinear media". In: *Soviet physics JETP* 34.1 (1972), p. 62.

[53] L. Salasnich, A. Parola, and L. Reatto. "Modulational Instability and Complex Dynamics of Confined Matter-Wave Solitons". In: *Physical Review Letters* 91.8 (Aug. 2003). ISSN: 1079-7114. DOI: 10.1103/physrevlett.91.080405. URL: http://dx.doi.org/10.1103/PhysRevLett.91.080405.

[54] Wilf H.S. (eds.) Ralston A. *Mathematical methods for digital computers,* vol. Vol.1. Wiley, 1960.

[55] Jason HV Nguyen et al. "Collisions of matter-wave solitons". In: *Nature Physics* 10.12 (2014), pp. 918–922.

[56] S. K. Adhikari. "Statics and dynamics of a self-bound matter-wave quantum ball". In: *Physical Review A* 95.2 (Feb. 2017). ISSN: 2469-9934. DOI: 10.1103/physreva.95.023606. URL: http://dx.doi.org/10.1103/PhysRevA.95.023606.

[57] Francesco Fassò. *Istituzioni di Fisica Matematica*. Cleup, 2016-2017.